C H A P T E R - VI

OBSERVATIONS, DISCUSSIONS AND CONCLUSIONS

6.0 General:

The object of this chapter is to analyse the mechanical behaviour of rocks under the theoretical background developed in previous chapter. A series of tests on discs and annuli subjected to diametral loading are presented with a view to verify the theoretical cencepts developed from first principles. The rock material for testing is an igneous rock of basalt formation of eocene age. The analysis aims to evolve a mechanistic picture of failure in igneous basaltic rock and establish a failure criterion. It also proposes to suggest a simple constitutive relationship amneable to mathematical analysis. It should contribute towards derivation of useful engineering parameters to explain the engineering behaviour of structures constituted of rock.

6.1 Material properties:

The material for the present investigation is the basalt rock from the Narmada Dam site. The physical properties of the samples and their petrographic properties are given below:

6.1.1 Physical properties:

a) Disc samples:

Radius = 2.7 cm.

Thickness = Ranges from 2.57 to 2.88 cm.

Apprent specific gravity = 2.59

% porosity = 7.48

% water absorption = 2.98

Air dried samples

b) Ring samples

Radius = 2.7 cm.

Thickness = Ranges from 2.533cm to 2.738cm

Density = 2.70 gm/c.c.

Apparent specific gravity = 2.78

% water absorption = 0.91

% porosity = 1.94

Air dried samples

6.1.2 Petrographic properties:

a) Disc samples:

Rock type : Basalt amygdalodal type

Magascopic characteristics : Shades of light green and grey with specks of white and dark green fine grained and homogeneous.

Microscopic characteristics:

I) Texture : Amygdaloidal, amygdals of calcite, zeolite (white) and chlorite (dark green)

II) Mineral composition : Plagioclase, felspar and augite

b) Ring samples:

Rock type : Dolerite and porphyritic amygdaloidal basalt

Megascopic characteristics : Fresh black coloured medium to fine grained and homogeneous

Microscopic characteristics:

I) Texture : Ophific texture, inequigranular and hemicrystalline in nature phenocrysts are of plagioclase felspar and are seen embedded in ground mass of plagioclase felspar laths and augite. Cavity of green earth is seen.

II) Mineral composition : Plagioclase felspar and augite

6.2 Observations:

The experiments are carried out employing Brazillian test technique. The specimens are given designations as below:

6.2.1 Disc specimens:

The specimens have been designated as Nx/D/0.48 μ/1, Nx/D/0.66 μ/2, Nx/D/0.96 μ/3 etc. where the notation Nx represents Nx core size i.e.5.4 cm. diameter and D represents disc. Notations 0.48 μ, 0.66 μ, 0.96 μ stands for head speed per minute such as 0.48 μ means 0.48×10^{-3}mm/min, 0.66 μ means 0.66×10^{-3}mm/min, and 0.96 μ means 0.96×10^{-3}mm/min and so on respectively.

Notation 1,2 or 3 stands for sample number one, two or three respectively.

6.2.2 Ring specimens:

The samples have been designated as Nx/R/3Ø/1, Nx/R/4Ø/5, Nx/R/5Ø/11 etc. where notation Nx represents Nx size i.e. 5.4 cm diameter and R stands for ring. Notation 3Ø, 4Ø and 5Ø stands for central hole diameter of 3,4 and 5mm respectively. Notation 1,5 or 11 represents the number of sample for example first fifth or eleventh.

6.2.3 Observations on failure of discs and rings:

The behaviour of the test specimens during fracturing is described below. The associated load displacement curve alongwith photograph is also presented.

6.2.3.1 Observations on failure of discs:

Nx/D/0.48 μ/1 The primary fracture is feebly visible along the load axis. The fracture crack is seen running along the flaw at the top left upper portion of the disc. A secondary crack is also visible at the bottom right of the disc. (Fig 6.1)

Nx/D/0.66 μ/2 The primary fracture in the form of a crack is distinctly observed along the diametral loading. A small secondary crack is also visible at the top left upper portion of the disc. (Fig 6.2)

Nx/D/0.96 μ/3 Only primary fracture in the form of a crack running along the loading line is observed. The crack does not appear to extend upto top and bottom indicating that crack does not start from the

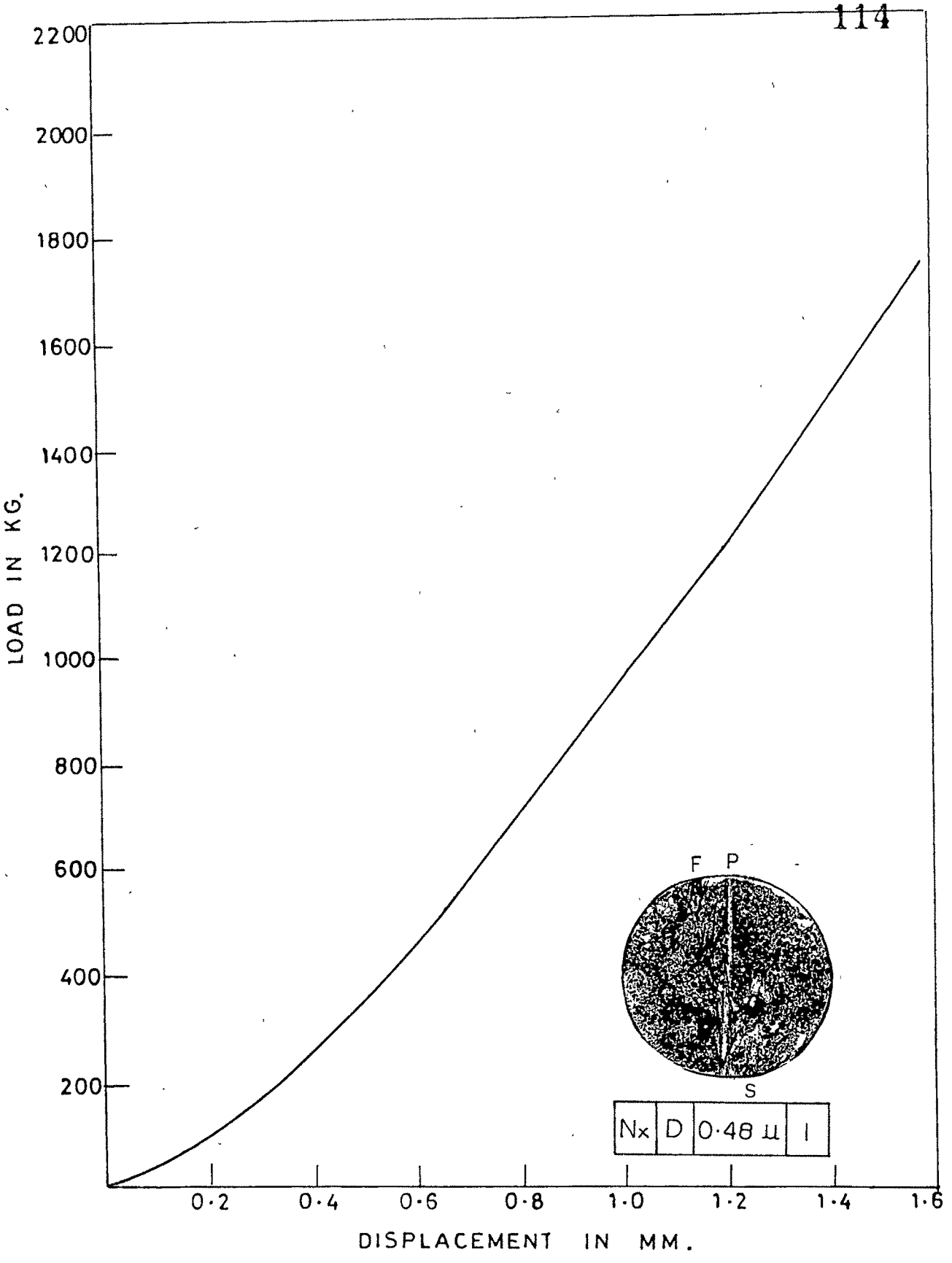

FIG. 6·1 : LOAD DISPLACEMENT CHARACTERISTICS.

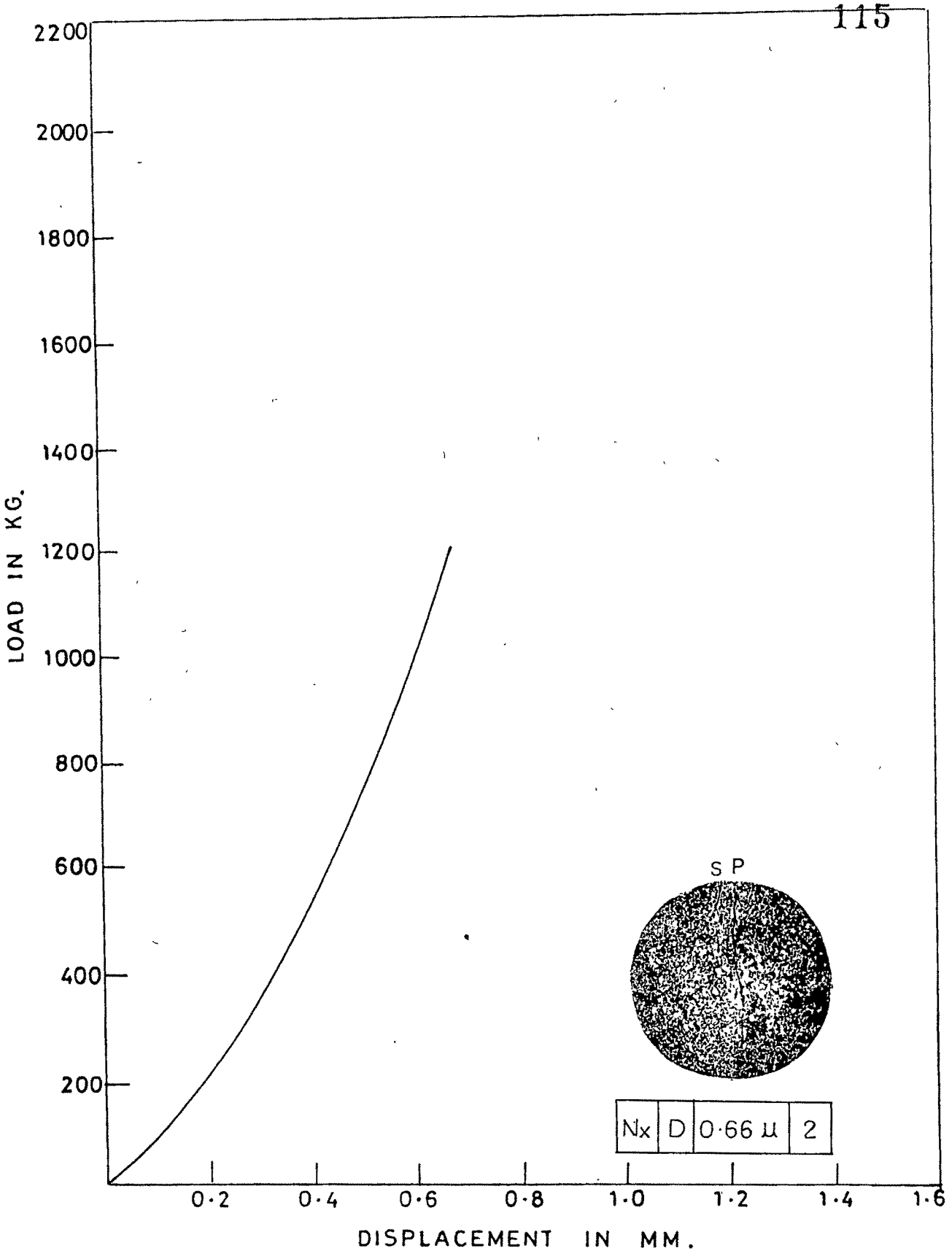

FIG.6·2 : LOAD DISPLACEMENT CHARACTERISTICS.

loading points. (Fig 6.3)

Nx/D/1.4 μ/4 The primary fracture is visible in the form of a crack along the load axis. A through secondary fracture in the form of a crack starting from a point situated at a little distance from the loading point at the top right portion of the disc is also observed. Some tertiary cracks are also seen at the bottom left portion of the disc, away from primary fracture. (Fig 6.4)

Nx/D/1.95 μ/5 Simultaneously with the primary fracture in the form of a crack along the diametral loading a crack is also observed through a flaw in the form of a calcite vein of semi spherical shape. At the centre of the disc a hair crack is discernible which means that the maximum stress concentration is joined by a flaw. (Fig 6.5)

Nx/D/2.4 μ/6 Only primary fracture in the form of a crack along the loading is seen. One more crack which springs up from a main primary crack at bottom one third point is visible at a little distance from main crack. (Fig 6.6)

Nx/D/3.3 μ/7 A primary crack is observed through the loading points. A small secondary crack is also seen at the bottom just little left from main crack. (Fig 6.7)

Nx/D/4.8 μ/8 The primary fracture in the form of a crack is visible along the loading line. A through secondary crack starting from a point situated

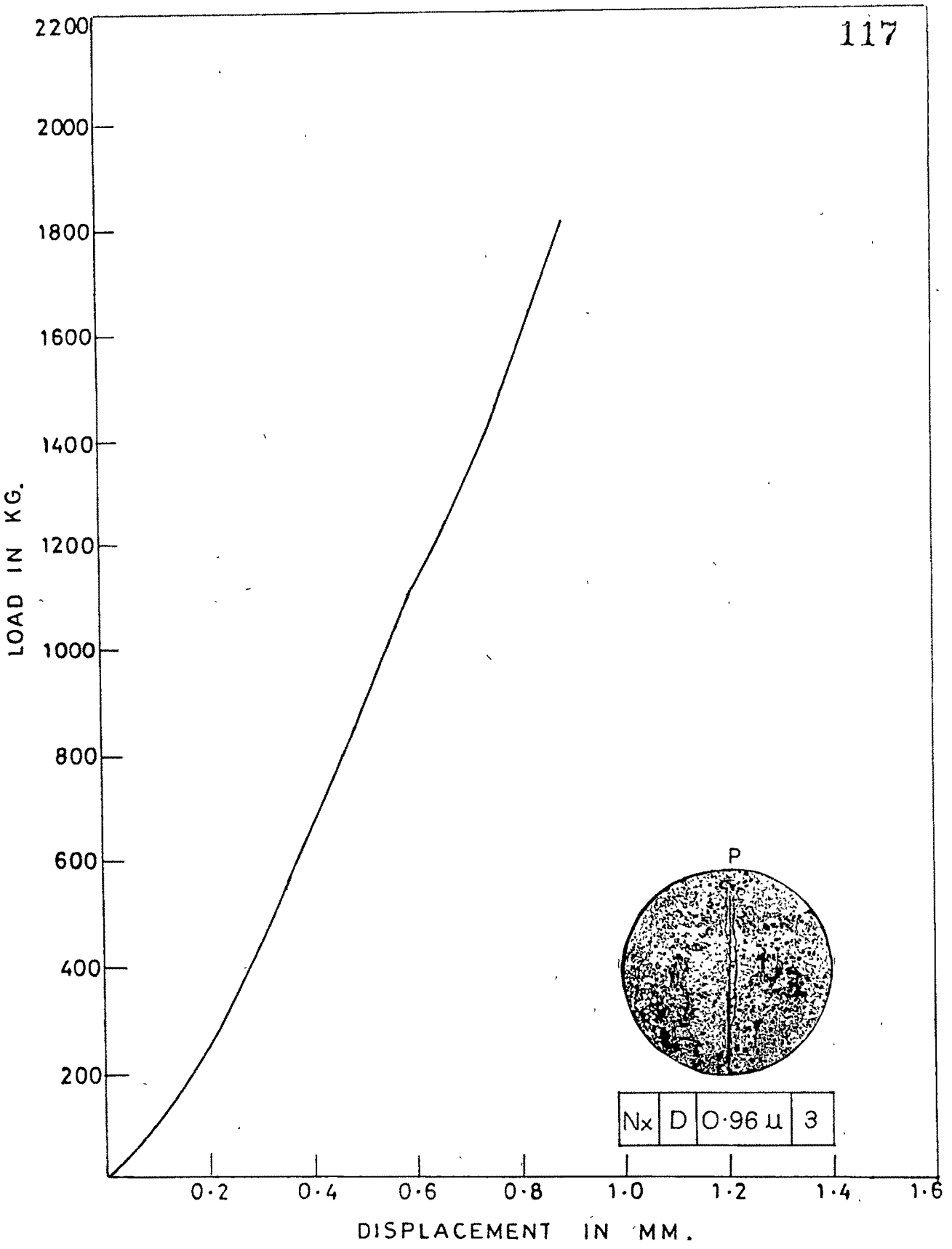

FIG. 6·3 : LOAD DISPLACEMENT CHARACTERISTICS.

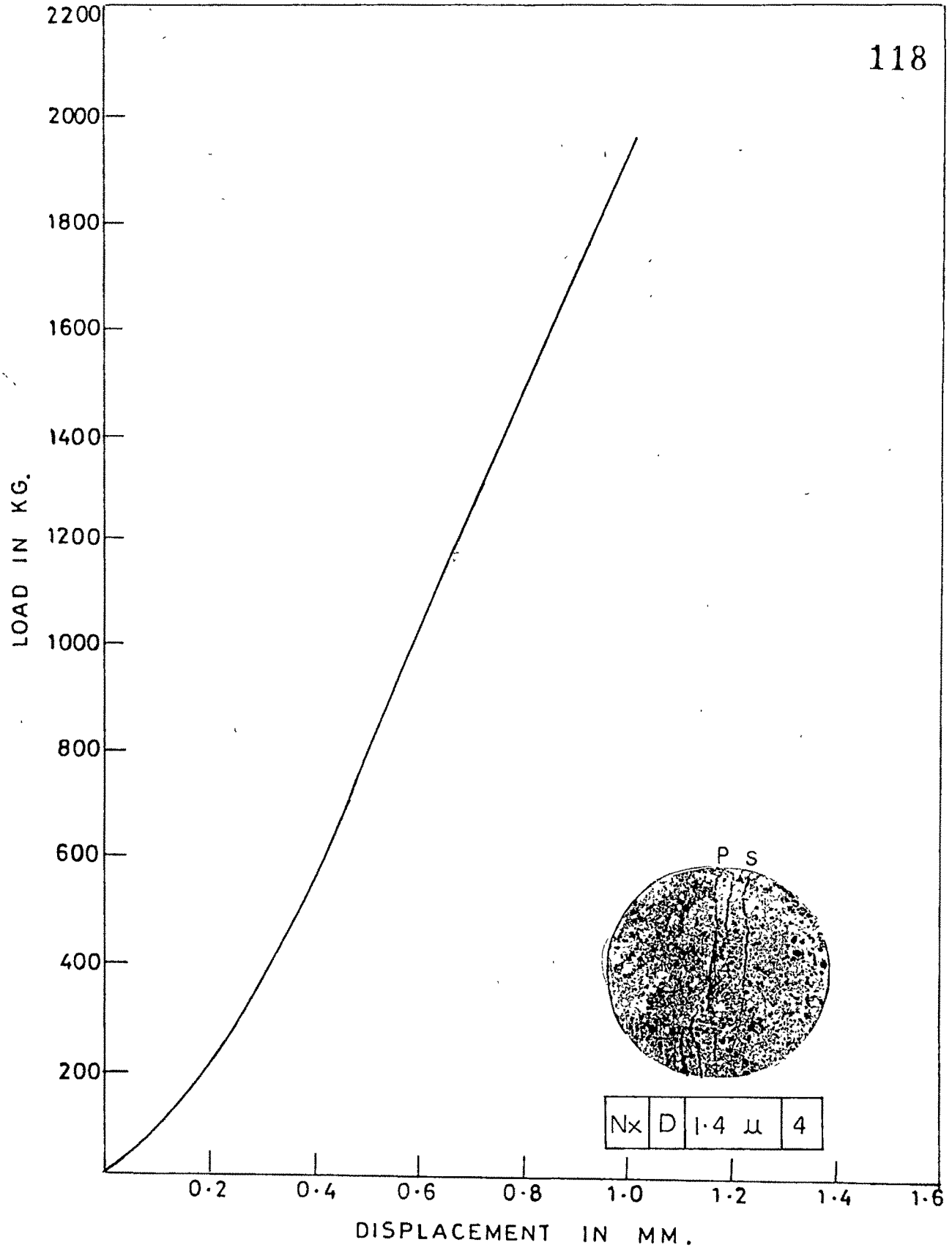

FIG. 6·4 : LOAD DISPLACEMENT CHARACTERISTICS.

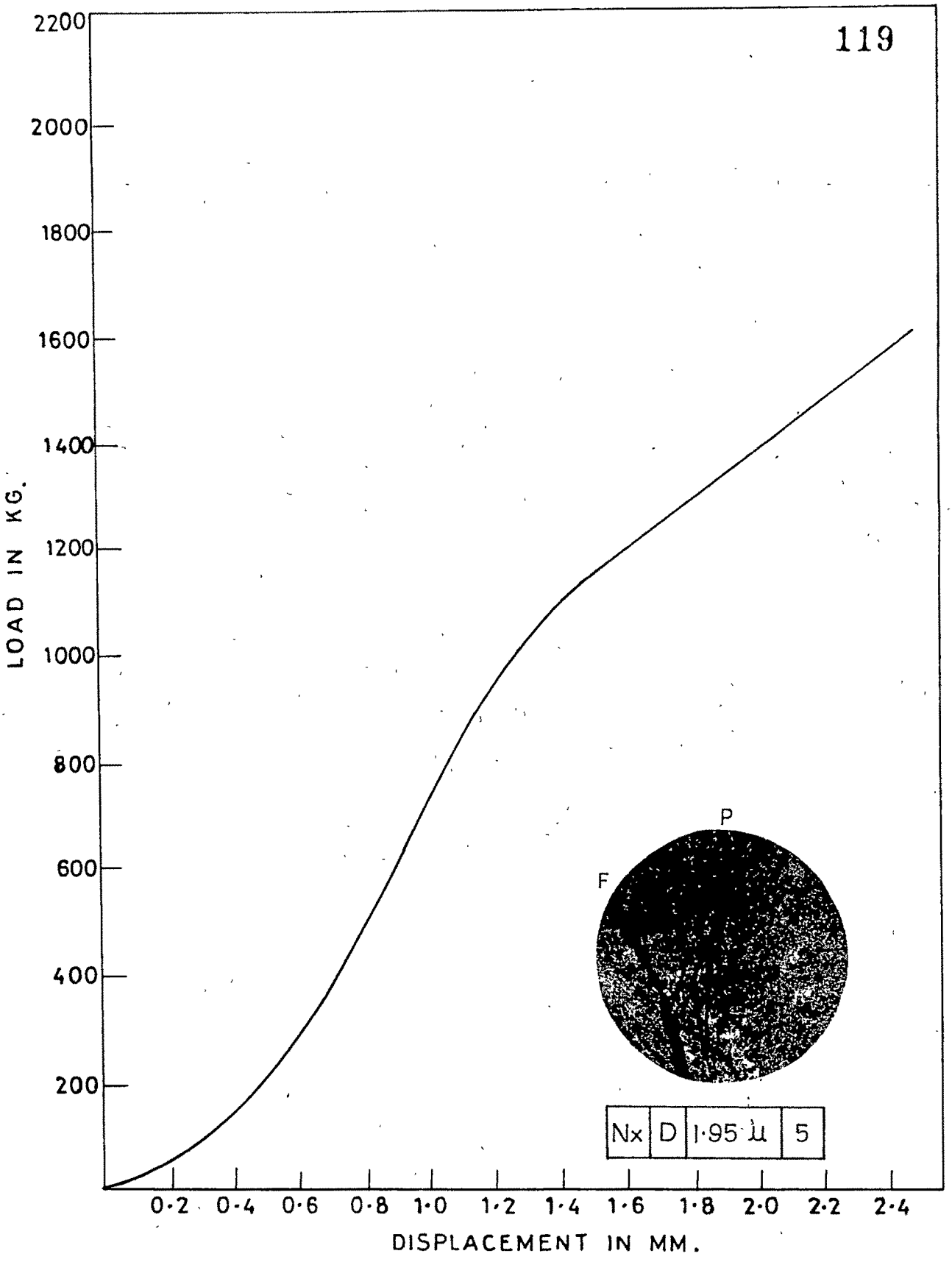

FIG.6·5 : LOAD DISPLACEMENT CHARACTERISTICS.

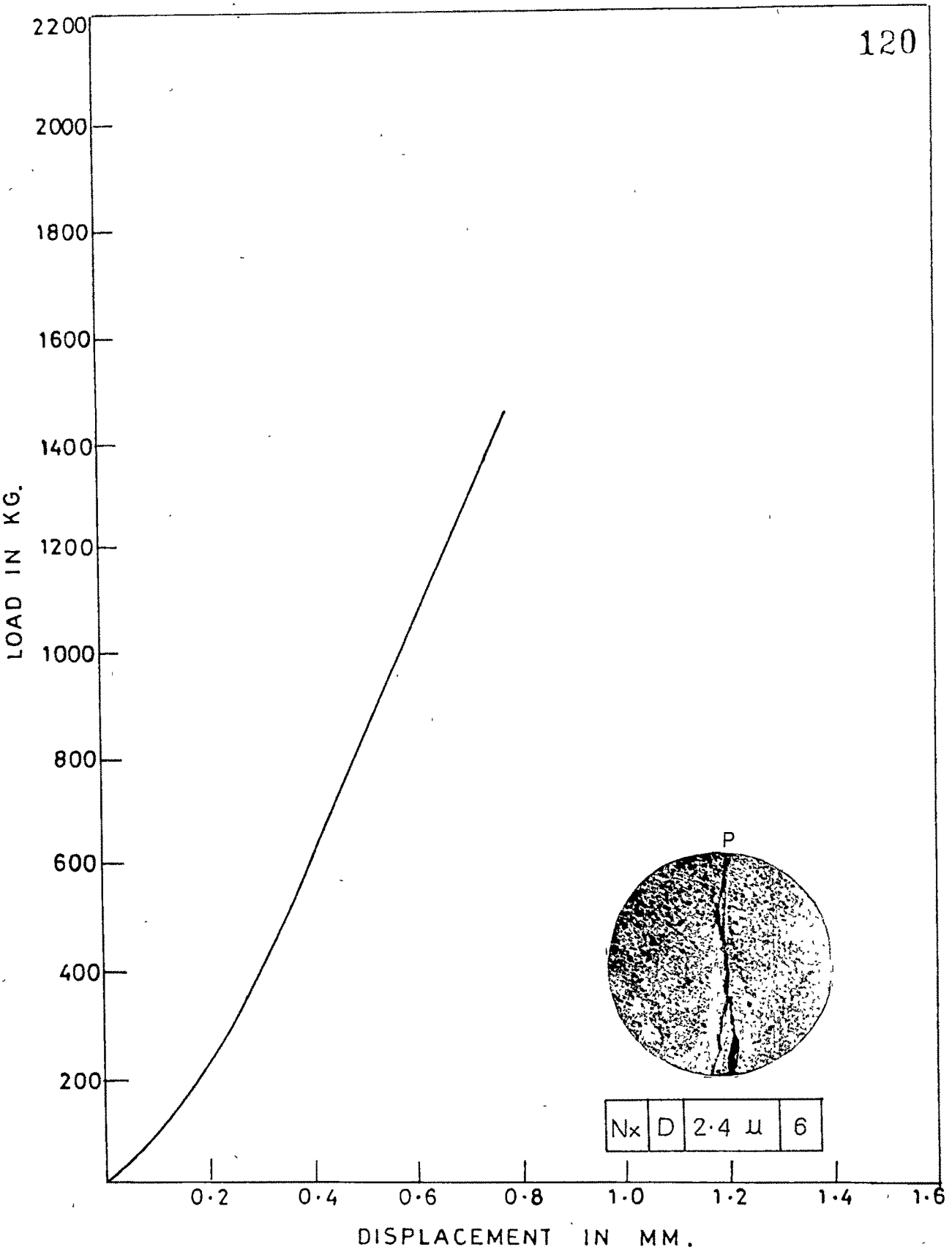

FIG. 6·6 : LOAD DISPLACEMENT CHARACTERISTICS.

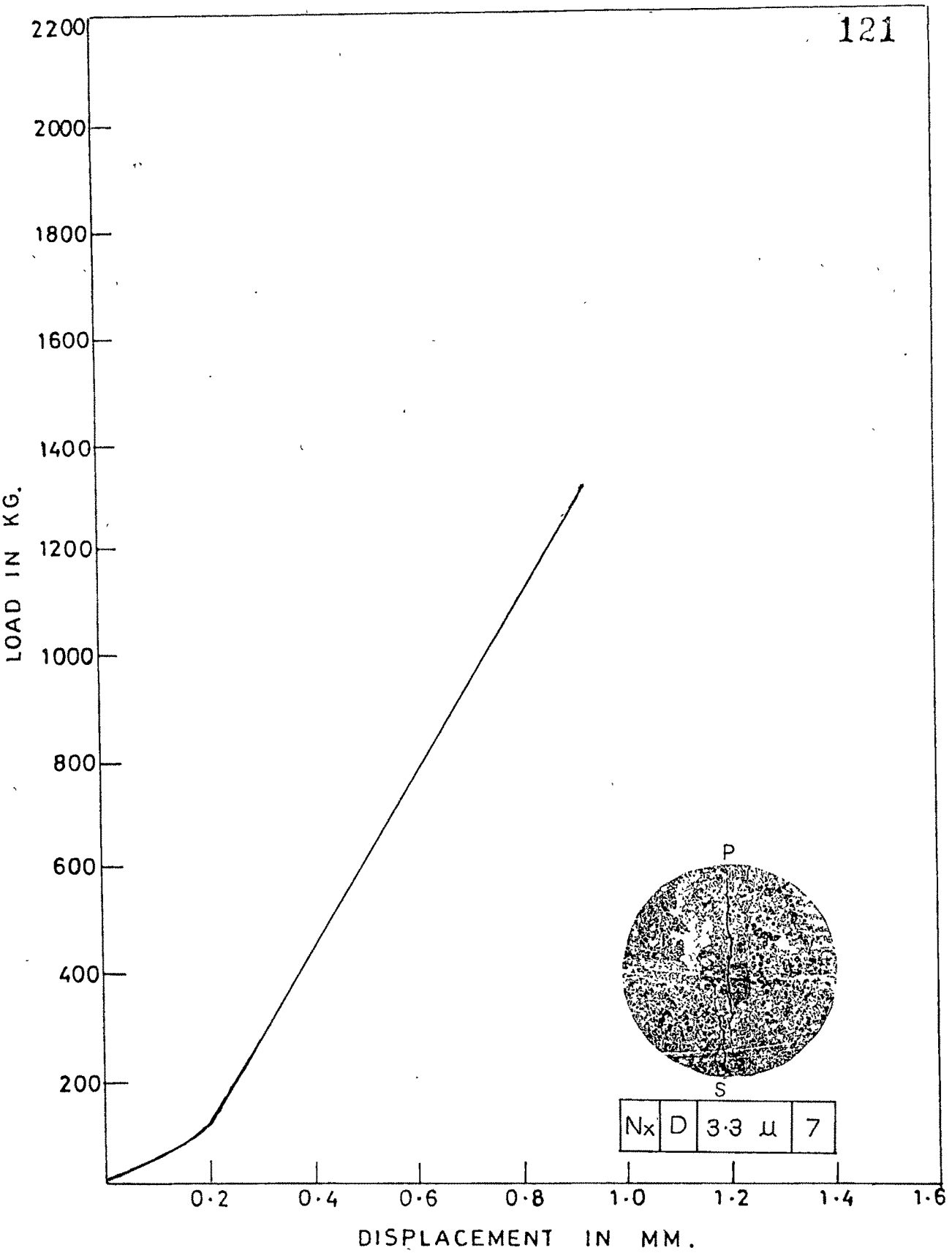

FIG. 6·7 : LOAD DISPLACEMENT CHARACTERISTICS.

at a little distance right from the top loading point of the disc is also seen. Some more secondary hair cracks are also visible at bottom left of the disc. (Fig 6.8)

Nx/D/7.2 μ/9 The primary fracture and a flaw is joined at the centre showing crack widened at the centre. Secondary fracture in the form of a crack is observed at the top right portion of the disc. A minute hair crack is also visible at the flaw in the form of a calcite vein at the end of the horizontal diameter of the disc. A tertiary crack is also seen running parallel to the primary crack on the bottom left half portion of the disc. (Fig 6.9)

Nx/D/9.6 μ/10 The primary fracture in the form of a crack is seen along the loading diameter. A secondary crack which just starts near the bottom left of primary crack runs parallel up to the centre of the disc. A crack is also seen through the flaw in the form of calcite vein situated at the top right quadrant of the disc. The crack runs across the disc and ends just near to the bottom right of the primary crack. (Fig 6.10)

Nx/D/12 μ/11 Besides a primary crack running along the loading diameter a more distinct crack along the calcite vein is observed. The flaw is oriented from the top first quadrant of the disc and running across the disc joint at the bottom with the primary crack.(Fig 6.11)

Nx/D/16 μ/12 The primary fracture is visible in the form of a crack running along the load axis.

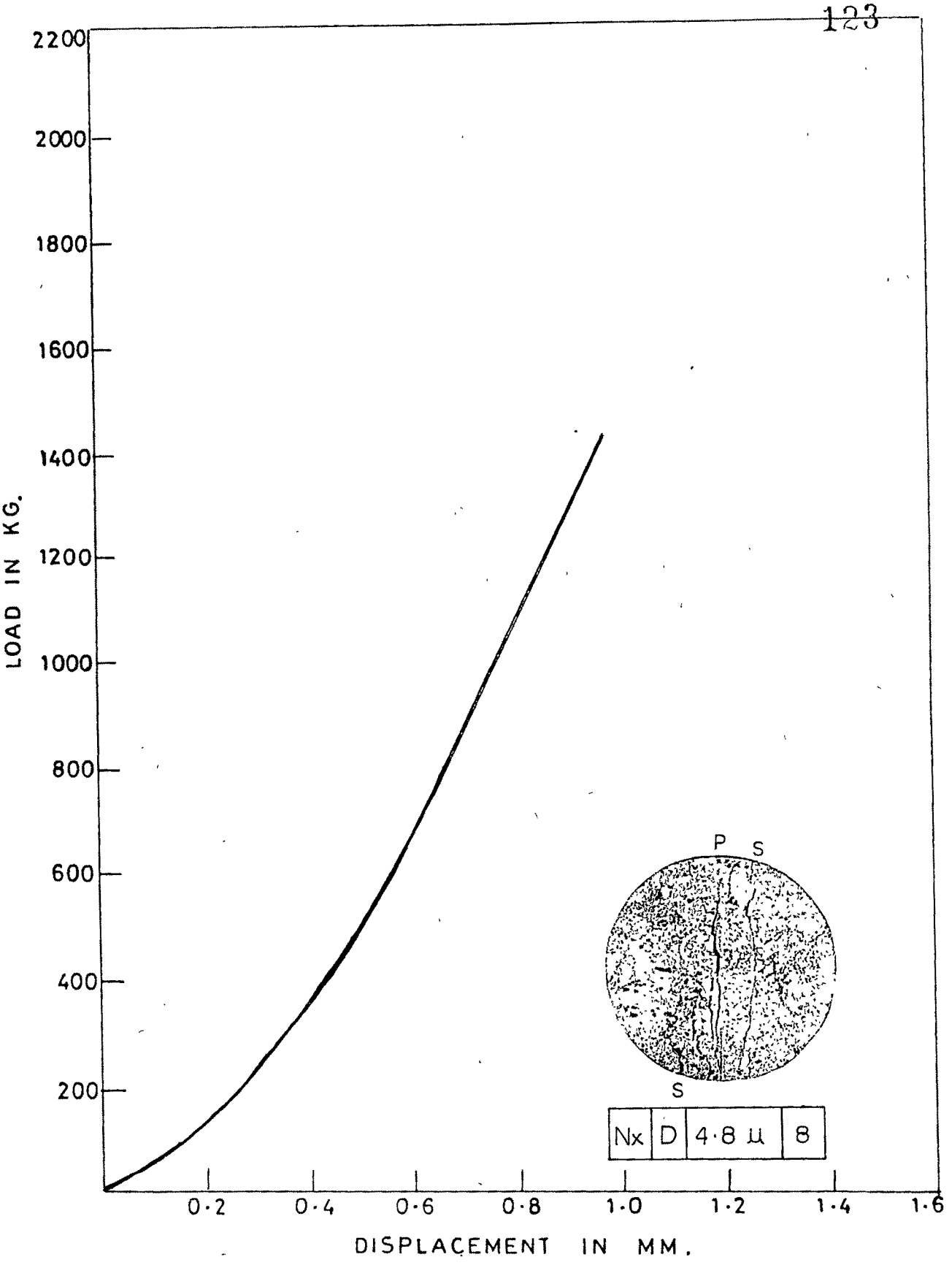

FIG. 6·8 : LOAD DISPLACEMENT CHARACTERISTICS.

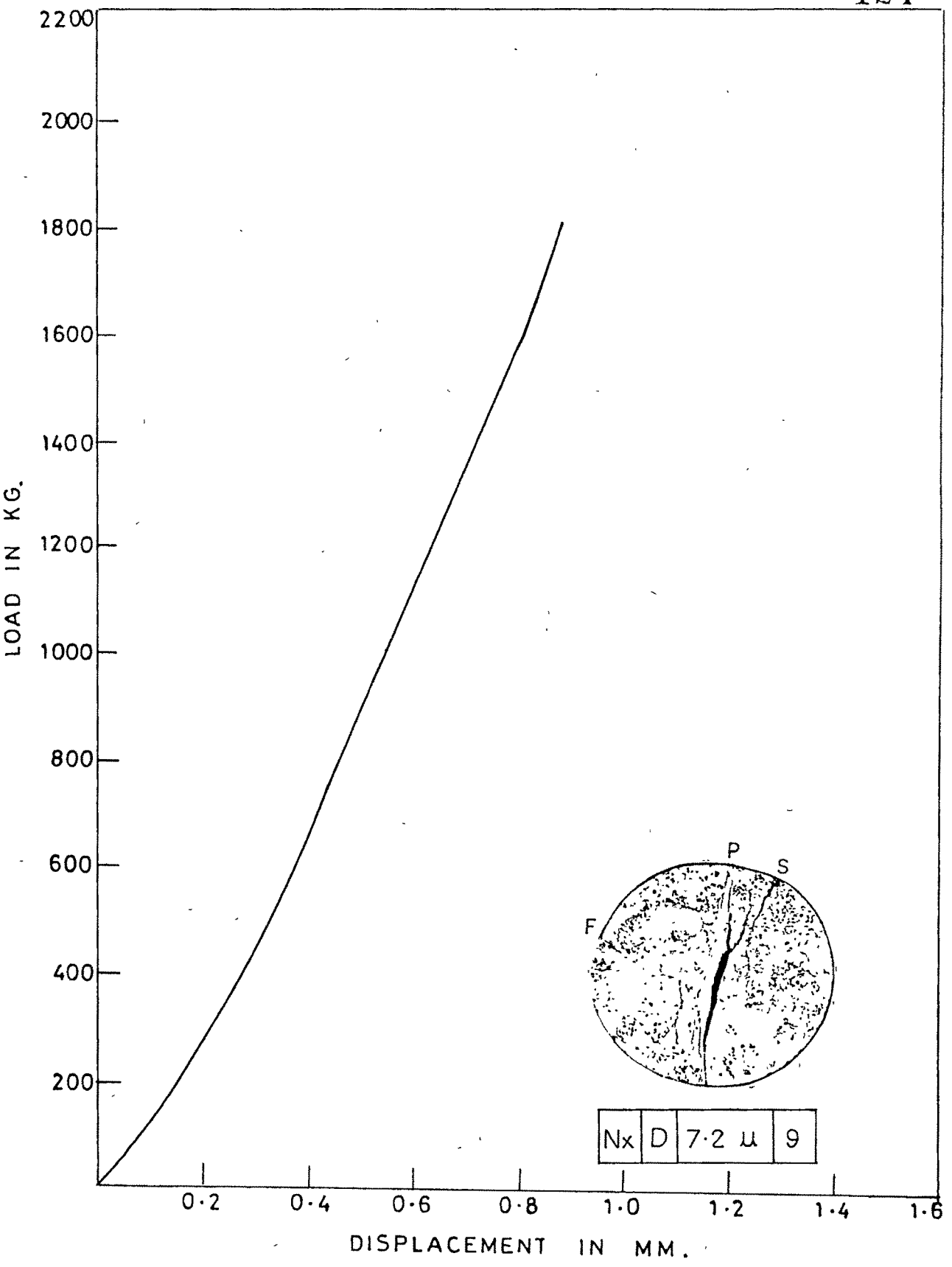

FIG. 6·9 : LOAD DISPLACEMENT CHARACTERISTICS.

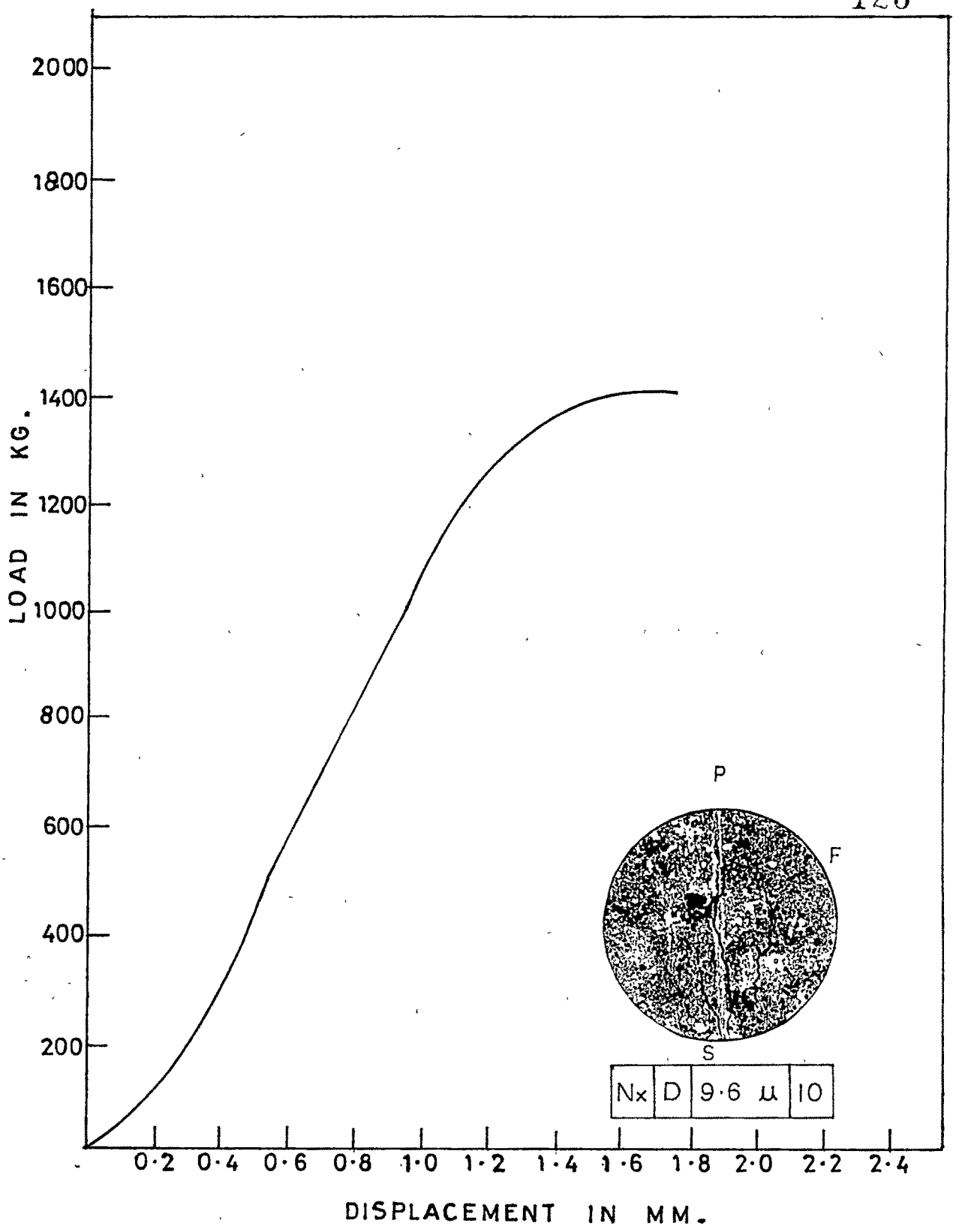

FIG. 6·10 : LOAD DISPLACEMENT CHARACTERISTICS.

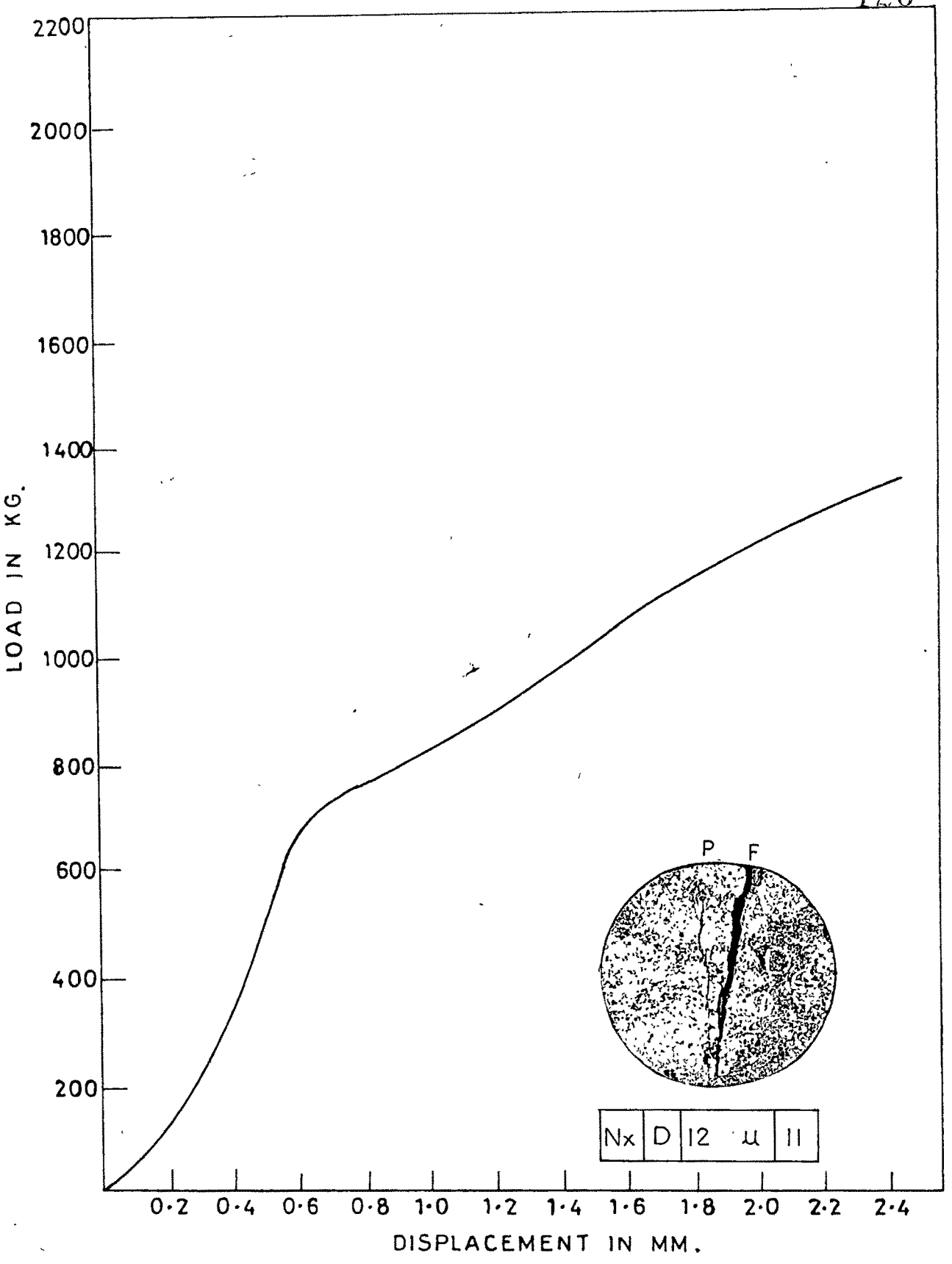

FIG.6·11: LOAD DISPLACEMENT CHARACTERISTICS.

A secondary crack is also observed at the bottom right of the primary crack. (Fig 6.12)

Nx/D/24 μ/13 The primary fractureis observed only in the form of a crack along diametral loading points. (Fig 6.13)

Nx/D/36 μ/14 A flaw is oriented across the disc starting from first quadrant at the top right ending at third quadrant at bottom left of the diametral loading at bottom left of the diametral loading line. The disc is only broken through the flaw which is in the form of a calcite vein. (Fig 6.14)

Nx/D/48 μ/15 The primary fracture in the form of a crack is observed along the load. Two secondary cracks one situated at just near the loading point at top right and the other one located near the loading point at bottom left are also visible. (Fig 6.15)

Nx/D/60 μ/16 The primary fracture is visible in the form of a heavy crack line along the load. Two point calcite flaws are joined with the crack along the loading line. Secondary cracking is also observed to the left and right of the loading line at top and bottom respectively. The tertiary cracking is also seen right to the loading line at bottom. (Fig 6.16)

Nx/D/82 μ/17 The primary fracture in the form of a crack along the load and a horizontal crack through the flaw situated at extreme left nearly at 1/4th on horizontal diameter occured simultaneously. The flaw is

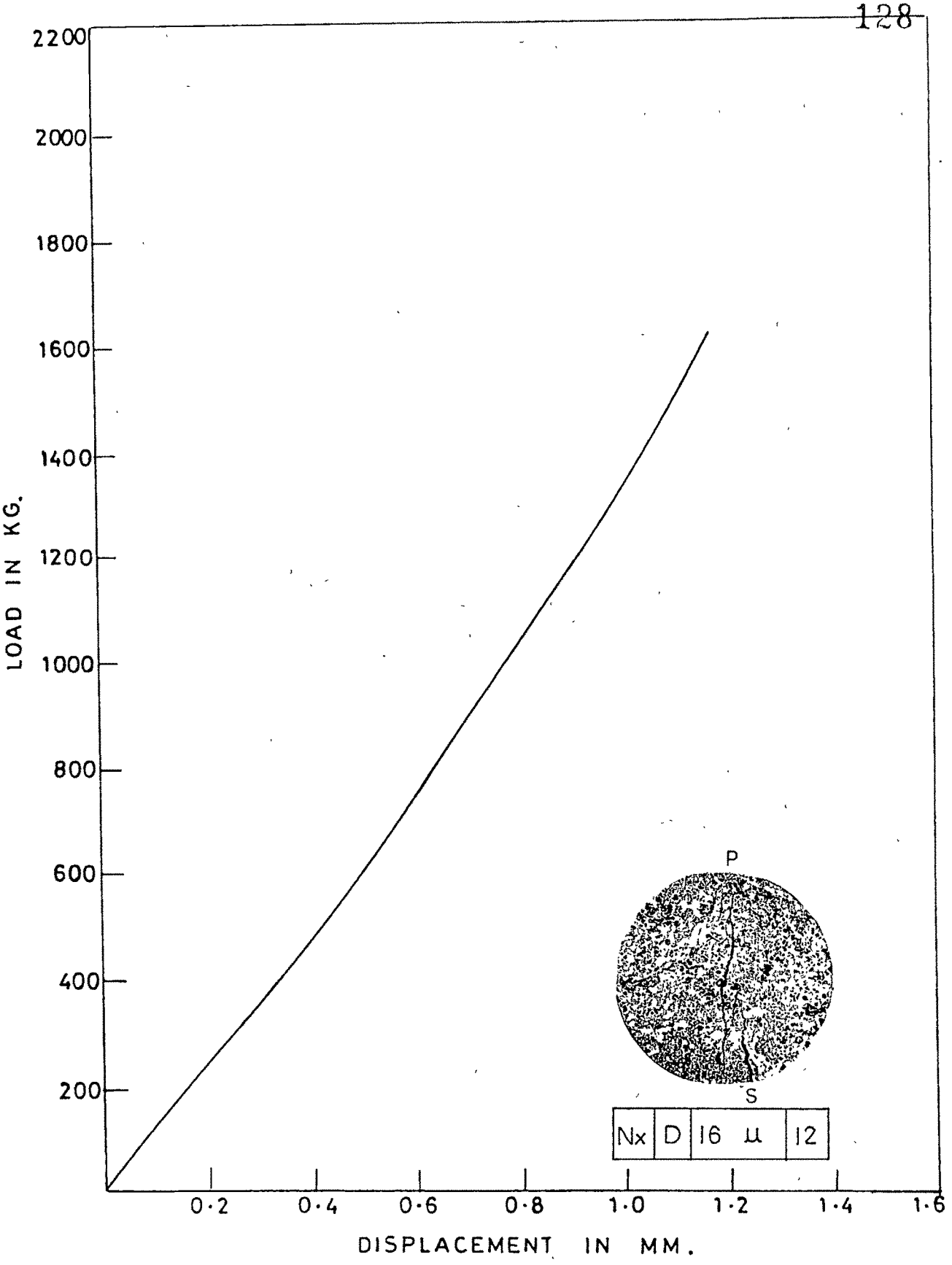

FIG. 6·12 : LOAD DISPLACEMENT CHARACTERISTICS.

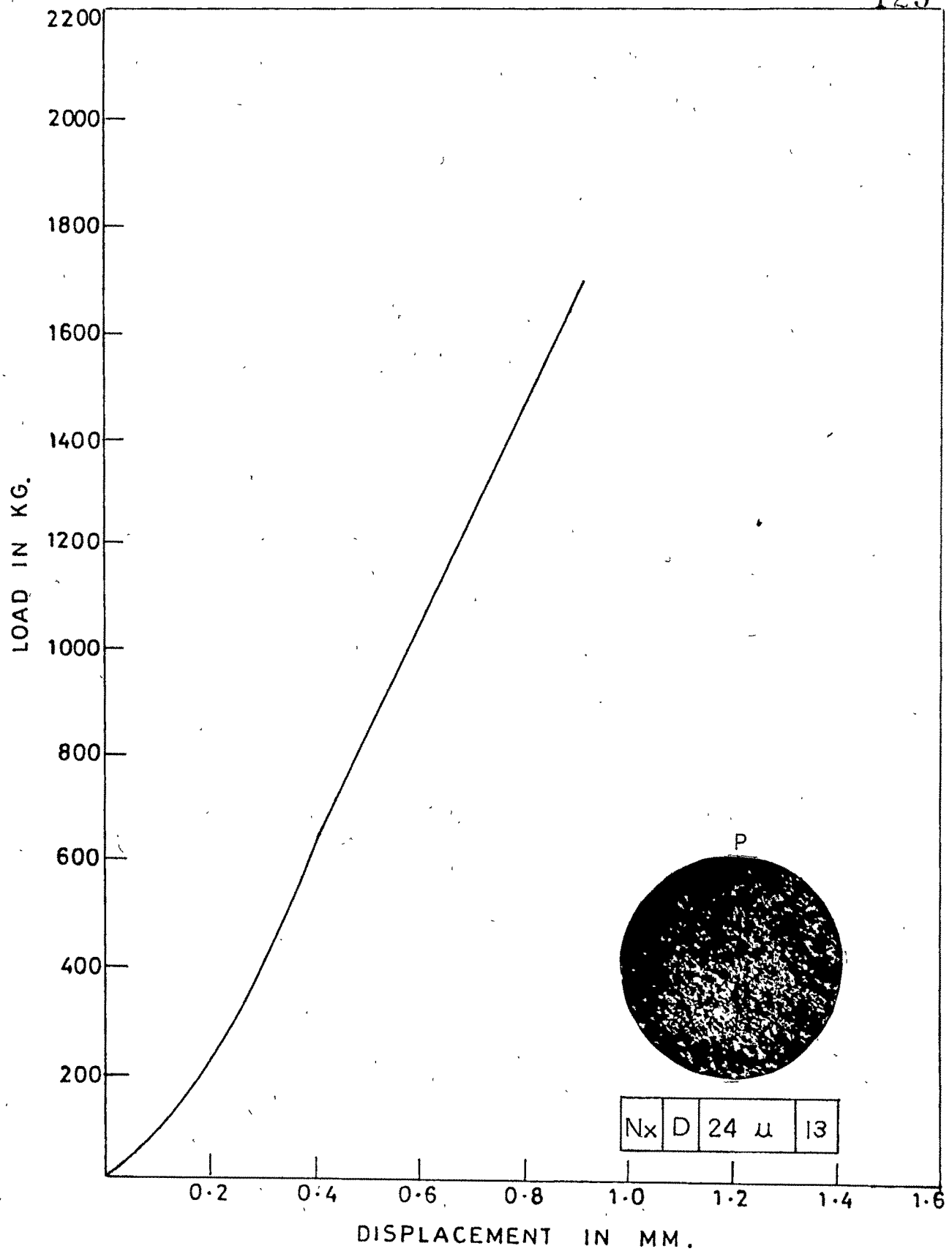

FIG. 6·13 : LOAD DISPLACEMENT CHARACTERISTICS.

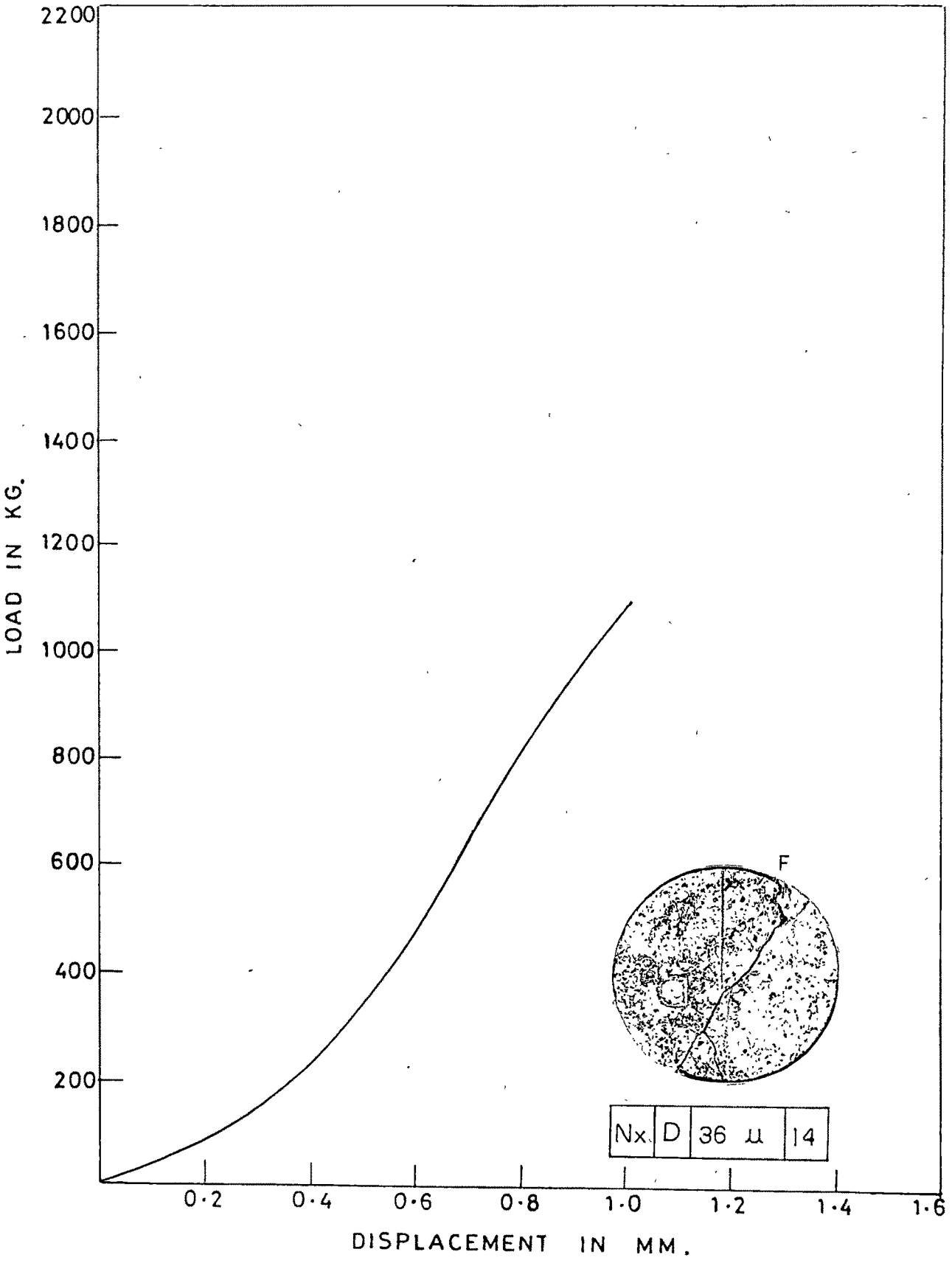

FIG. 6·14 : LOAD DISPLACEMENT CHARACTERISTICS.

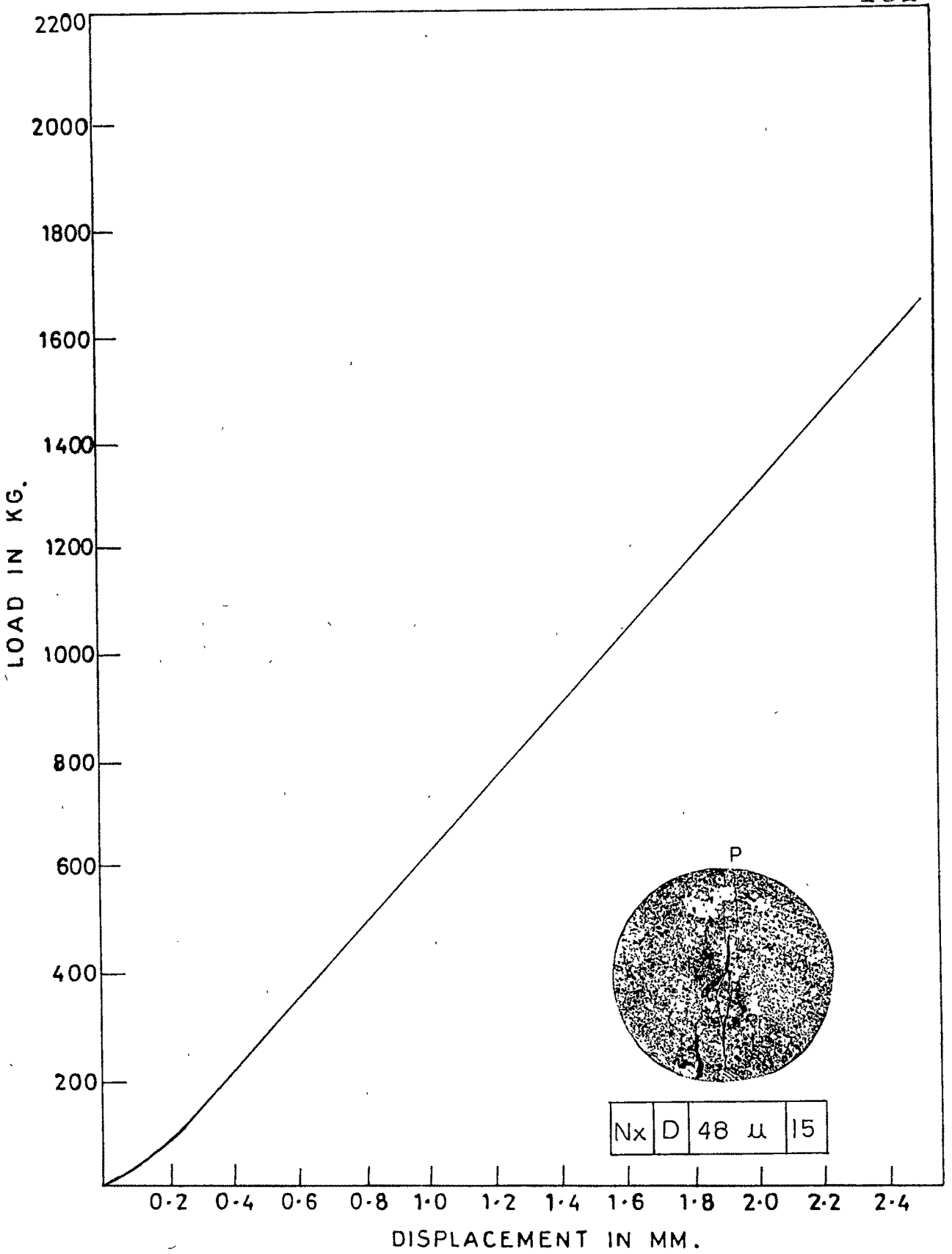

FIG.6·15: LOAD DISPLACEMENT CHARACTERISTICS.

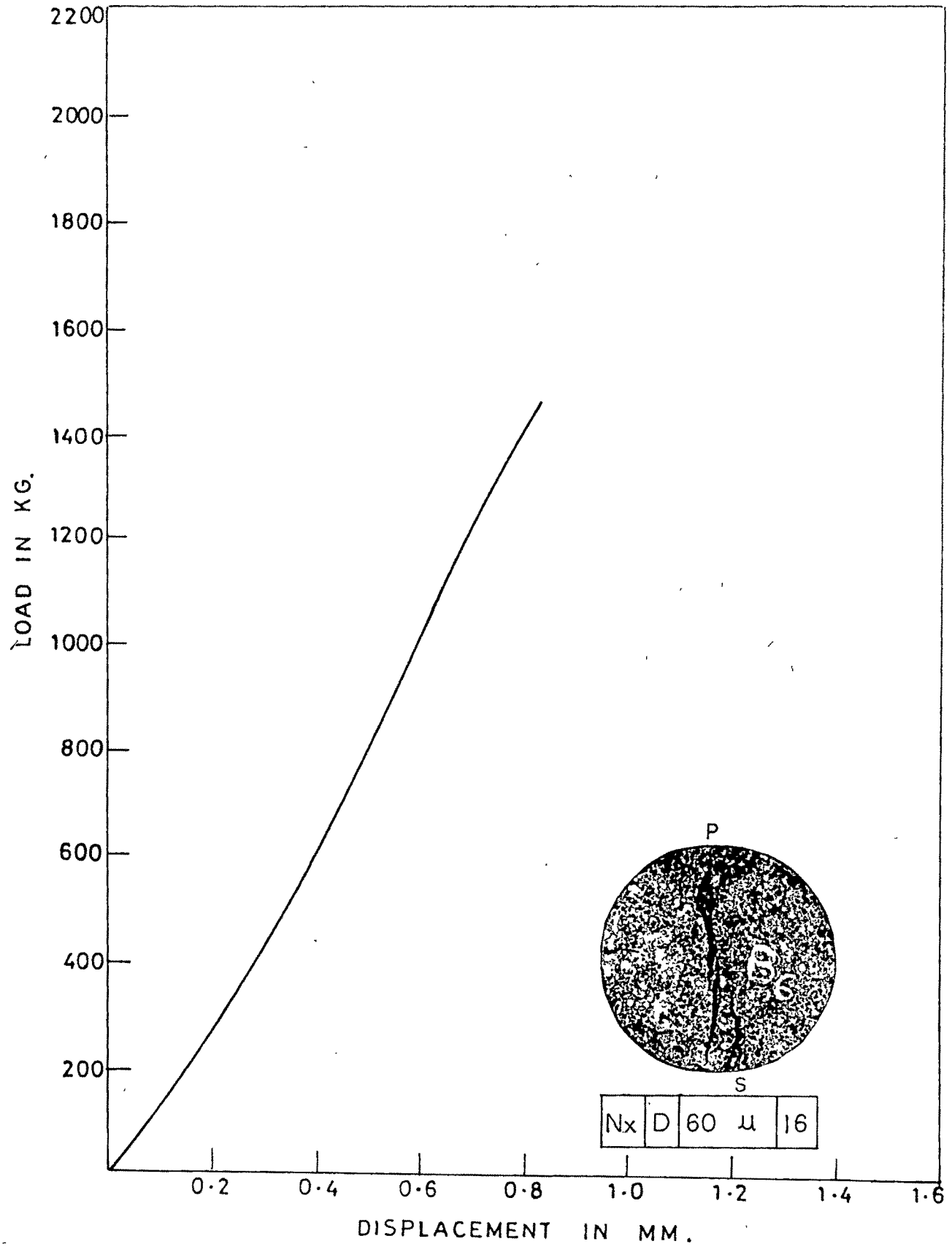

FIG.6·16 : LOAD DISPLACEMENT CHARACTERISTICS.

a typical calcite vein. A secondary crack is also visible just near the primary crack at top right of the disc. (Fig 6.17)

Nx/D/120 μ/18 Only secondary cracking is observed in the form of a crack running just parellel to loading line starting from bottom left of the disc. The crack is taking a semispherical turn and joins the loading line at a distance 1/5th. from the top. (Fig 6.18)

Nx/D/180 μ/19 The primary fracture in the form a crack joining the diametral loading line. The secondary and tertiary cracks are also visible at top right of the disc just near the loading point.(Fig 6.19)

Nx/D/240 μ/20 The primary fracture in the form of a crack running along loading line but terminating just before the loading points at top and bottom. The secondary and tertiary cracking is also observed at top right and bottom left of the disc respectively.(Fig 6.20)

Nx/D/300 μ/21 A clear primary fracture is observed along the diametral loading points. A minute hair crack also visible at bottom right of the loading point as a secondary crack. (Fig 6.21)

Nx/D/410 μ/22 The primary fracture in the form of a crack running throughout the loading diameter except a little distance at top loading point is clearly seen. At bottom right a little distance away from loading point a minute secondary crack is also observed.(Fig 6.22)

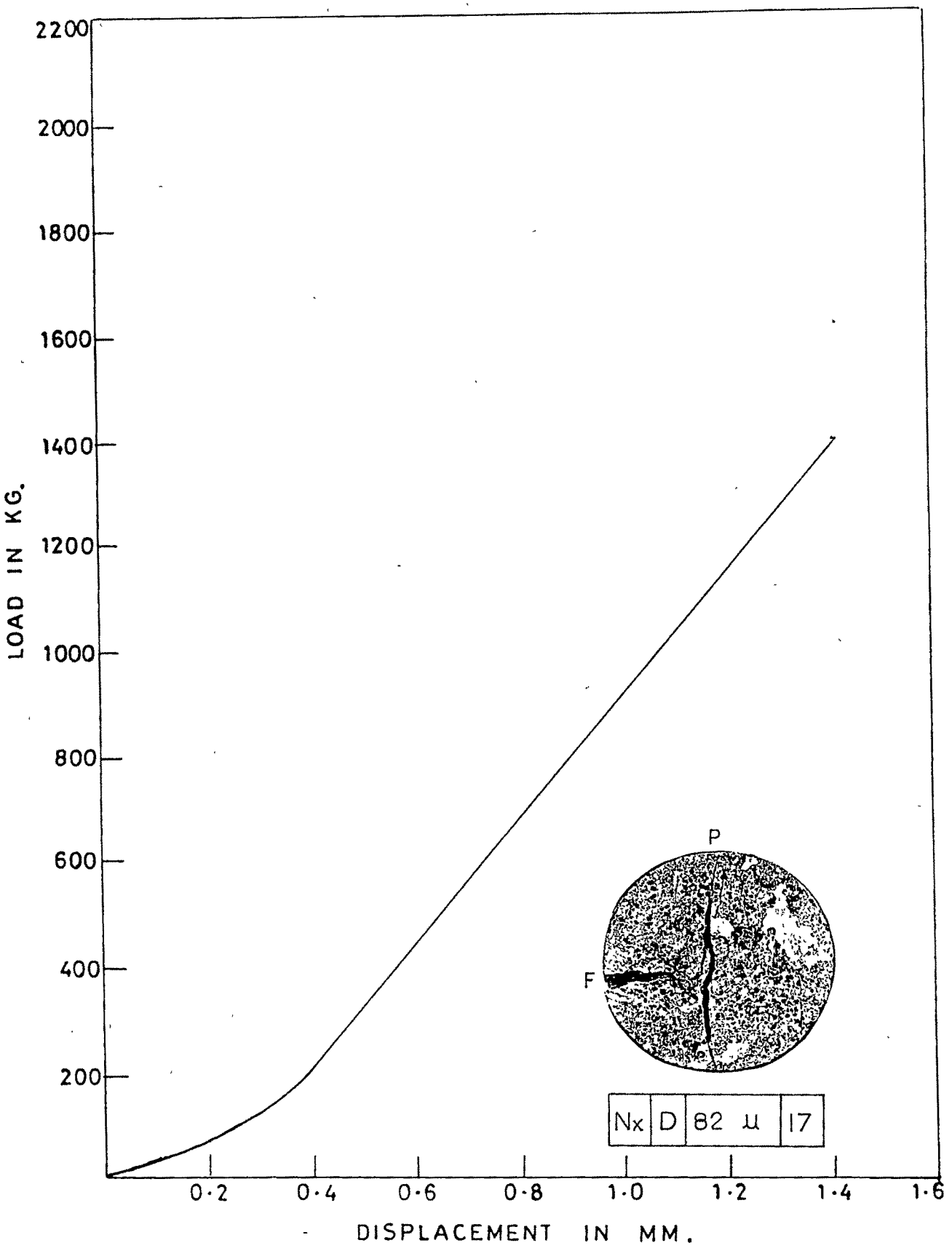

FIG. 6·17 : LOAD DISPLACEMENT CHARACTERISTICS.

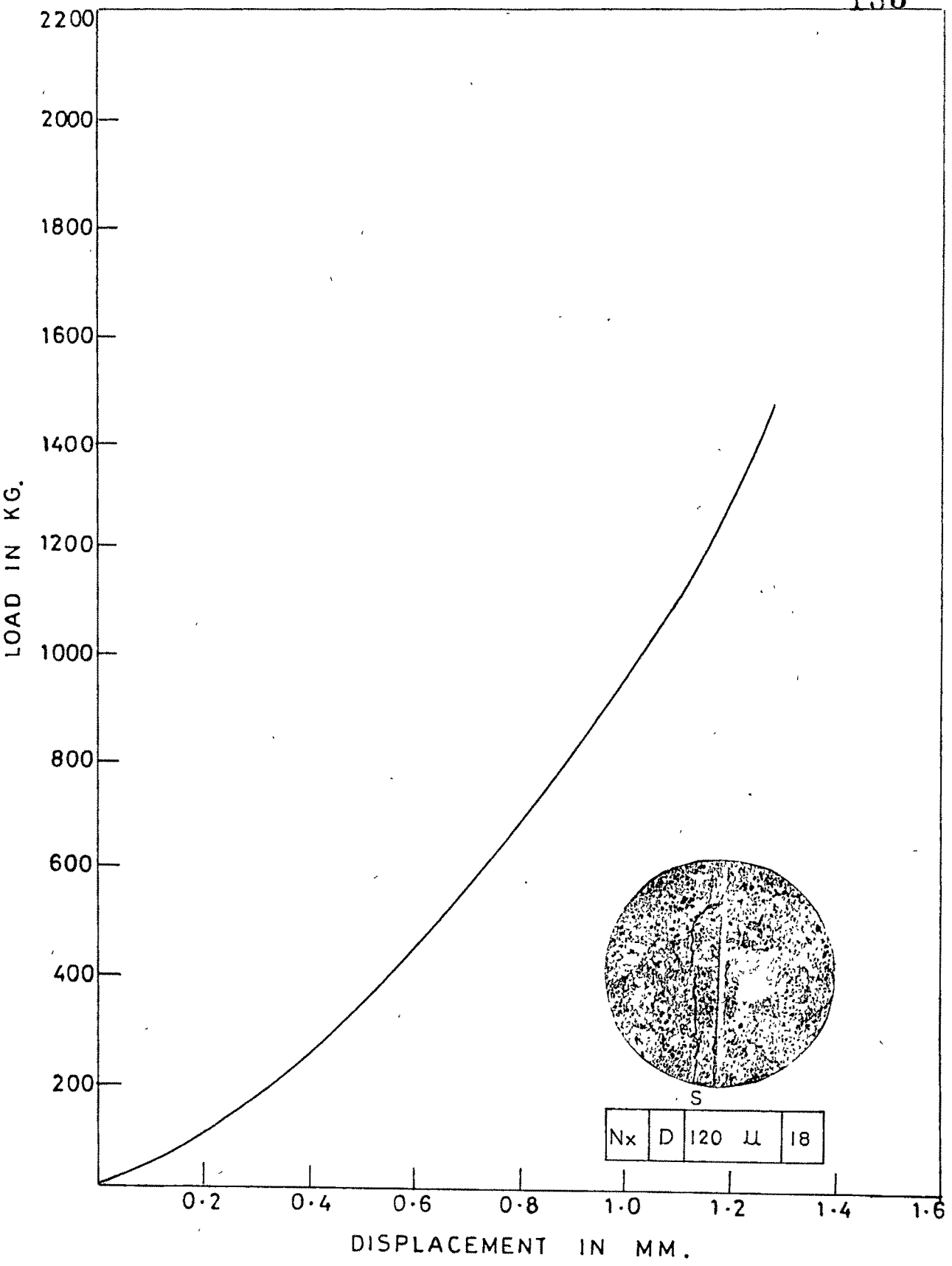

FIG.6·18 : LOAD DISPLACEMENT CHARACTERISTICS.

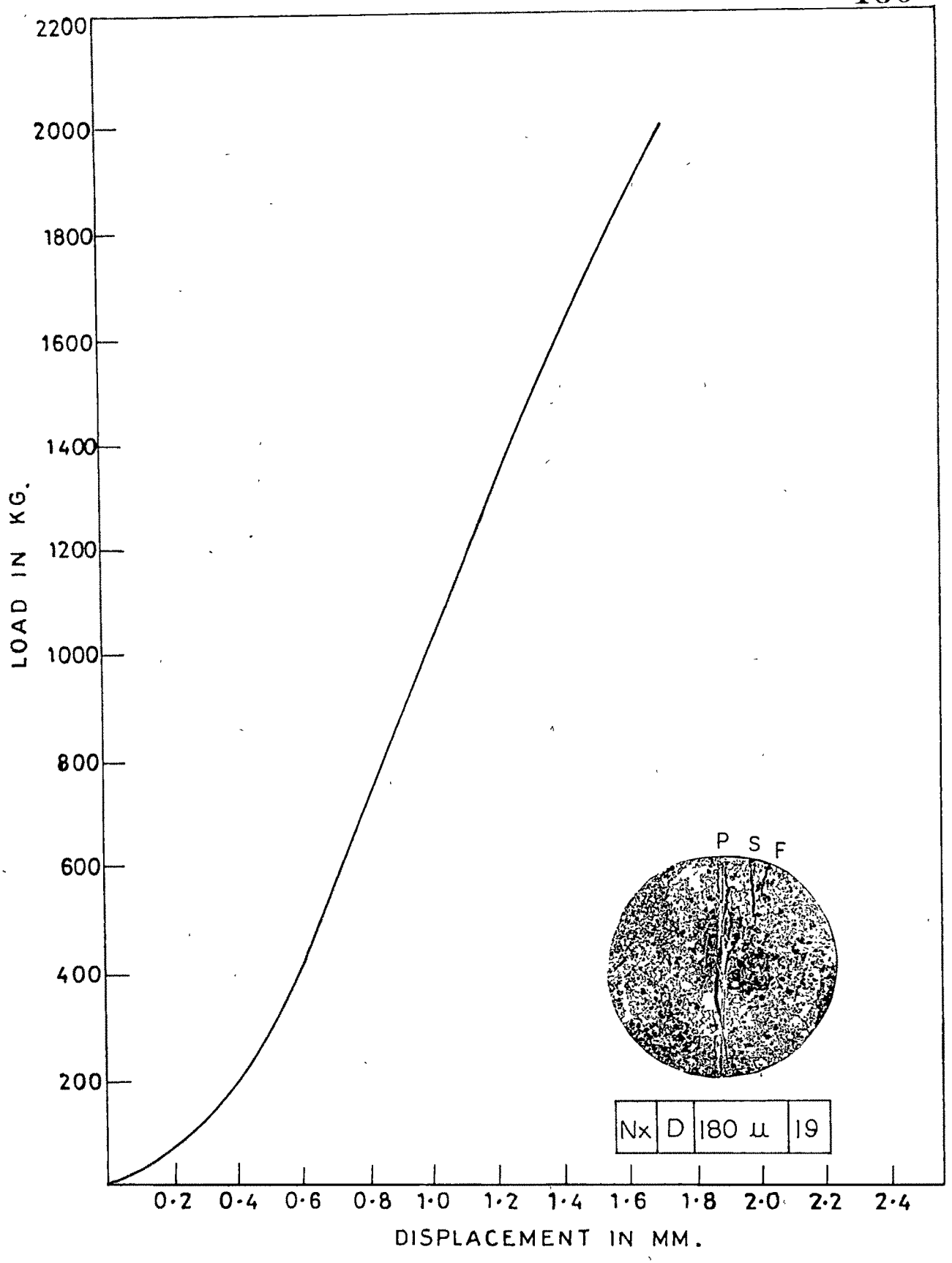

FIG.6·19: LOAD DISPLACEMENT CHARACTERISTICS.

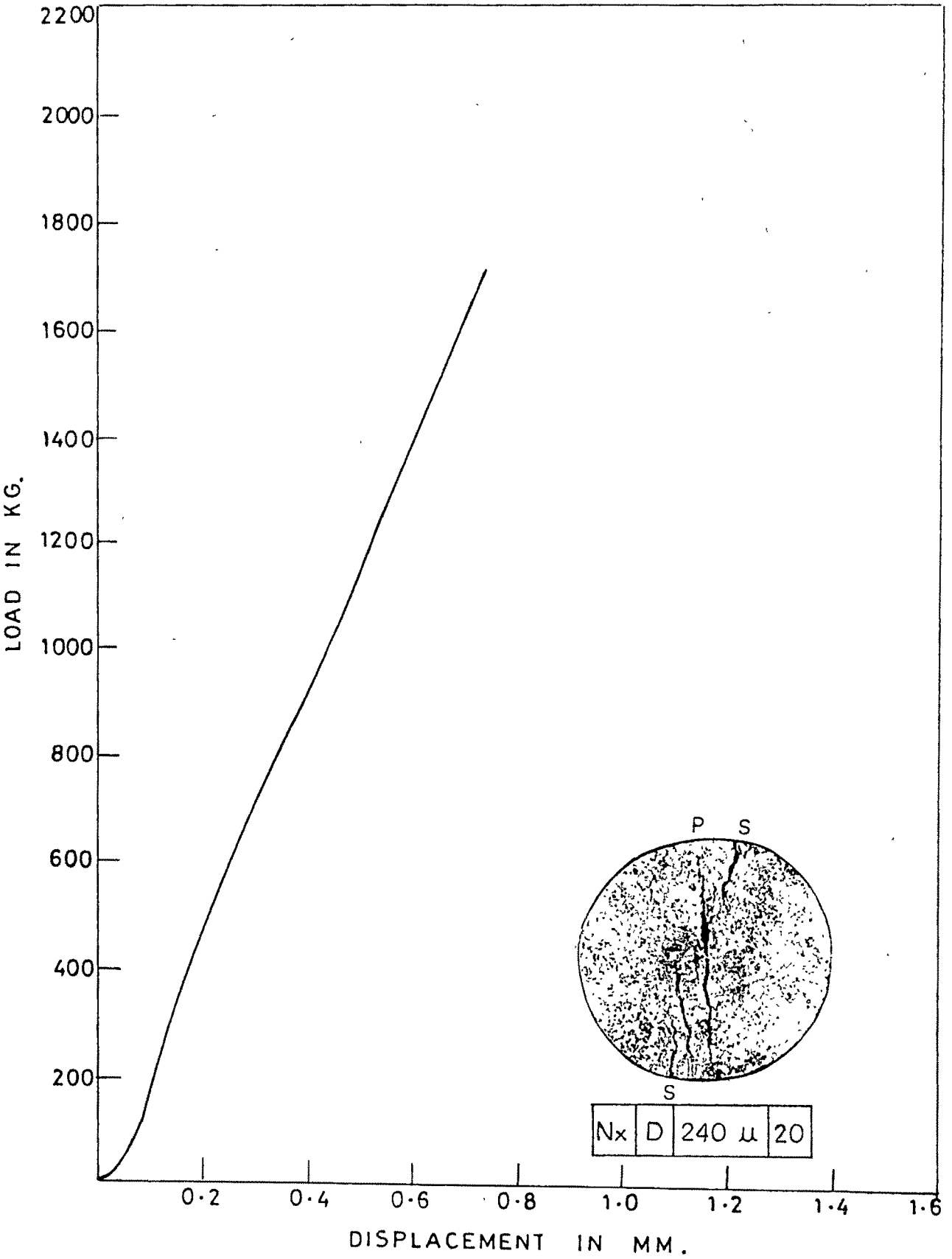

FIG. 6·20 : LOAD DISPLACEMENT CHARACTERISTICS.

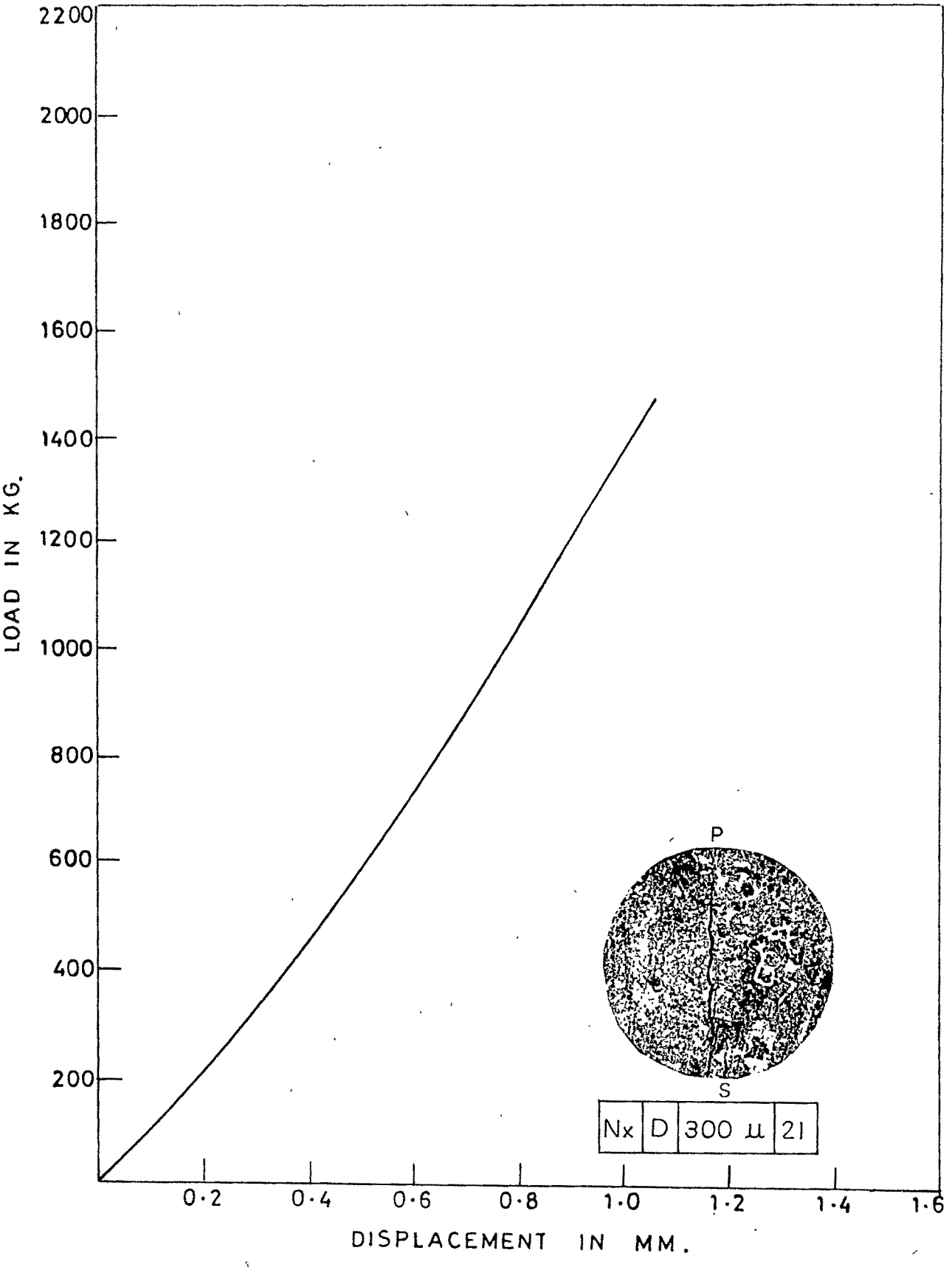

FIG. 6·21 : LOAD DISPLACEMENT CHARACTERISTICS.

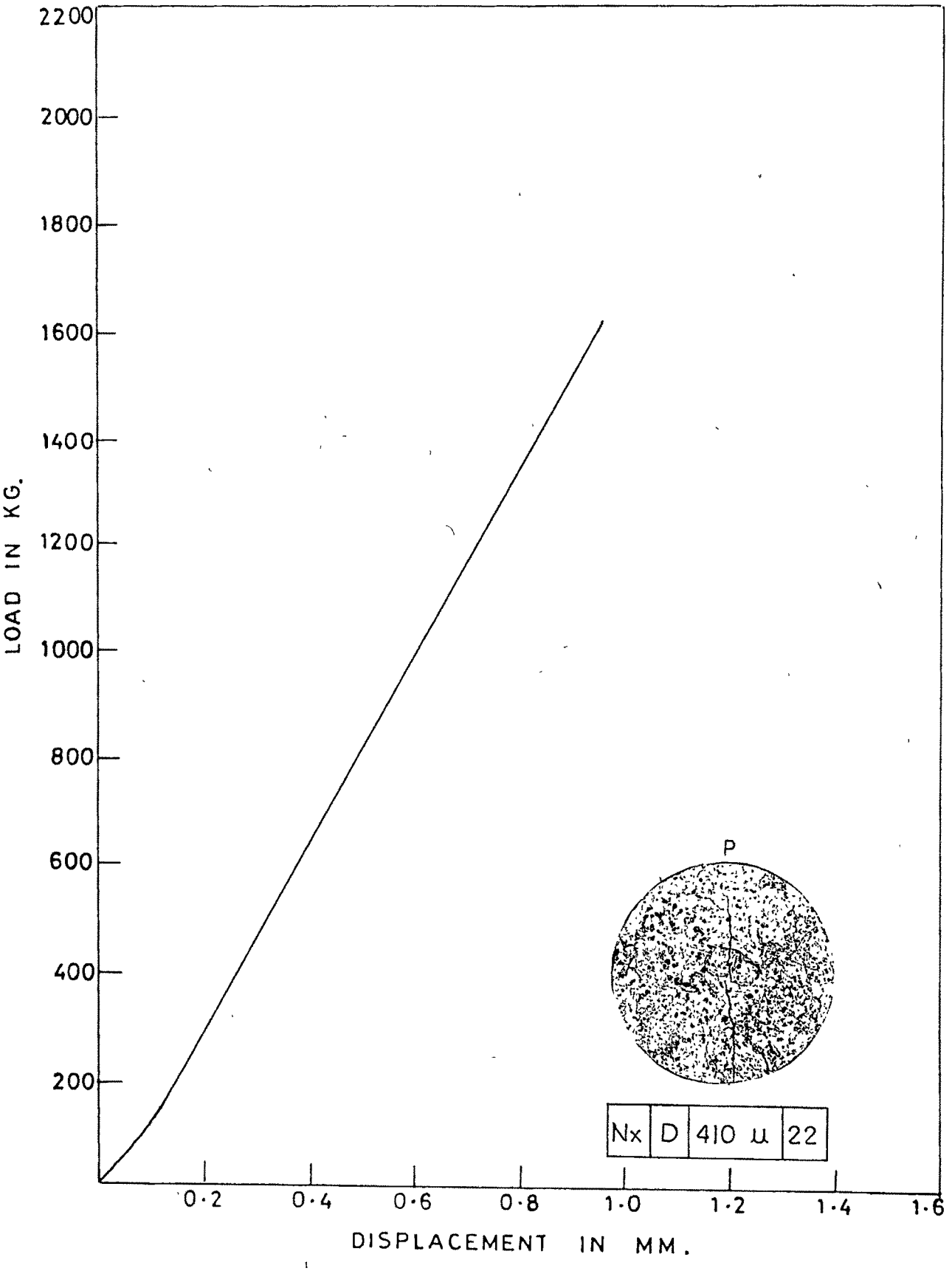

FIG. 6·22 : LOAD DISPLACEMENT CHARACTERISTICS.

Nx/D/610 μ/23 The primary fracture in the form of a crack is little twisted at the centre on the loading line. The flaw joins at this point and runs up to the end of the disc in the first quadrant at the top right of the loading point. The cracking is also seen through the flaw simultaneously. A secondary crack running parallel to the left of the primary crack is also visible. This crack covers the whole disc except a little part on the top of the disc. (Fig 6.23)

Nx/D/900 μ/24 The primary fracture in the form of a crack running along the loading points is observed. Secondary cracking and tertiary cracking is also seen a little distance away right at the top loading. (Fig 6.24)

Nx/D/1220 μ/25 The primary fracture is observed along the loading point in the form of a crack. Secondary and tertiary cracking is also seen just near the loading point and at the right of the bottom loading point. (Fig 6.25)

Nx/D/1520 μ/26 The primary fracture is observed in the form of a diametral crack along the load. Secondary cracking to the right of the top loading point and to the left of the bottom loading point is also visible. The secondary cracking is more pronounced to the left of the bottom loading point. (Fig 6.26)

Nx/D/2560 μ/27 The primary fracture in the form of a diametral crack is more pronounced in the middle third of the diameter. The diametral crack does not seem

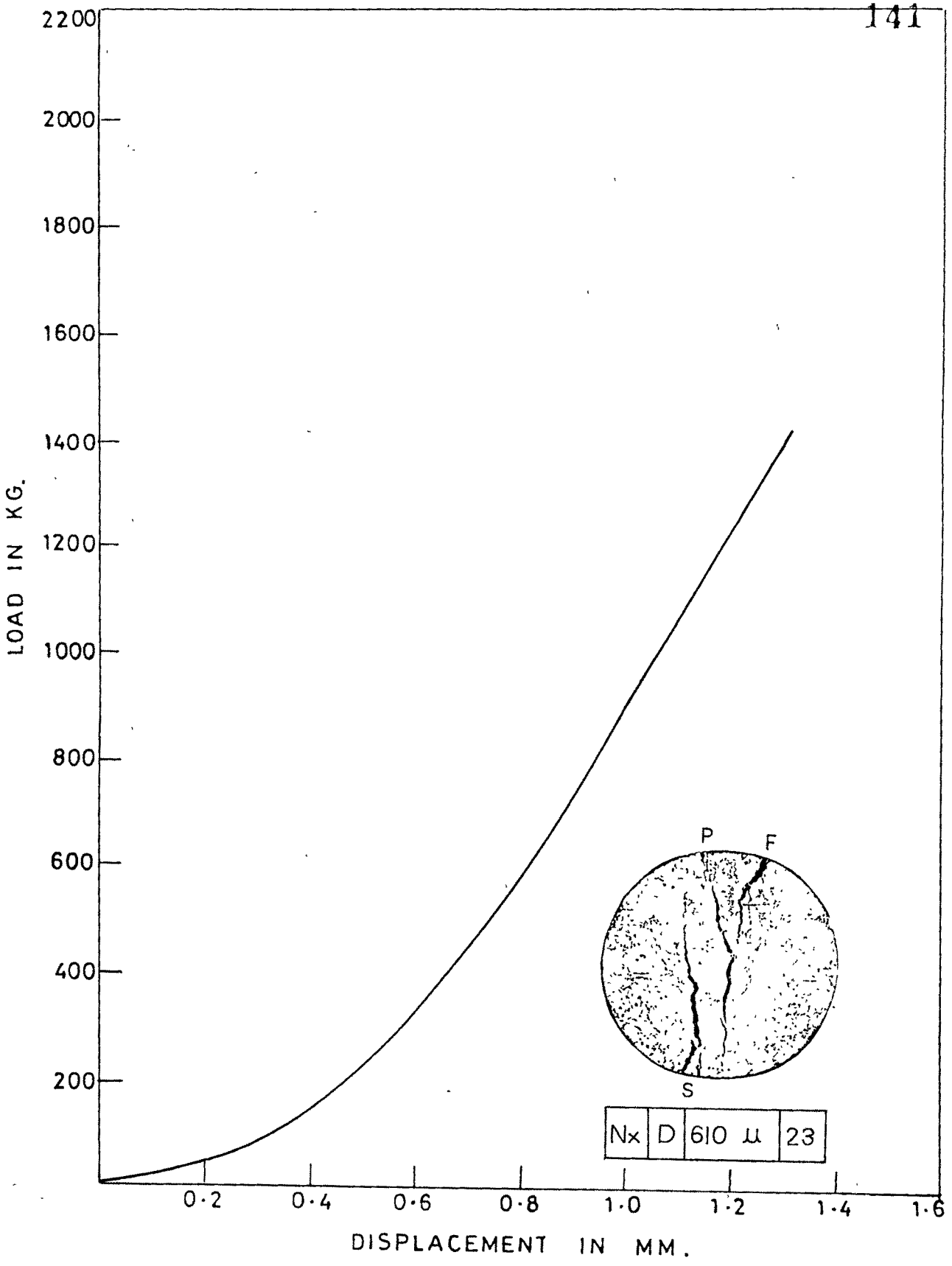

FIG.6·23 : LOAD DISPLACEMENT CHARACTERISTICS.

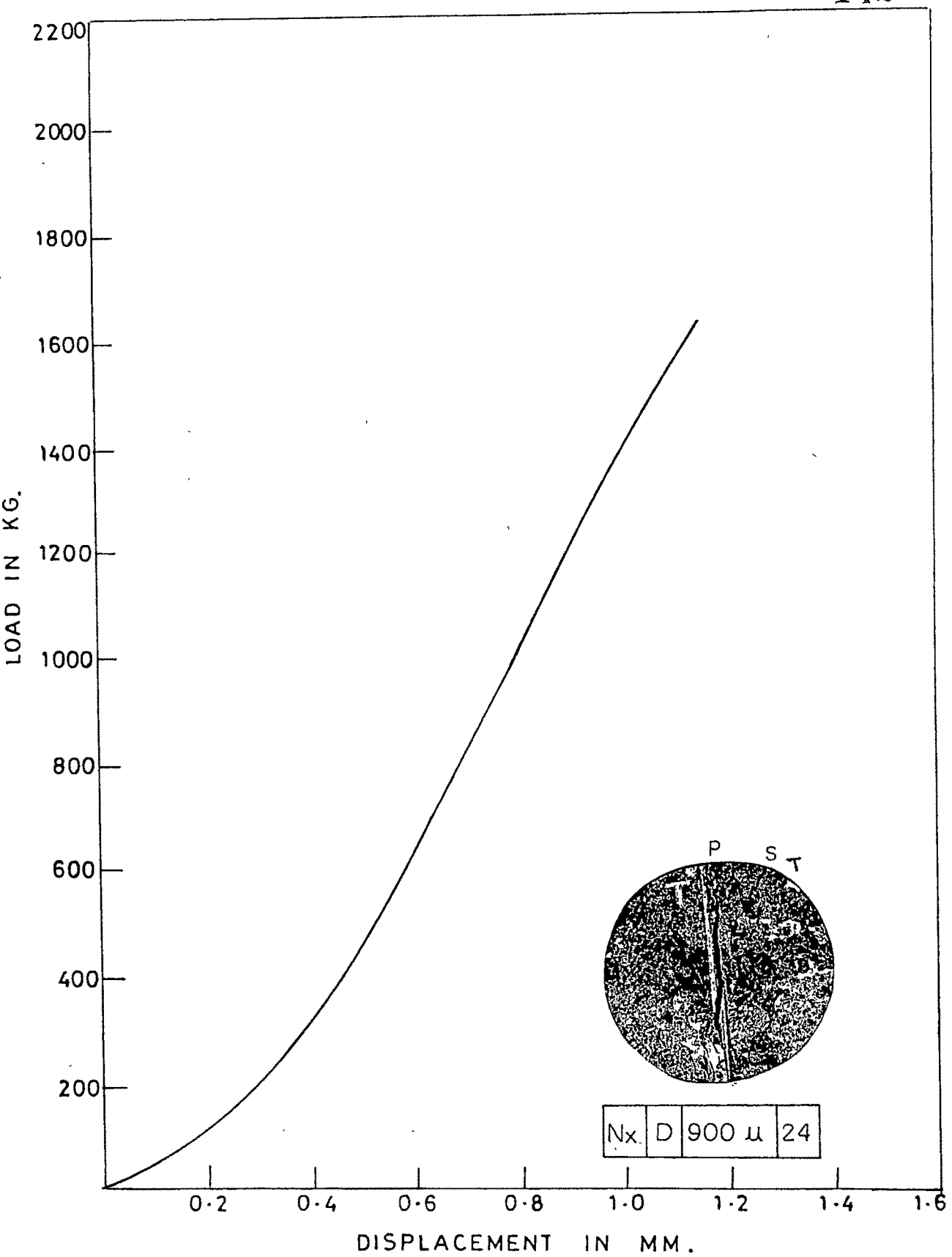

FIG.6·24 : LOAD DISPLACEMENT CHARACTERISTICS.

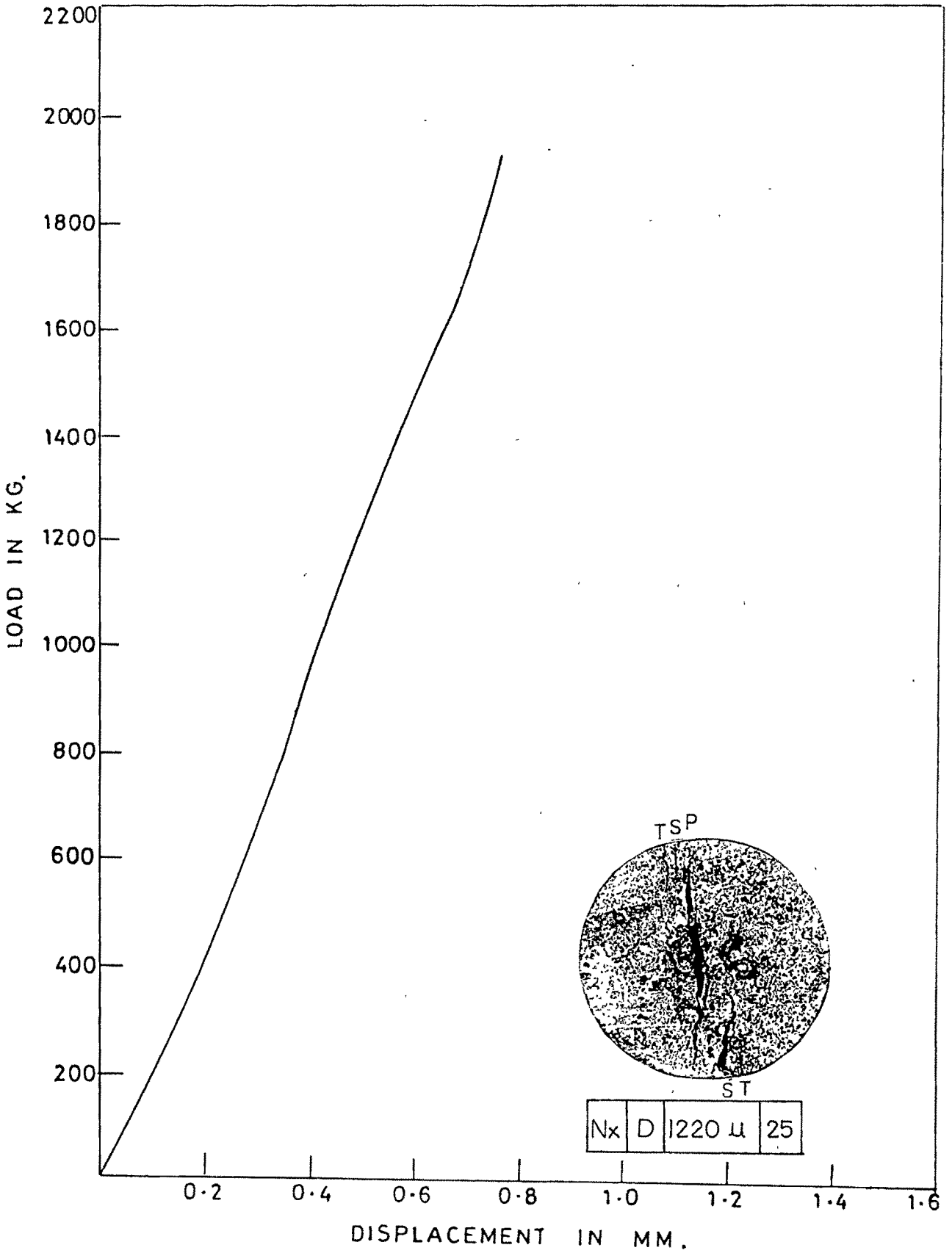

FIG. 6·25 : LOAD DISPLACEMENT CHARACTERISTICS.

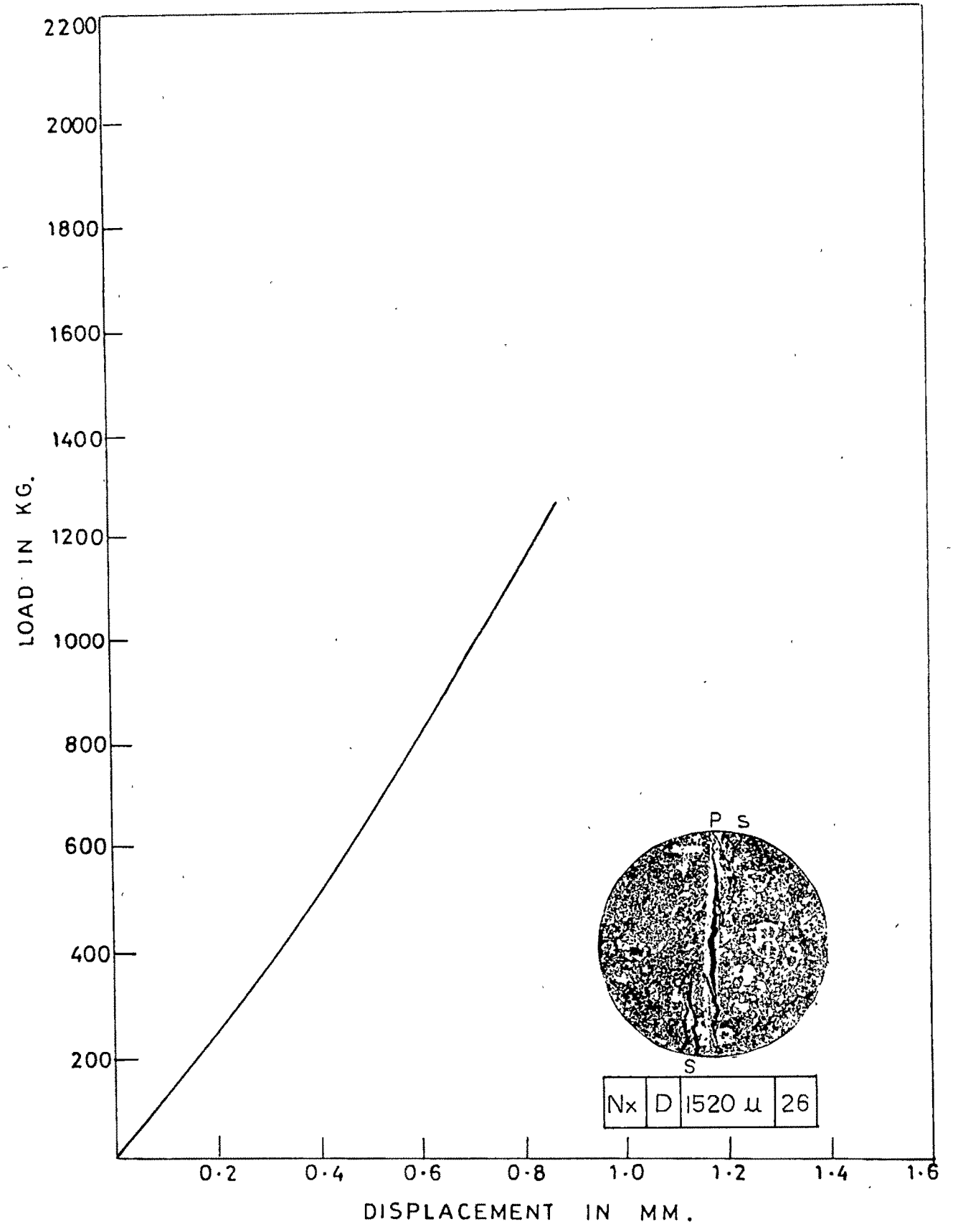

FIG. 6·26 : LOAD DISPLACEMENT CHARACTERISTICS.

to go up to the loading points specially the bottom loading point. A flaw is situated at the left of the top loading point in the fourth quadrant of the disc. A crack simultaneously sparked off from the flaw with the diametral crack. (Fig 6.27)

Nx/D/3050 μ/28 The primary fracture is observed as a diametral crack along the load. The second crack along with the diametral crack is also visible. This crack is due to flaw in the form of a calcite vein. The flaw terminates to the right of the top loading point in the first quadrant. (Fig 6.28)

Nx/D/4520 μ/29 The primary fracture in the form of a crack along the diameter is observed. This diametral crack takes a little triangular crack form at the centre of the disc. Along with the primary cracking it is observed that a crack from the flaw sparks off. The flaw is located in the second quadrant right of the bottom loading point in the form of a calcite vein. The secondary and tertiary cracking is also seen at the left of the bottom loading point. (Fig 6.29)

Nx/D/6100 μ/30 The failure is instantaneous. The diametral crack as a primary fracture and a parallel secondary crack running just right to the top loading point up to the centre have been observed. At the left of the bottom loading point secondary cracking is also seen. (Fig 6.30)

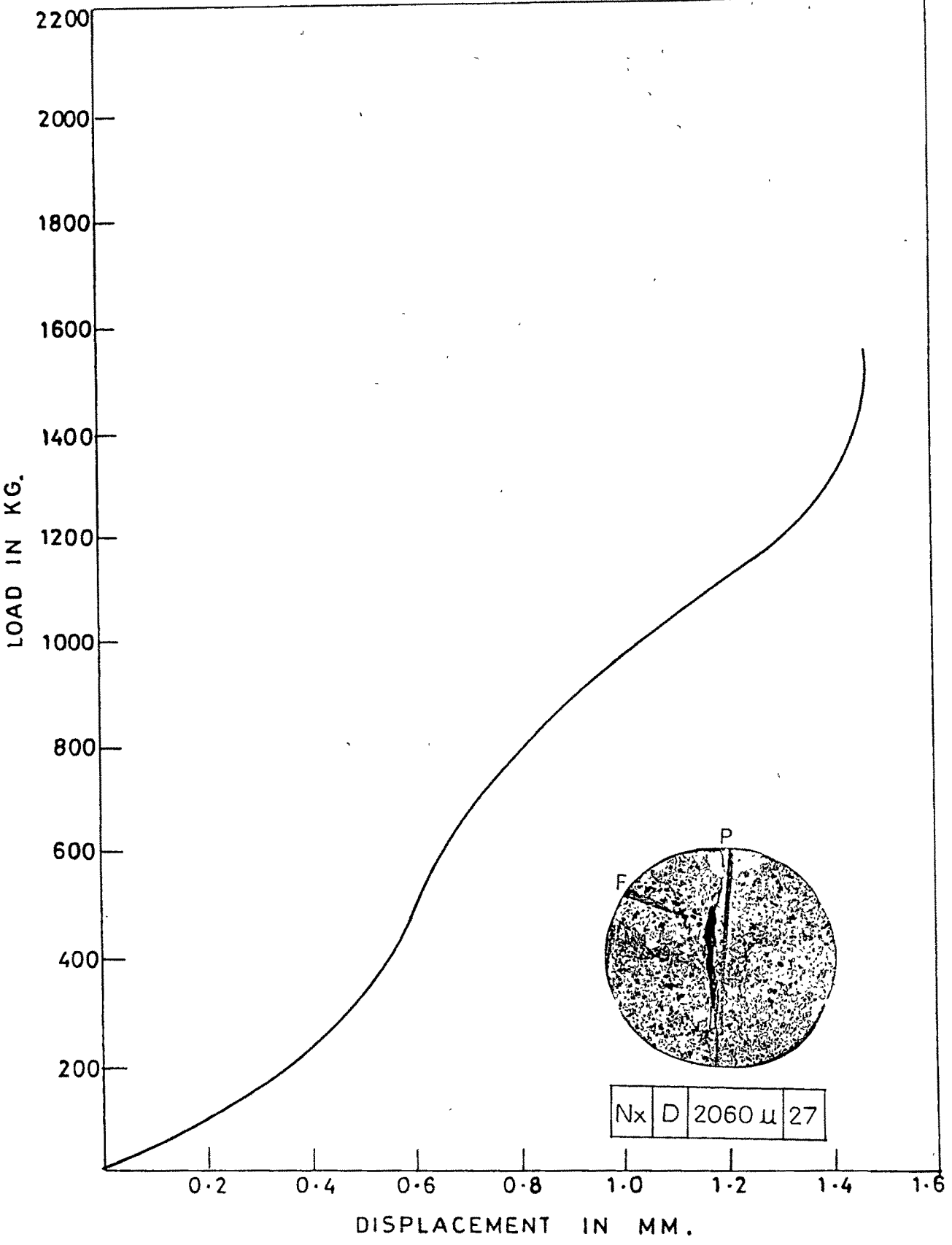

FIG.6·27 : LOAD DISPLACEMENT CHARACTERISTICS.

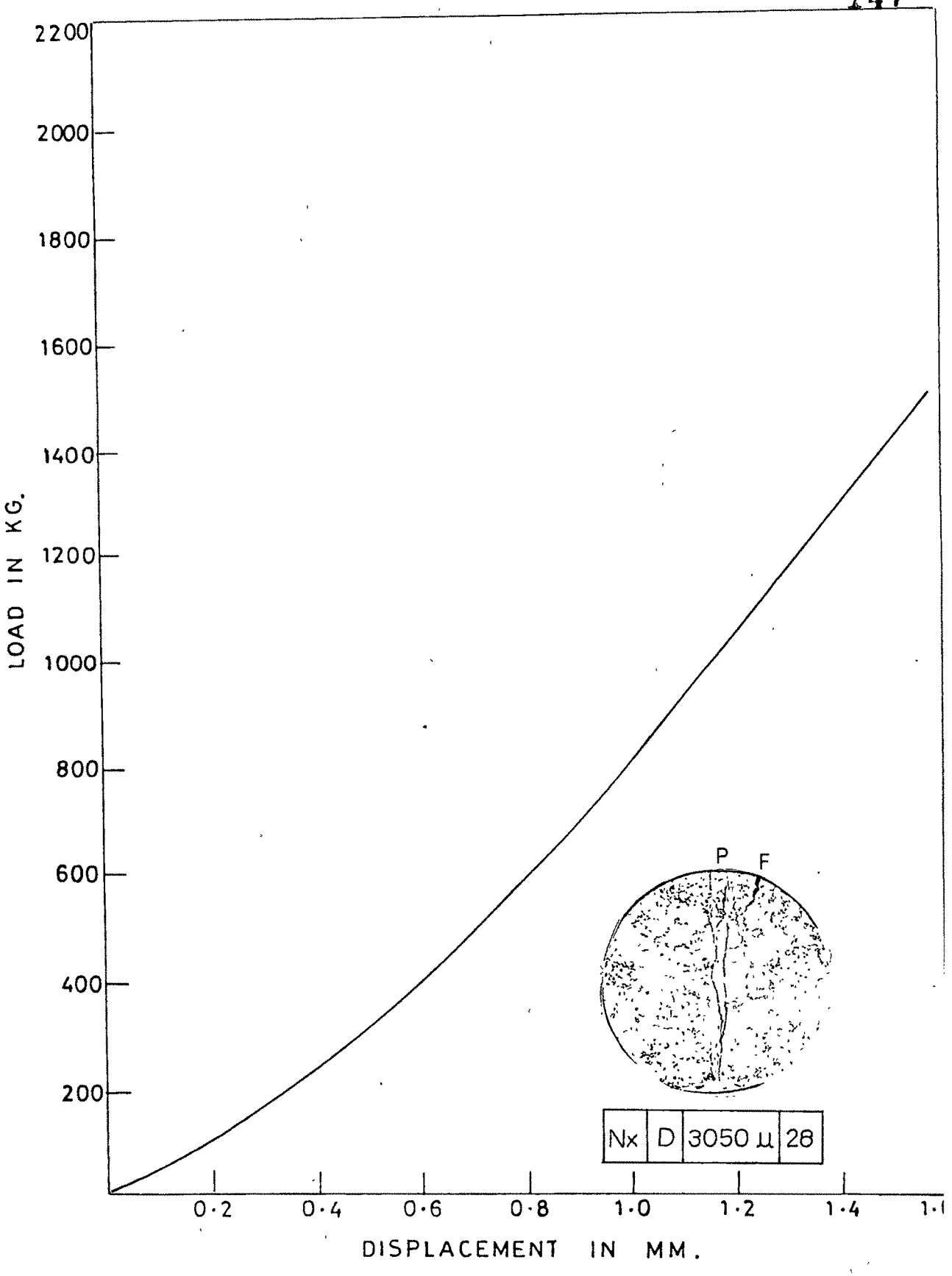

FIG. 6·28 : LOAD DISPLACEMENT CHARACTERISTICS.

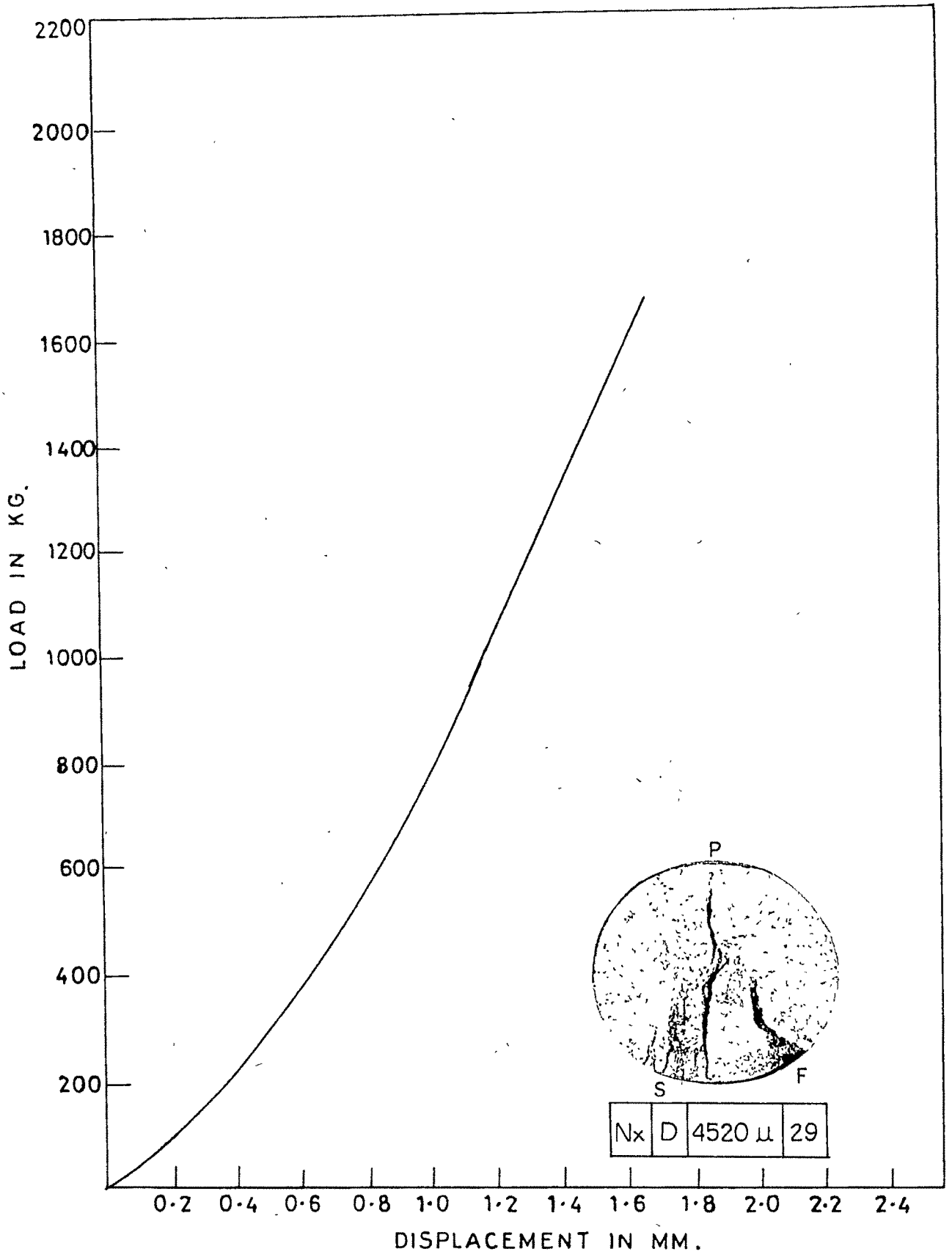

FIG.6·29: LOAD DISPLACEMENT CHARACTERISTICS.

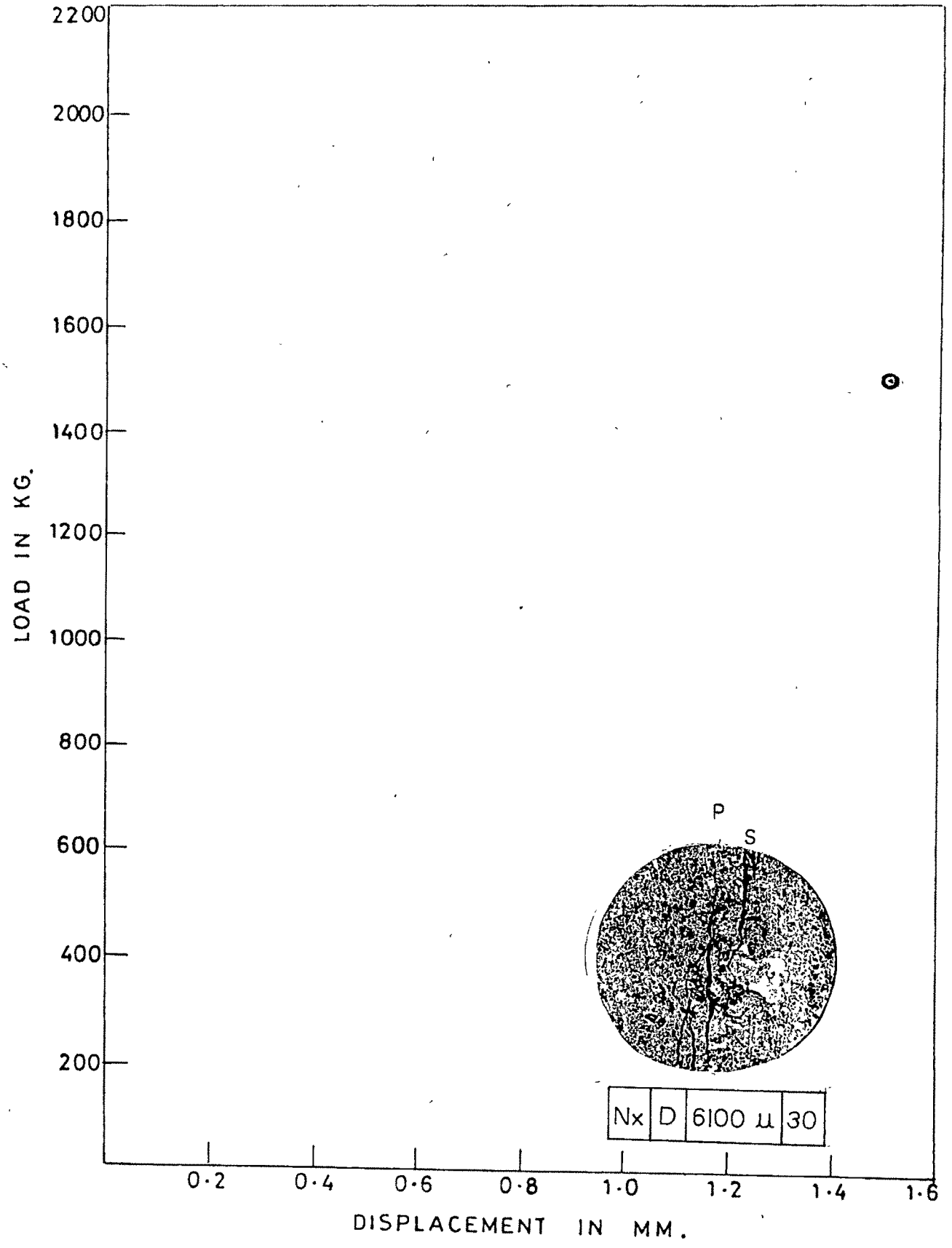

FIG. 6·30 : LOAD DISPLACEMENT CHARACTERISTICS.

6.2.3.2 Observations on failure of rings:

Nx/R/3Ø/1 Failure was instantaneous with a cracking sound with simultaneous development of a primary crack which was seen to initiate from the centre of the sample along the loaded diameter. The primary crack was wider near the hole and got reduced in width towards the top and bottom loading platens. On one face, the primary crack was seen to terminate at some distance away from the periphery of the samples. The secondary cracks developed along the end points of platen contact but their propagation could not be observed due to a sudden failure. Some higher order cracking including hair cracking was also observed being more prominent in the lower half of the sample. (Fig.6.31)

Nx/R/3Ø/2 Failure was instantaneous with a cracking sound with simultaneous development of a primary crack which was seen to initiated from the centre of the sample. The primary crack on one face was almost along the loaded diameter on one face and elightly off-centre on the other face. On both the faces of the sample, the secondary cracks are seen on one side of the loaded diameter only. Secondary cracks are wider at the loading platens becoming hair like towards the centre of the sample terminating in the central portion. Some hair cracking was seen near the loading platens.(Fig 6.32)

Nx/R/3Ø/3 Failure was more sudden compared to the earlier two tests hence neither the crack initiation nor the crack propagation could be seen. The primary crack

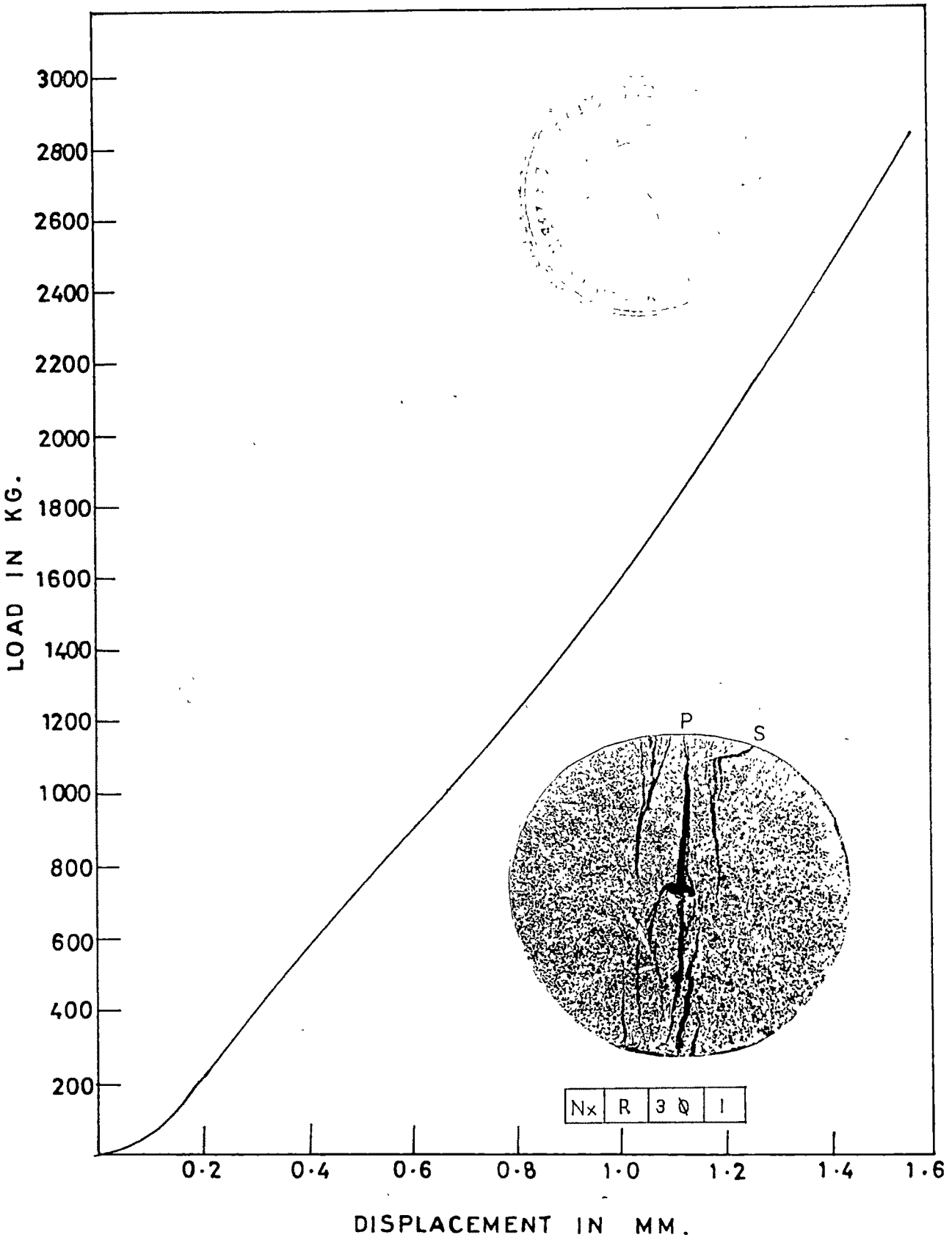

FIG. 6·31 : LOAD DISPLACEMENT CHARACTERISTICS.

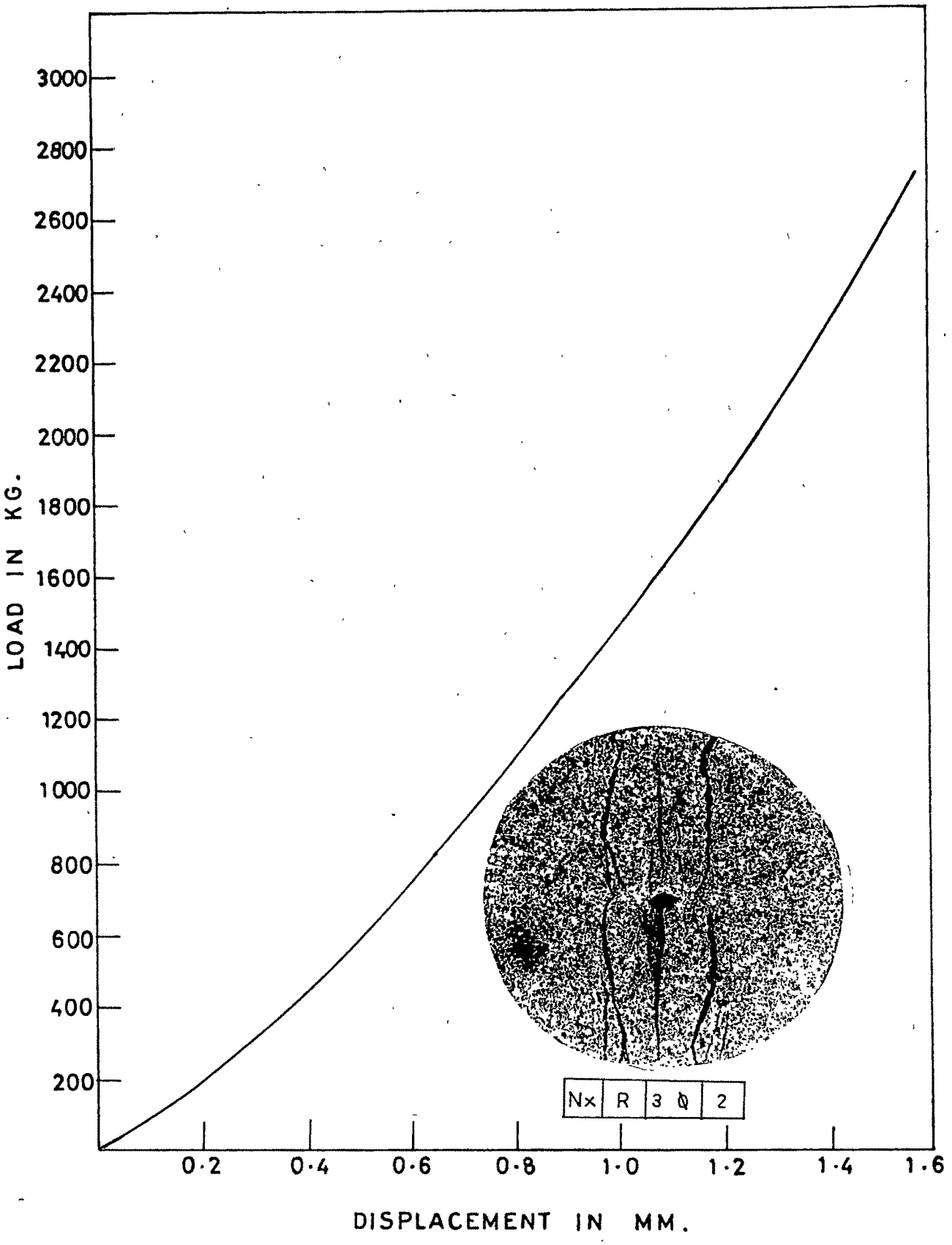

FIG. 6·32 : LOAD DISPLACEMENT CHARACTERISTICS.

on both the faces was along the loaded diameter being wider near the hole and reducing in width towards the upper platens. The crack on one face was of uniform width starting from the hole but terminating at some distance away from the lower loading platen. The secondary cracks on both the faces, on one side of the hole were comparable to the earlier cases of the same hole diameter. Hair cracking was more prominent near both the top and bottom loading platens. (Fig 6.33)

Nx/R/3Ø/4 Some intrusions were present on the sample being more prominent on one face as seen in the photograph. Sample failed without giving any sort of sound indication prior to failure. Primary failure did not take place along the loaded diameter. Primary crack initiation could not be observed. On one face there is a prominent hair like cracking in the upper half of the sample which just touches the periphery of the hole. The crack in the lower half of the sample is seen to terminate at a considerable distance away from the sample periphery. A nominal amount of secondary cracking is seen in the upper half initiating from the sample periphery. Fracture load and test duration are remarkably less as compared to the all earlier cases with 3mm diameter central hole.(Fig 6.34)

Nx/R/4Ø/5 Primary crack at the very instant of failure was seen to initiate exactly from the centre of the sample along the loaded diameter. Secondary cracks in the form of a curly bracket were observed on both sides of

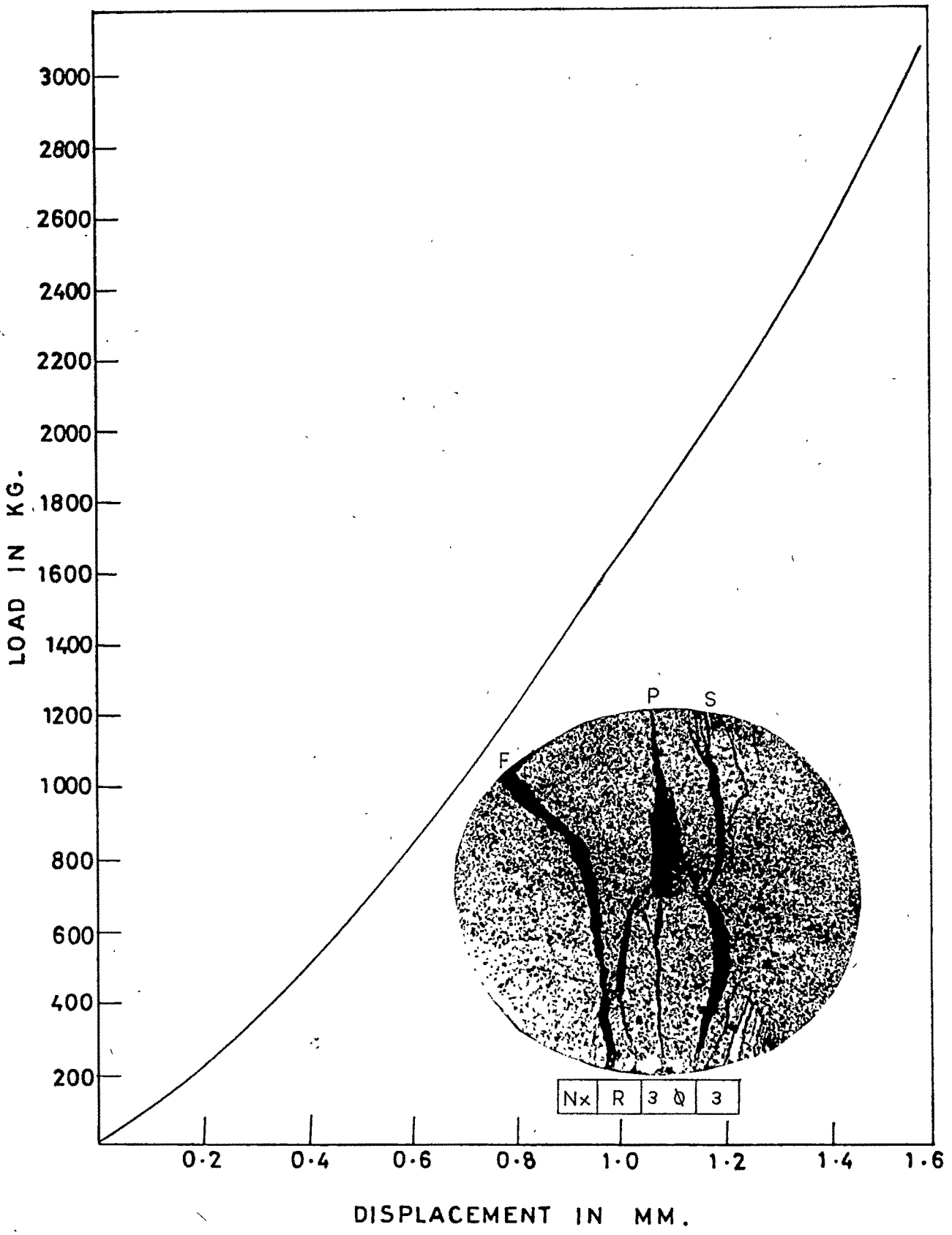

FIG.633 : LOAD DISPLACEMENT CHARACTERISTICS.

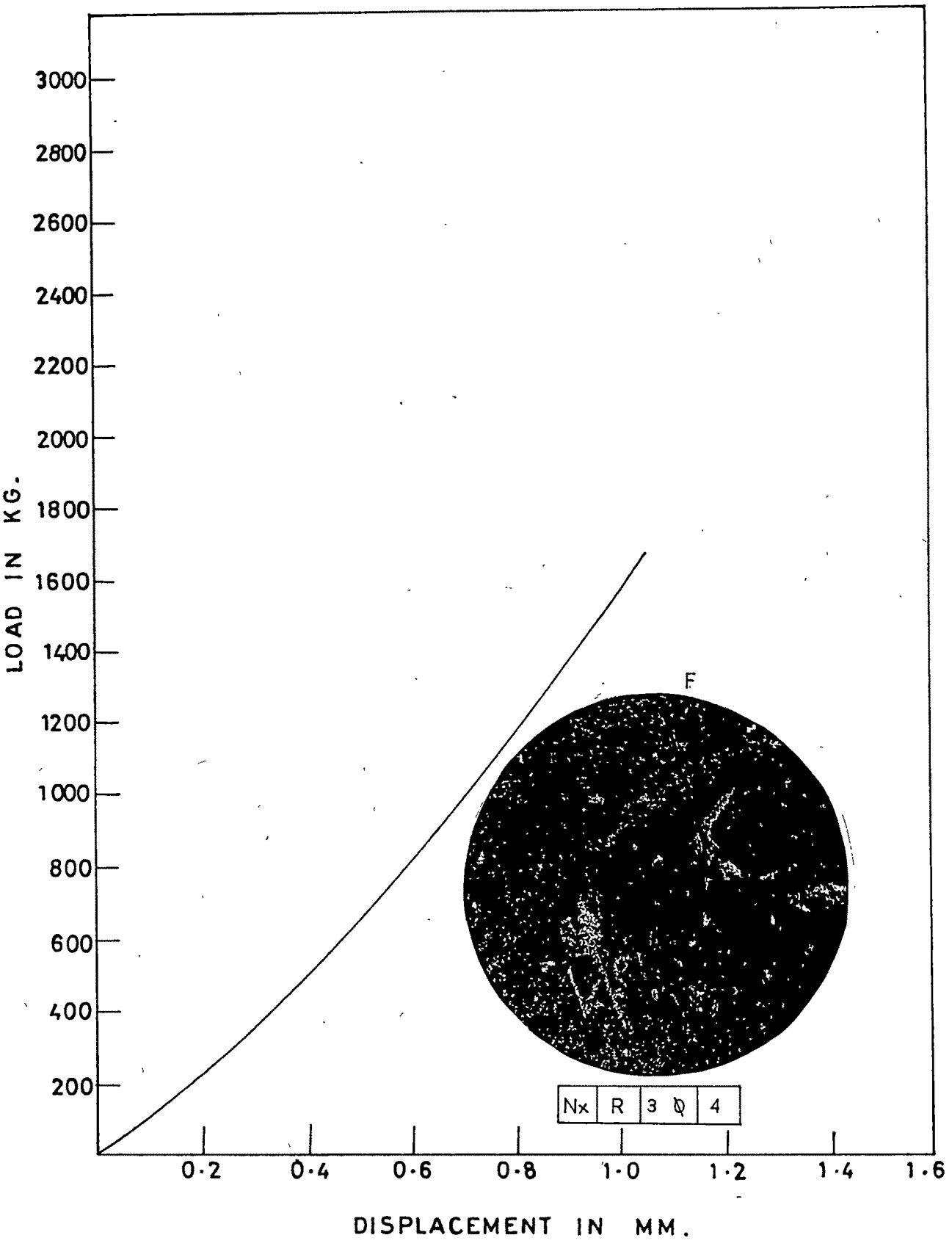

FIG. 6·34 : LOAD DISPLACEMENT CHARACTERISTICS.

the central hole being more prominent in the lower half of the sample. Some higher order cracking were also observed in the lower of the sample. Fracture load was less in comparison with the samples with 3mm diameter central hole though the test duration was comparable. (Fig 6.35)

Nx/R/4Ø/6 Failure was instantaneous immediately followed by a shatters of the sample and crack initiation could not be seen. Photograph reveals that the primary crack developed from the exact centre of the sample along the loaded diameter with a simultaneous cracking along a vein which was barely visible prior to testing.(Fig 6.36)

Nx/R/4Ø/7 Hair like veins were visible on the sample prior to testing. Failure was instantaneous. Primary crack was seen to initiate from the centre of the sample along the loaded diameter on one face but slightly off-centre on the other face. As it can be seen from the photograph, the primary crack becomes hair like towards the upper and lower loading platens implying thereby that the crack initiated from the centre of the sample. The secondary cracks were seen to develop immediately after the machine was switched off after primary failure took place. Secondary cracking on one side of the loaded diameter is more prominent in the lower half of the sample whereas it does not extend in the lower half on other side of the loaded diameter. One prominent crack initiated from the lower half periphery of the samples as seen in the photograph. (Fig 6.37)

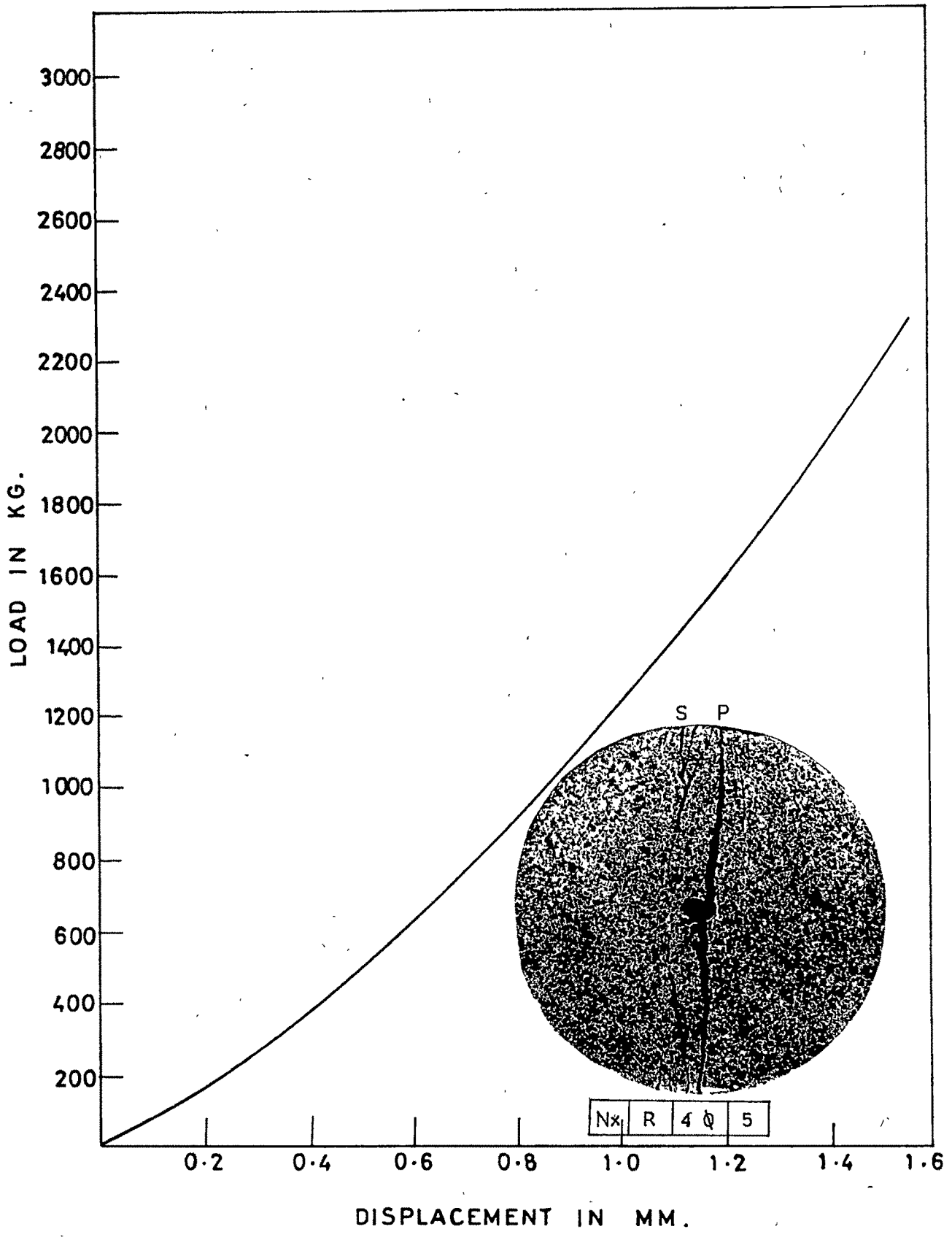

FIG. 6·35 : LOAD DISPLACEMENT CHARACTERISTICS.

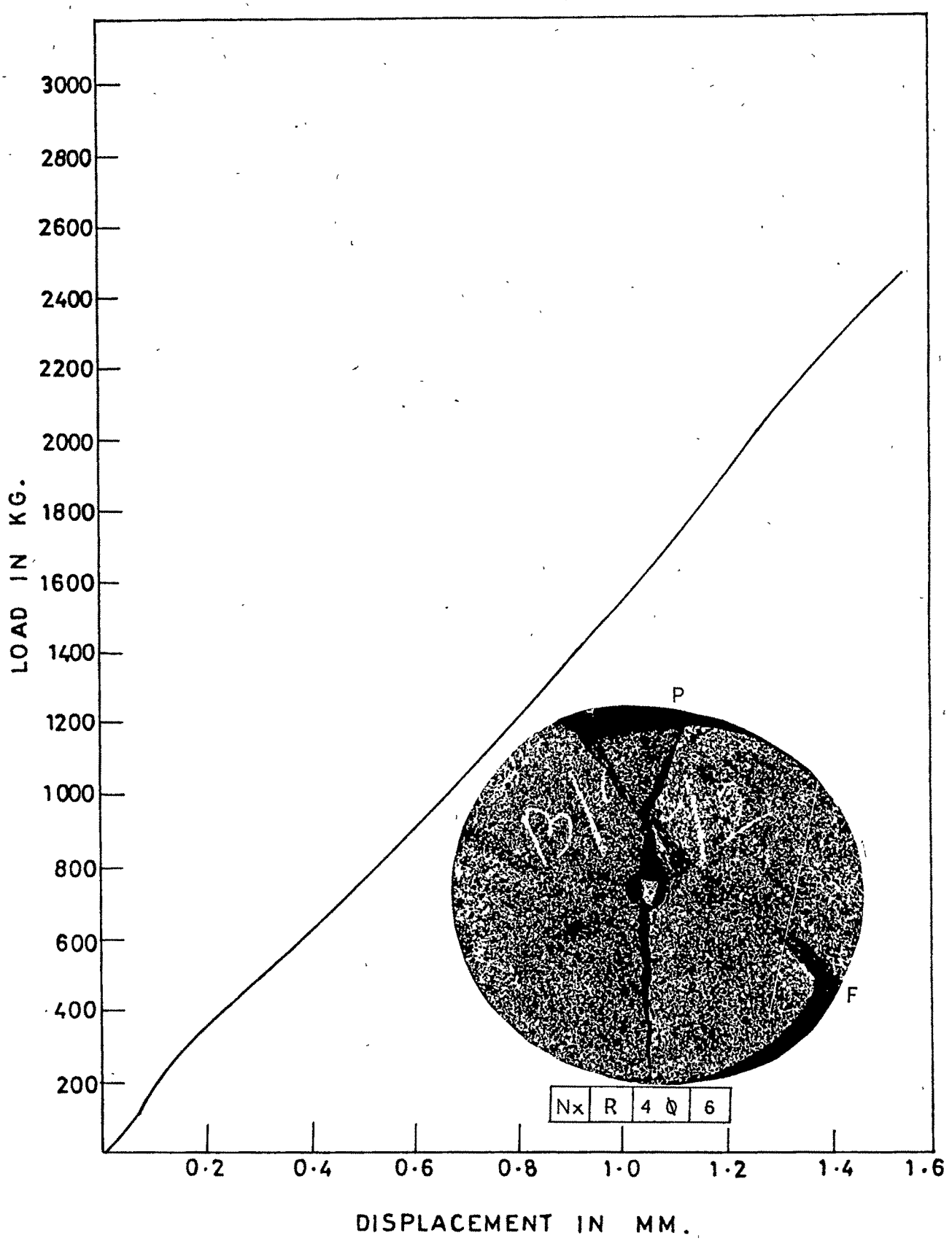

FIG.6·36 : LOAD DISPLACEMENT CHARACTERISTICS.

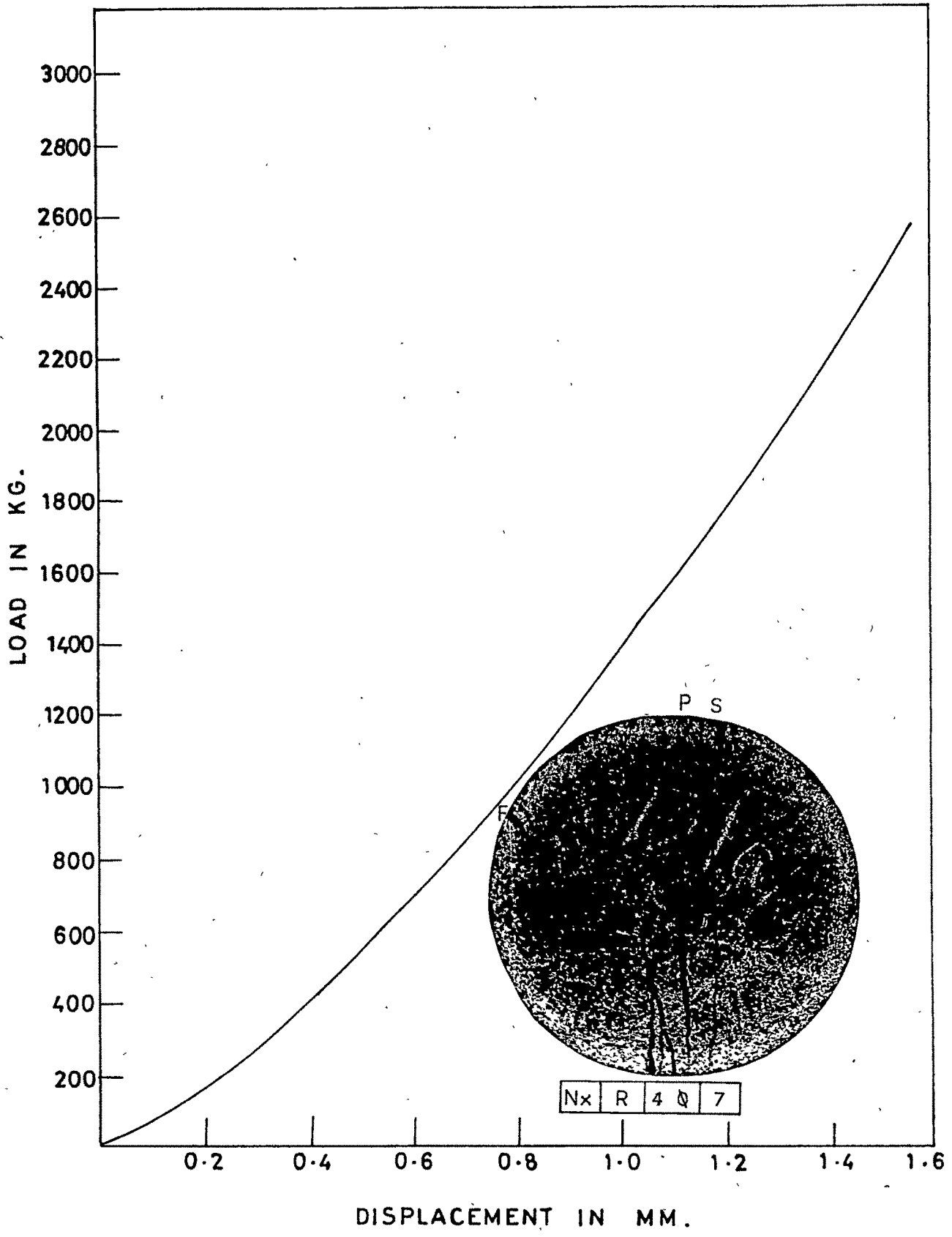

FIG. 6·37 : LOAD DISPLACEMENT CHARACTERISTICS.

Nx/R/4Ø/8 Failure was instantaneous with primary crack seen to initiate from the centre of the sample along the loaded diameter on one face and slightly off-centre on the other face. As it can be seen from the photographs, primary crack on one face terminated at some distance away from the periphery of the sample whereas it become hair like near the periphery on the other face. Secondary cracking in the form of a'curly bracket' was seen on one side of the loaded diameter only on both the faces but it took place in the lower half of the sample only on other side of the loaded diameter on both the faces. Secondary cracking, in general, was more prominent in the lower half of the sample. It is interesting to note here that the cracks opened out after the machine was switched off after failure took place. (Fig 6.38)

Nx/R/4Ø/9 Failure was instantaneous. No veins were apparently visible prior to testing. Failure on both the faces took place exactly along the loaded diameter. The crack initiation however, could not be seen due to sudden mode of failure. But as it is clear from the photograph, primary crack was wider near the hole periphery becoming gradually hair like and terminating at some nominal distance away from the periphery of the sample implying thereby that the crack initiated from the centre. Failure along the loaded diameter took place with a simultaneous failure by sliding along a vein. Secondary cracking was observed in the upper half only.(Fig 6.39)

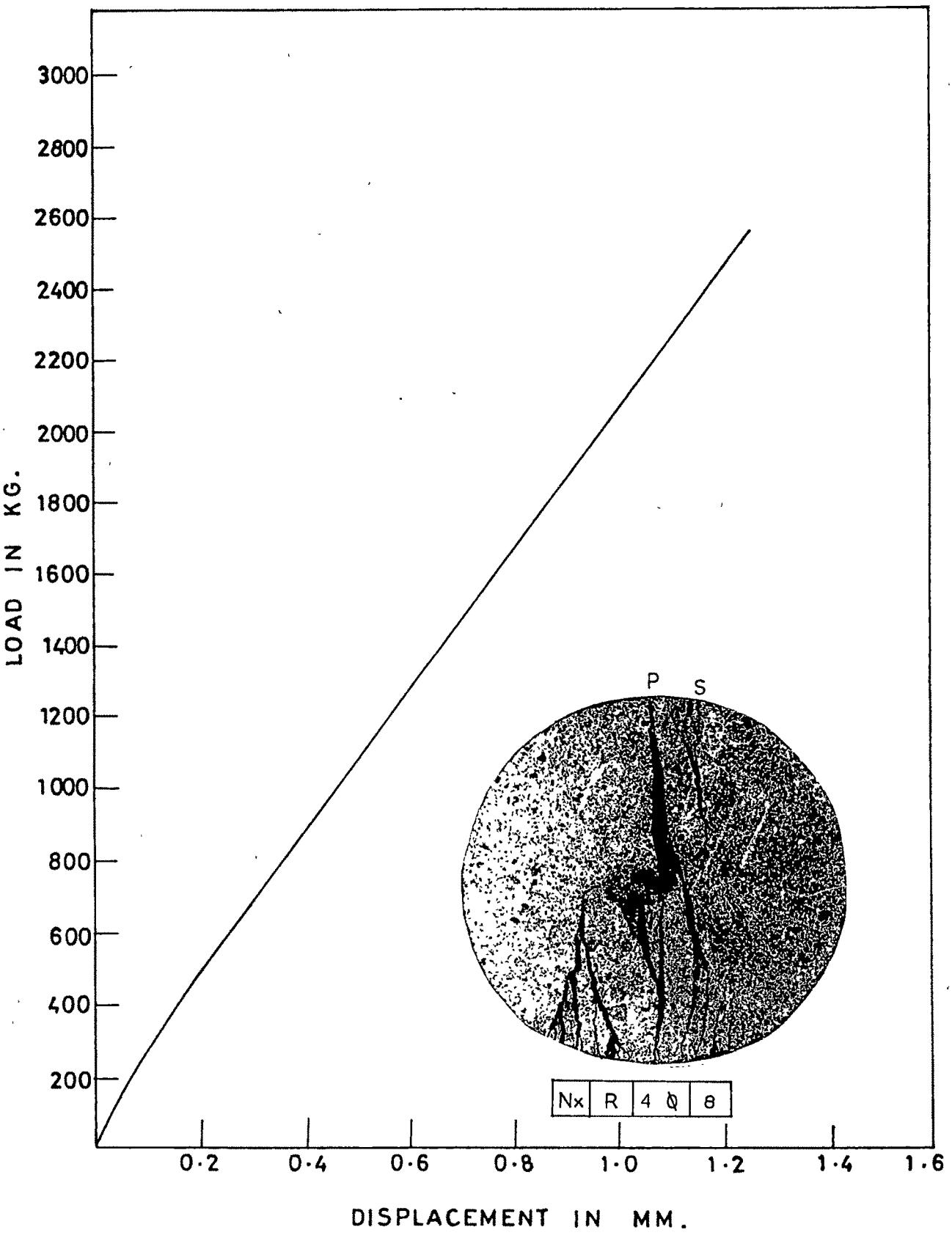

FIG. 6·38: LOAD DISPLACEMENT CHARACTERISTICS.

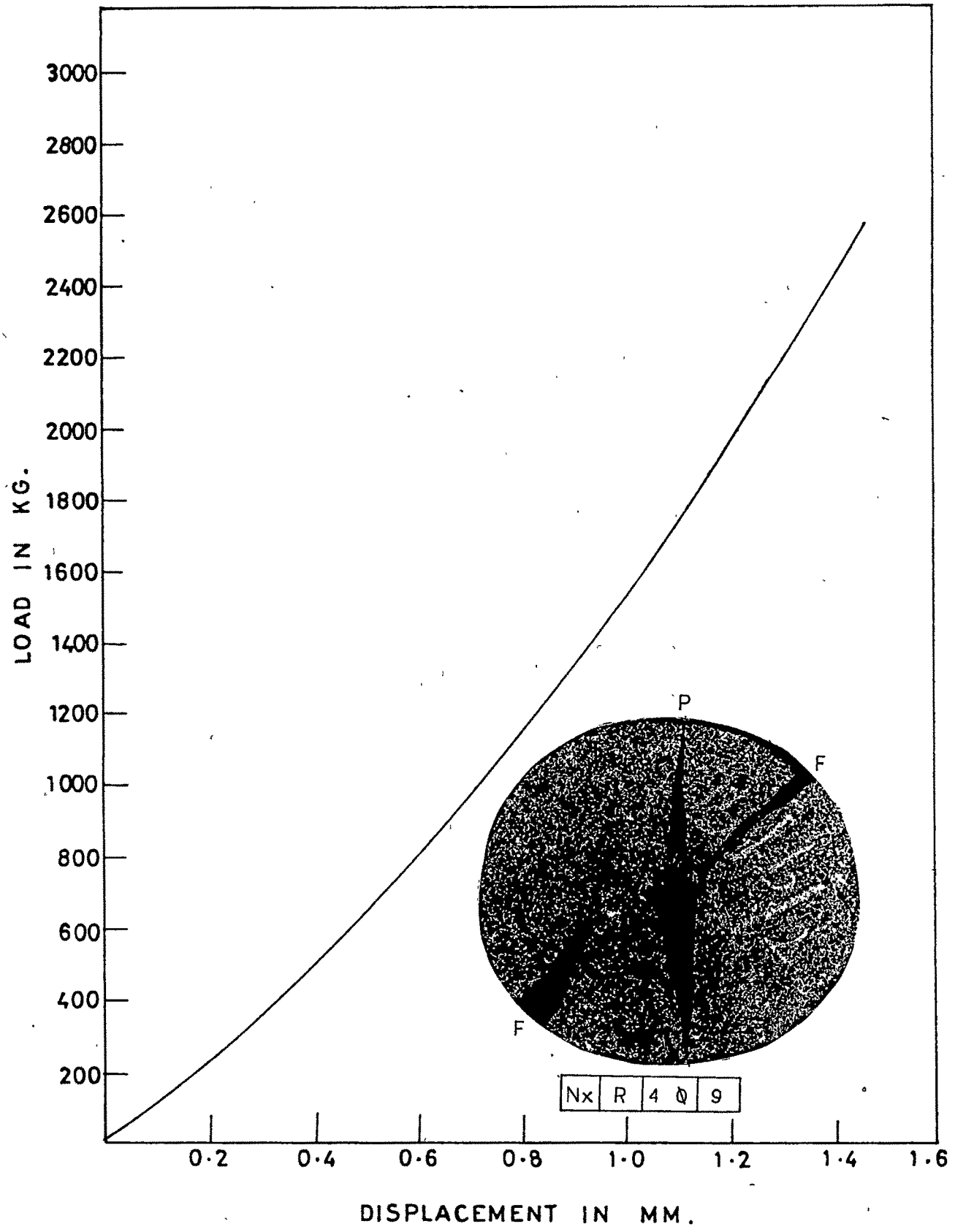

FIG. 6·39 : LOAD DISPLACEMENT CHARACTERISTICS.

Nx/R/5Ø/10 As it can be seen from the photograph the vein present was kept along the loaded axis of the sample prior to testing primary crack initiation could not be observed as the failure was very instantaneous accompanied by a shattering effect. Moreover the primary fracture and the fracture along the vein took place simultaneously. Secondary and higher order cracking was more prominent on the side of the loaded diameter opposite to the side with the vein. (Fig 6.40)

Nx/R/5Ø/11 As it can be seen from the photograph, vein was kept along the axis perpendicular to the loaded diameter. Failure was instantaneous. The primary crack was along the loaded diameter in the form of an 'inverted vee', that is, wider at the centre becoming hair like near the periphery of the sample implying thereby that the crack initiated from the centre. Failure along the vein occured simultaneously with the primary failure. Secondary cracking, as seen in the photograph, was almost absent. (Fig 6.41)

Nx/R/5Ø/12 As it can be seen from the photograph, vein was kept along the axis perpendicular to the loaded diameter. Failure was instantaneous with a simultaneous fracturing along the loaded diameter as well as along the vein. Primary crack was seen to initiate exactly from the centre of the sample and exactly along the loaded diameter. It is seen to terminate at some distance away from both upper and lower loading platens

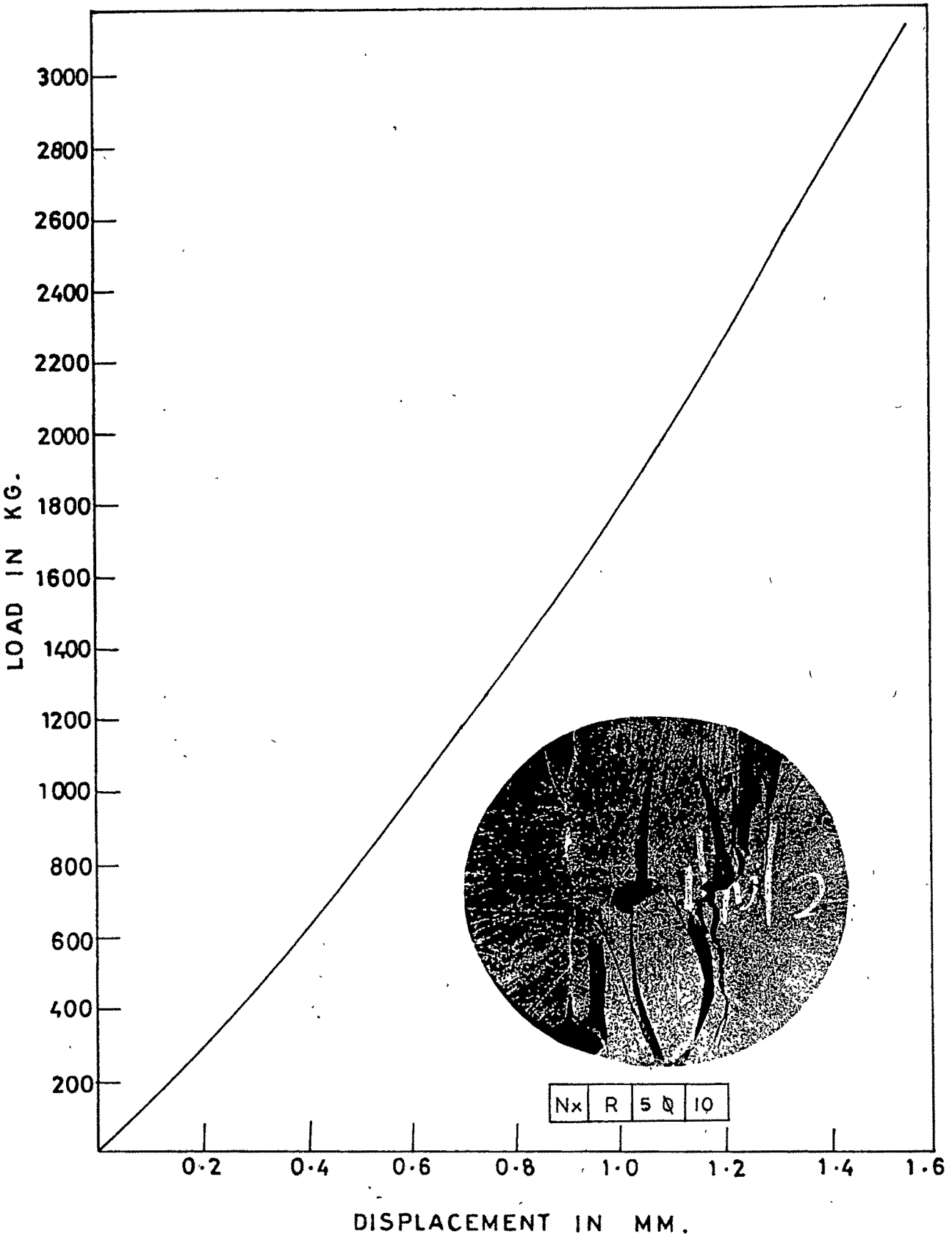

FIG. 6·40: LOAD DISPLACEMENT CHARACTERISTICS.

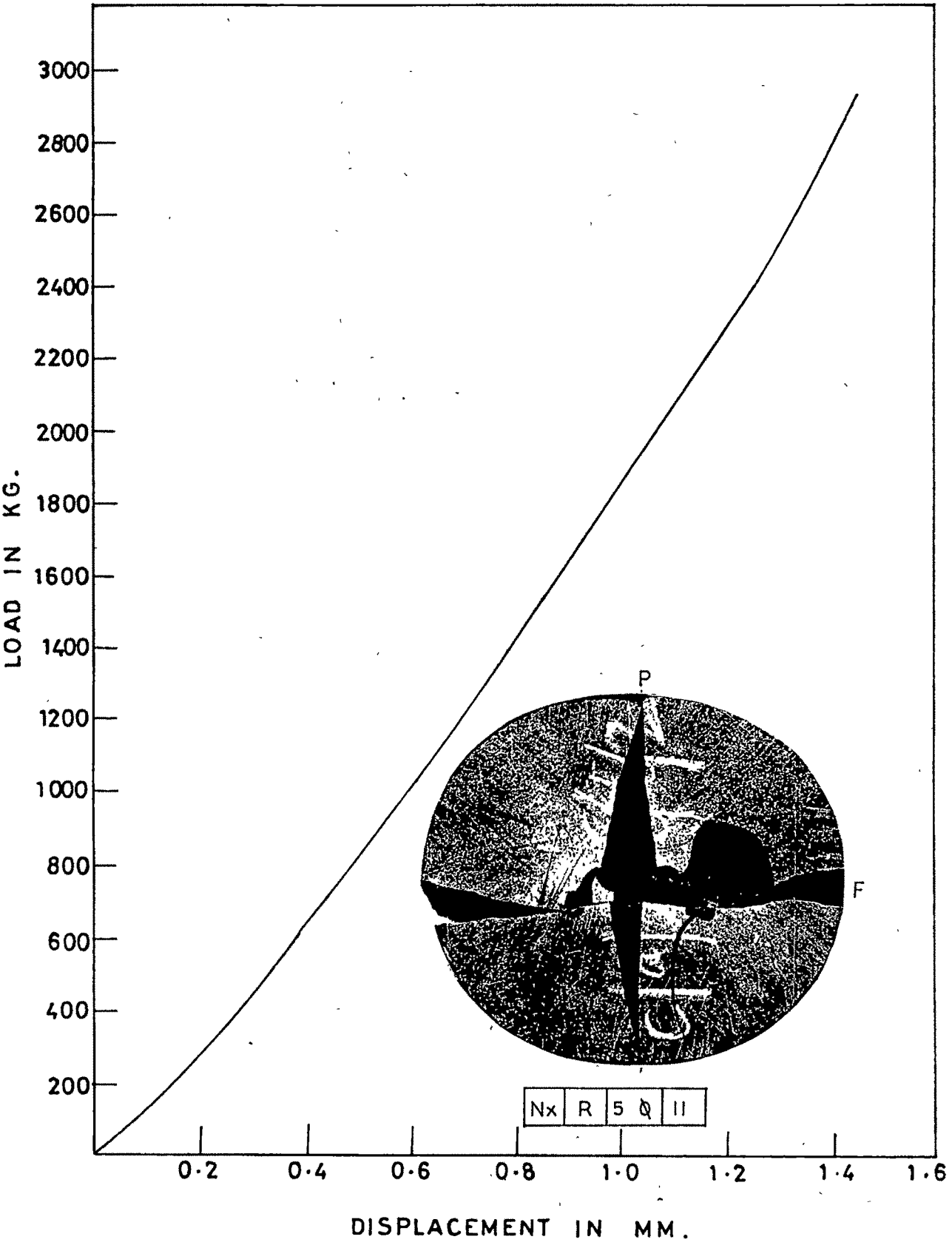

FIG.6·41 : LOAD DISPLACEMENT CHARACTERISTICS.

implying thereby that the crack initiated from the centre. The crack along the vein was wider at as is revealed from the photograph. (Fig 6.42)

Nx/R/5Ø/13 Failure was instanteneous. Primary crack was seen to initiate from the centre of the sample exactly along the loaded diameter terminating at some distance away from both upper and lower loading platens. This phenomenon also implies that the crack initiated from the centre. Moreover the crack was wider at the centre becoming hair like towards the periphery. It was possible to minimize secondary cracking perhaps due to absence of flaws. Some higher order cracking is more prominent in the lower half of the sample. Each secondary crack starting from the loading platen terminated near the hole periphery. (Fig 6.43)

Nx/R/5Ø/14 Failure was instantaneous. Primary crack was seen to initiate from the centre of the sample exactly along the loaded diameter. It is wider at the hole than at the periphery implying thereby its initiation from the centre. Secondary cracking was in the form of a 'curly bracket' on one side of the hole running between opposite loading platens but did not extend in the upper half beyond the hole periphery. Higher order cracking was more prominent in the lower half of the sample. (Fig 6.44)

6.2.4 Results:

The tables 6.1 A and 6.1 B show the load at fracture and its corresponding displacement for discs and

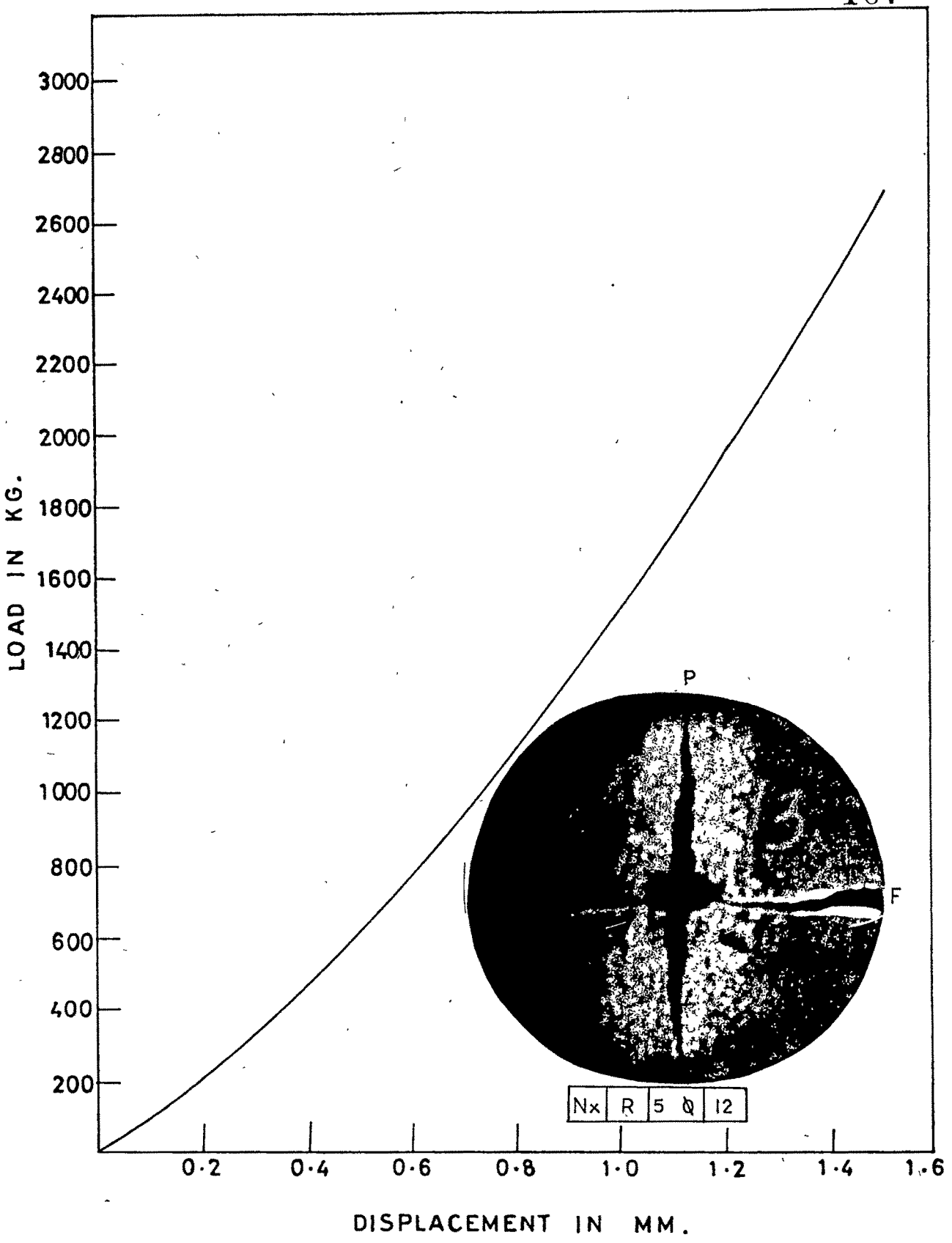

FIG.6·42 : LOAD DISPLACEMENT CHARACTERISTICS.

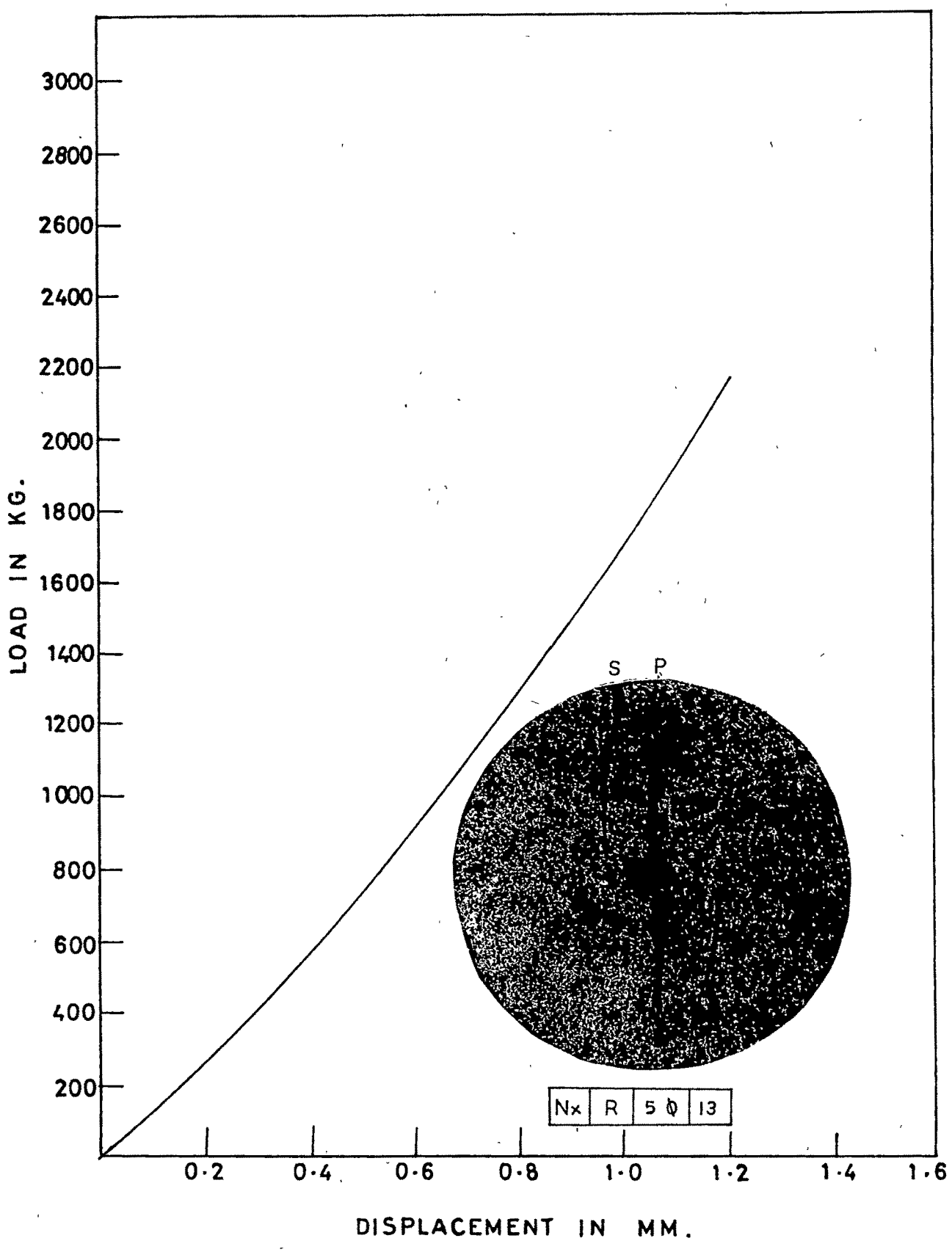

FIG. 6·43 : LOAD DISPLACEMENT CHARACTERISTICS.

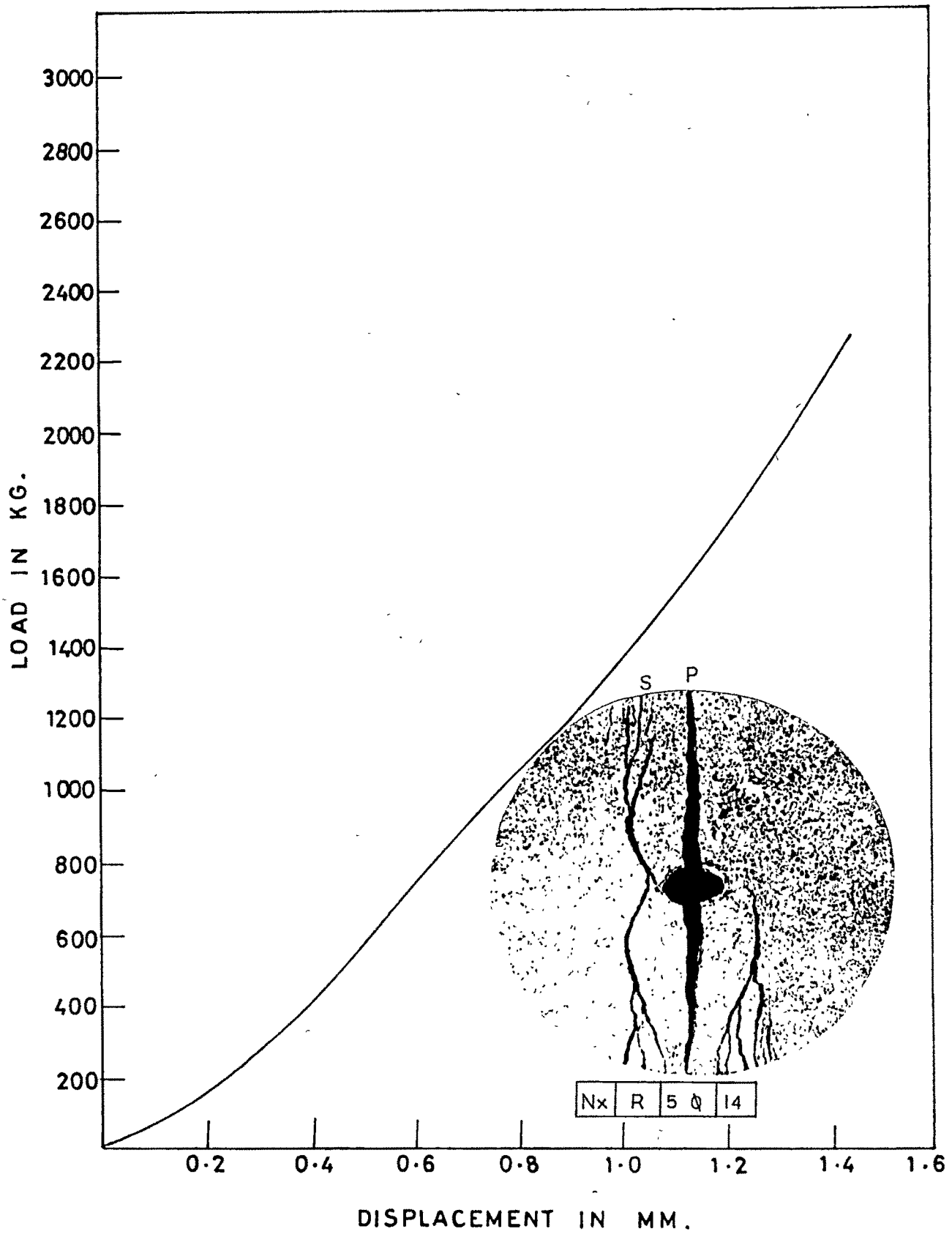

FIG.6·44: LOAD DISPLACEMENT CHARACTERISTICS.

TABLE - 6.1 A RESULTS FOR DISCS

Sr. No. (1)	Disc Designation (2)	Fracture Load in Kg. (3)	Maximum Displacement mm. (4)
1.	Nx/D/0.48 μ/1	1848.32	1.61
2.	Nx/D/0.66 μ/2	1191.3	0.65
3.	Nx/D/0.96 μ/3	1810.42	0.904
4.	Nx/D/1.4 μ/4	1913.3	1.003
5.	Nx/D/1.95 μ/5	1716.00	2.55
6.	Nx/D/2.4 μ/6	1424.145	0.7969
7.	Nx/D/3.3 μ/7	1314.04	0.927
8.	Nx/D/4.8 μ/8	1418.73	0.965
9.	Nx/D/7.24 μ/9	1851.93	0.92
10.	Nx/D/9.6 μ/10	1407.51	1.76
11.	Nx/D/12 μ/11	1436.78	2.476
12.	Nx/D/16 μ/12	1617.28	1.155
13.	Nx/D/24 μ/13	1685.87	0.89
14.	Nx/D/36 μ/14	1104.66	0.99
15.	Nx/D/48 μ/15	1689.48	2.59
16.	Nx/D/60 μ/16	1422.34	0.765
17.	Nx/D/82 μ/17	1400.68	1.397
18.	Nx/D/120 μ/18	1465.66	1.3589
19.	Nx/D/180 μ/19	2003.55	1.70
20.	Nx/D/244 μ/20	1671.43	0.68
21.	Nx/D/300 μ/21	1480.10	1.14
22.	Nx/D/410 μ/22	1617.28	0.952
23.	Nx/D/610 μ/23	1415.12	1.295

Table 6.1 A continued.....

(1)	(2)	(3)	(4)
24.	Nx/D/900 μ/24	1631.72	1.13
25.	Nx/D/1220 μ/25	1945.79	0.75
26.	Nx/D/1520 μ/26	1270.72	0.855
27.	Nx/D/2060 μ/27	1530.64	1.46
28.	Nx/D/3050 μ/28	1740.02	1.34
29.	Nx/D/4520 μ/29	1660.60	1.657
30.	Nx/D/6100 μ/30	1494.54	1.498

TABLE - 6.1 B RESULTS FOR RINGS

Sr. No.	Ring Designation	Fracture Load in Kg.	Displacement at Fracture in mm
1.	Nx/R/3Ø/1	2837.46	1.562
2.	Nx/R/3Ø/2	2801.36	1.765
3.	Nx/R/3Ø/3	3104.60	1.587
4.	Nx/R/3Ø/4	1696.70	1.041
5.	Nx/R/4Ø/5	2700.28	1.568
6.	Nx/R/4Ø/6	2454.80	1.625
7.	Nx/R/4Ø/7	2830.24	1.651
8.	Nx/R/4Ø/8	2563.10	1.206
9.	Nx/R/4Ø/9	2685.84	1.511
10.	Nx/R/5Ø/10	3140.70	1.5136
11.	Nx/R/5Ø/11	2989.08	1.441
12.	Nx/R/5Ø/12	2591.98	1.454
13.	Nx/R/5Ø/13	2184.05	1.200
14.	Nx/R/5Ø/14	2295.96	1.435

rings respectively.

6.3 Stress-strain characteristics:

The plots in Fig 6.1 to Fig 6.44 are the load displacement curves obtained from experimental observations on the diametrally compressed rock discs and annuli.

6.3.1 Initial characteristics:

The initial portion of the stress-strain curve shows the concave curvature on upwards side meaning thereby that initially the rate of increase of displacement is rapid. From this initial concave curvature it may be implied that the locked stresses or pre-stress in the flaws and microcracks inherent in the rocks are getting released. As the size of the hole increases there appears a tendency of displacement to become smaller.

6.3.2 Pre-failure characteristics:

As the load increases the rate of displacement becomes slower than that obtained in initial curve. The pre-stress responsible for the initial higher displacements behave now act as triggering stress for the cracks to initiate and when the ratio of applied stress to pre-stress assumes unity a failure becomes imminent.

6.3.3 Post failure characteristics:

The observation of post failure behaviour in a rock is an untractable phenomenon. As the failure is approached there occurs a sudden and instaneous burst of energy which shatters the rock. It is therefore not

possible to record the observations with the presently available microphotographic technique and soft testing machines. It is absolutely essential that better readout systems, a stiff testing device and newer microphotographic techniques may be developed to ensure the precise recording of the post-failure phenomenon (Hudson,Crouch and Fairhurst)

6.4 Pre-stress in rocks:

In article 5.2.2 a geometrical construction is used to determine the value of pre-stress from observed load displacement curve. Also the value of pre-stress can be worked out by comparing the curvature of Griffith failure envelope and curvature of failure envelope of a rock material under test. The expression for σ_o is

$\sigma_o = n\ To/2 - 4\ To$

$= To\ (\ n - 8\ )/2$

if $n = 8$, $\sigma_o = 0$

The value of To is obtained from the formula used by Hondros for Brazil test, since tensile strength using Hondros formula for disc show one to one correspondece with the uniaxial tensile strength value. The Table 6.2 A and Table 6.2 B present the comparision between the two values and Fig 6.45 and Fig 6.46 are the corresponding plots. From this it bears out that value of pre-stress by graphical construction and that from formula tally fairly well. The inference is therefore that the concept of pre-stress has a valid basis.

TABLE - 6.2 A PRE-STRESS IN ROCKS

Sr. No.	Specimen Designation	σ_o (Graph.) Kg/cm^2	σ_o (Formula) Kg/cm^2
(1)	(2)	(3)	(4)
1.	Nx/D/0.48 μ/1	374.2	405.17
2.	Nx/D/0.66 μ/2	242.53	243.56
3.	Nx/D/0.96 μ/3	380.16	416.58
4.	Nx/D/1.44 μ/4	383.4	457.48
5.	Nx/D/1.95 μ/5	-	-
6.	Nx/D/2.4 μ/6	299.038	316.28
7.	Nx/D/3.3 μ/7	302.4	291.84
8.	Nx/D/4.8 μ/8	289.63	298.075
9.	Nx/D/7.2 μ/9	403.97	412.89
10.	Nx/D/9.6 μ/10	-	-
11.	Nx/D/12 μ/11	295.01	310.5
12.	Nx/D/16 μ/12	359.26	348.78
13.	Nx/D/24 μ/13	315.87	353.3
14.	Nx/D/36 μ/14	235.2	239.528
15.	Nx/D/48 μ/15	432.41	364.85
16.	Nx/D/60 μ/16	333.99	322.77
17.	Nx/D/82 μ/17	291.42	347.77
18.	Nx/D/120 μ/18	291.4	316.535
19.	Nx/D/180 μ/19	406.88	444.71
20.	Nx/D/240 μ/20	378.74	272.34
21.	Nx/D/300 μ/21	355.87	339.32
22.	Nx/D/410 μ/22	361.2	312.18

Table 6.2 A continued....

(1)	(2)	(3)	(4)
23.	Nx/D/610 μ/23	279.10	312.64
24.	Nx/D/900 μ/24	384.3	373.9
25.	Nx/D/1220 μ/25	396.34	412.94
26.	Nx/D/1520 μ/26	306.87	293.13
27.	Nx/D/2560 μ/27	332.87	319.61
28.	Nx/D/3050 μ/28	307.88	395.84
29.	Nx/D/4520 μ/29	349.59	372.84
30.	Nx/D/6100 μ/30	-	-

TABLE - 6.2 B PRE-STRESS IN ROCKS

Sr. No.	Specimen Designation	$\bar{\sigma}_o$ (Graph) Kg/cm^2	$\bar{\sigma}_o$ (Formula) Kg/cm^2
1.	Nx/R/3Ø/1	603.01	659.92
2.	Nx/R/3Ø/2	557.86	649.19
3.	Nx/R/3Ø/3	581.76	679.76
4.	Nx/R/3Ø/4	378.98	403.81
5.	Nx/R/4Ø/5	523.80	596.22
6.	Nx/R/4Ø/6	516.7	542.11
7.	Nx/R/4Ø/7	524.22	624.52
8.	Nx/R/4Ø/8	546.93	581.28
9.	Nx/R/4Ø/9	524.66	584.26
10.	Nx/R/5Ø/10	642.85	692.67
11.	Nx/R/5Ø/11	609.09	640.5
12.	Nx/R/5Ø/12	550.38	558.24
13.	Nx/R/5Ø/13	498.48	490.87
14.	Nx/R/5Ø/14	520.83	510,13

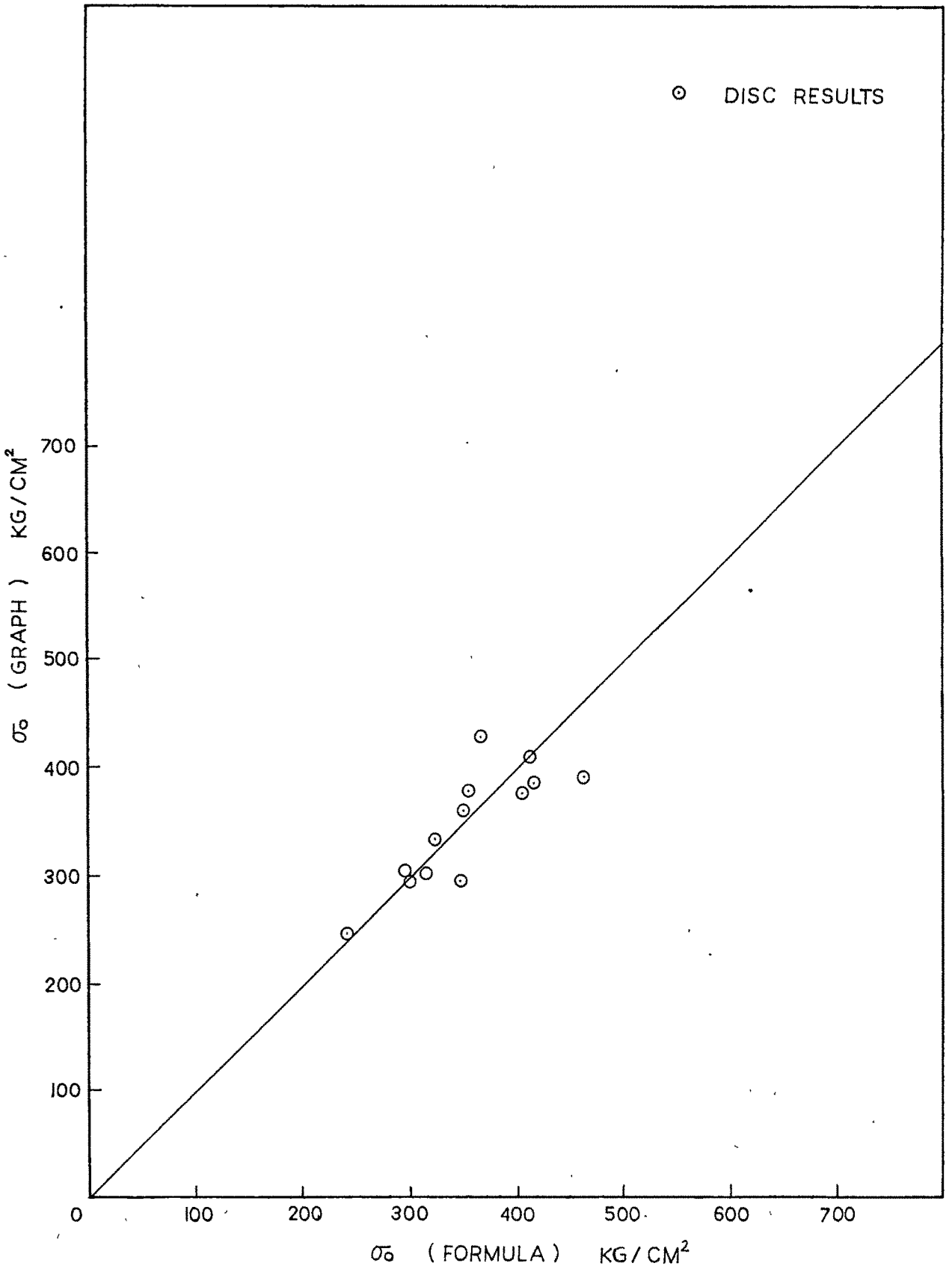

FIG. 6·45 σ_0 (GRAP) Vs σ_0 (FORMULA) IN BRAZIL TEST ON DISC SPECIMENS OF BASALT

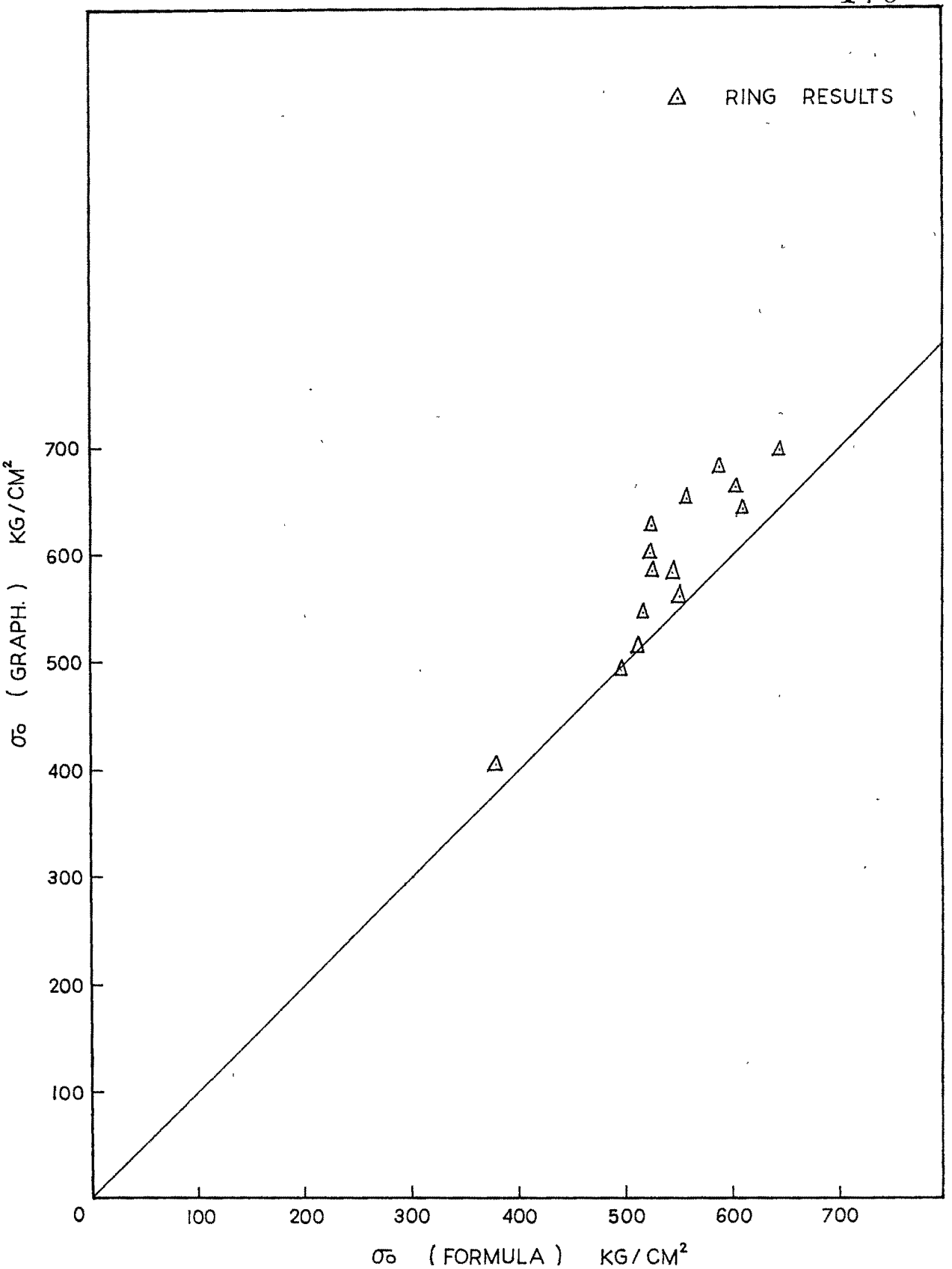

FIG. 6·46 σ_0 (GRAP) Vs σ_0 (FORMULA) IN BRAZIL TEST ON RING SPECIMENS OF BASALT

The plot between parameters σ_o, σ/σ_o, σ, Vs. rate of loading at Fig 6.47 reveal a pulsating curve which could be approximated to a straight line with a slight slope. The interpretation could be that there is no pronounced effect of rate of loading on these parameters. Or may be an effect of machine's stiffness or may be intriguing dynamic effect due to rate of loading getting displayed as pulsating curve. Fig 6.48 shows a plot between σ_o, σ/σ_o, σ Vs. radii ratio from which a decreasing trend can be noticed. The inference could be that there could be a influence of hole on the value of pre-stress.

6.5 Constitutive relationships:

In article 5.2.3 a general constitutive law for rock material is proposed which is expressed as

$$\sigma/\sigma_o = \text{Sinh}(\lambda \epsilon)$$

where σ/σ_o = $\frac{\text{Maximum compressive stress}}{\text{Maximum internal pre-stress}}$

ϵ = Axial strain

and λ = A Material constant

Fig 6.49 and Fig 6.50 depict comparisons from a series of Brazil tests on discs and rings from cores of two varieties of igneous basaltic rocks. It established that there is a constitutive relationship between stress ratio and strain. This stress ratio between maximum compressive stress and maximum internal pre-stress triggers the failure when it reaches a critical value of unity till then there occurs a deformation of submicrscopic

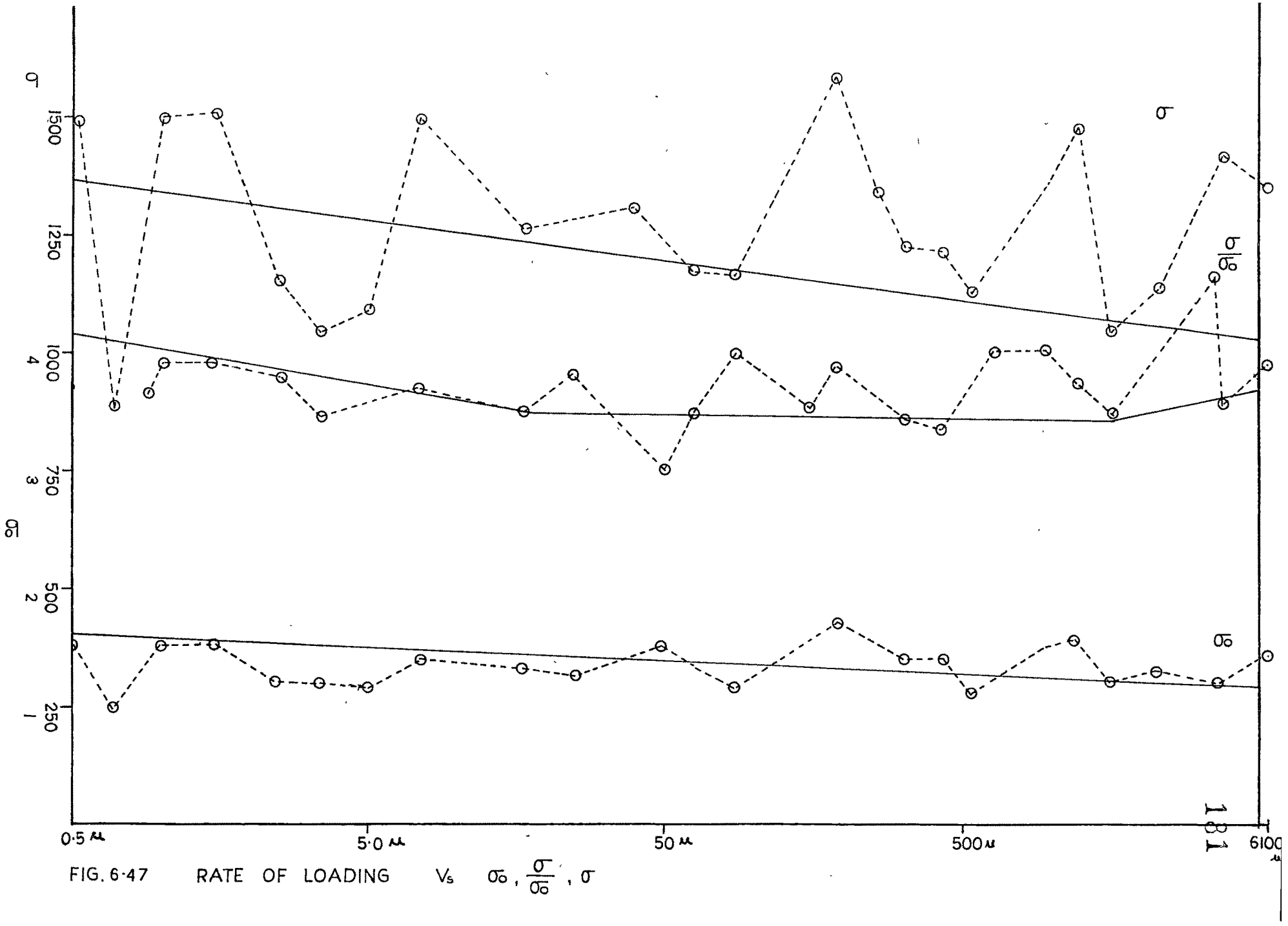

FIG. 6·47 RATE OF LOADING Vs σ_0, $\frac{\sigma}{\sigma_0}$, σ

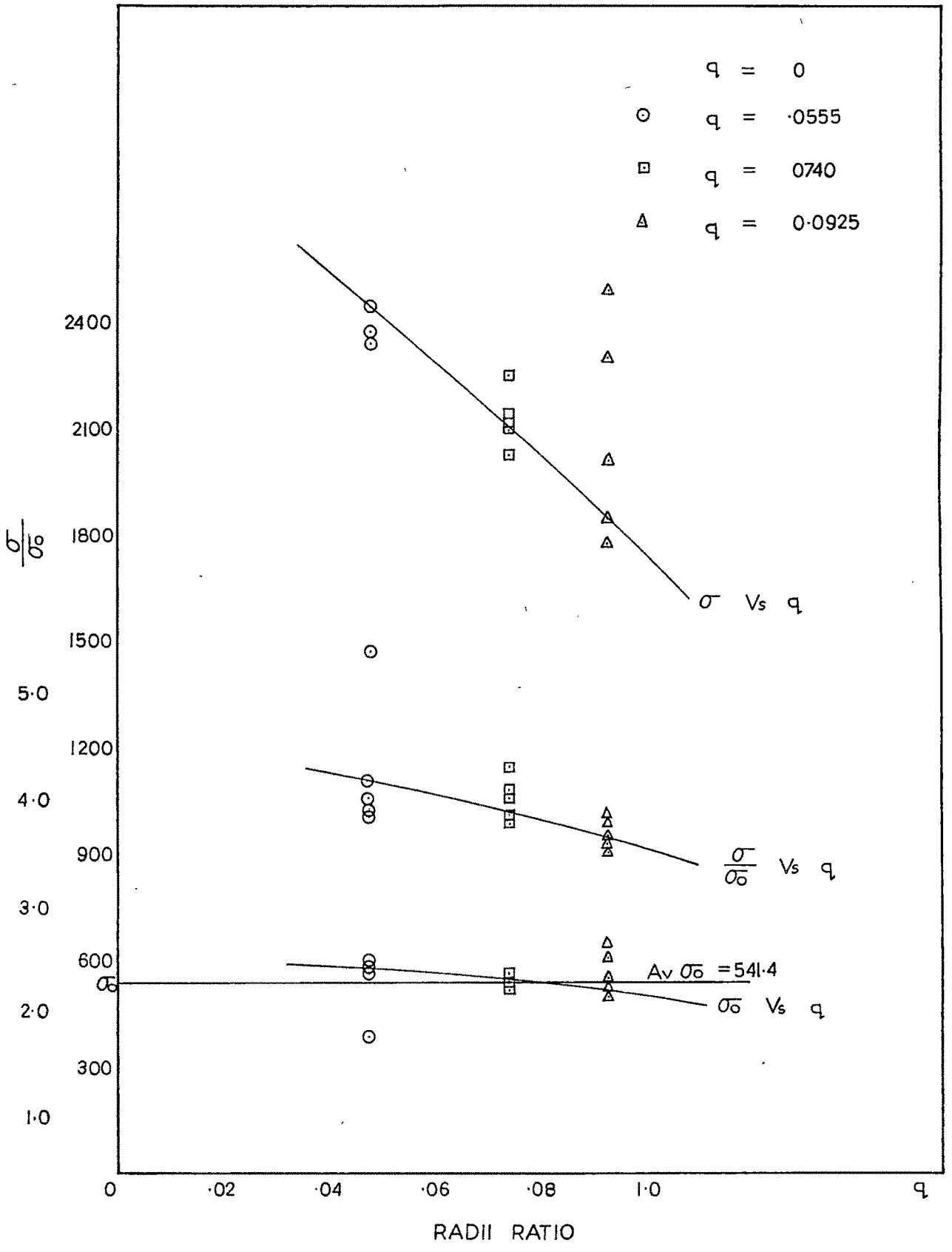

FIG. 6·48 σ_0, $\frac{\sigma}{\sigma_0}$, σ Vs q

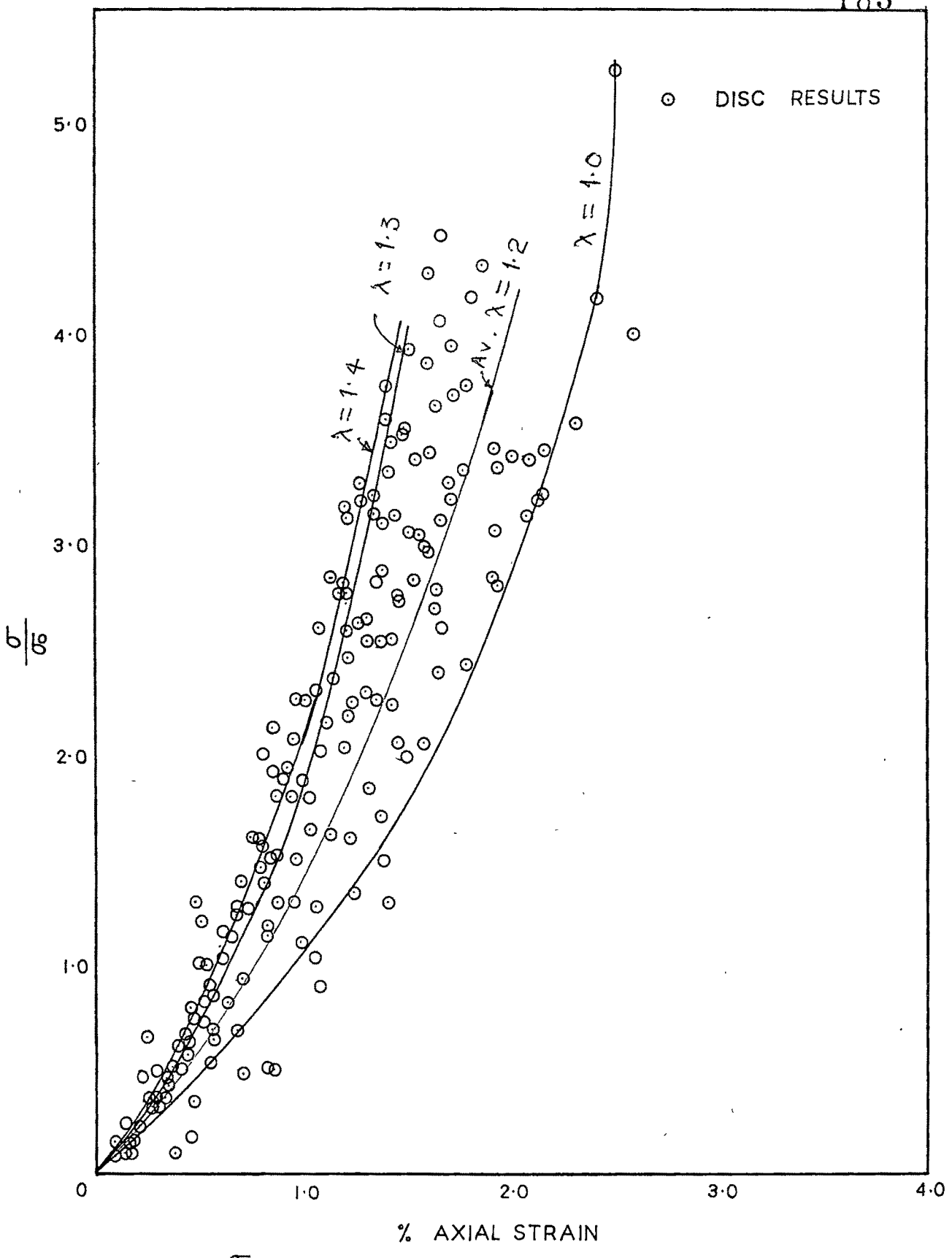

FIG. 6·49 $\frac{\sigma}{\sigma_0}$ Vs STRAIN

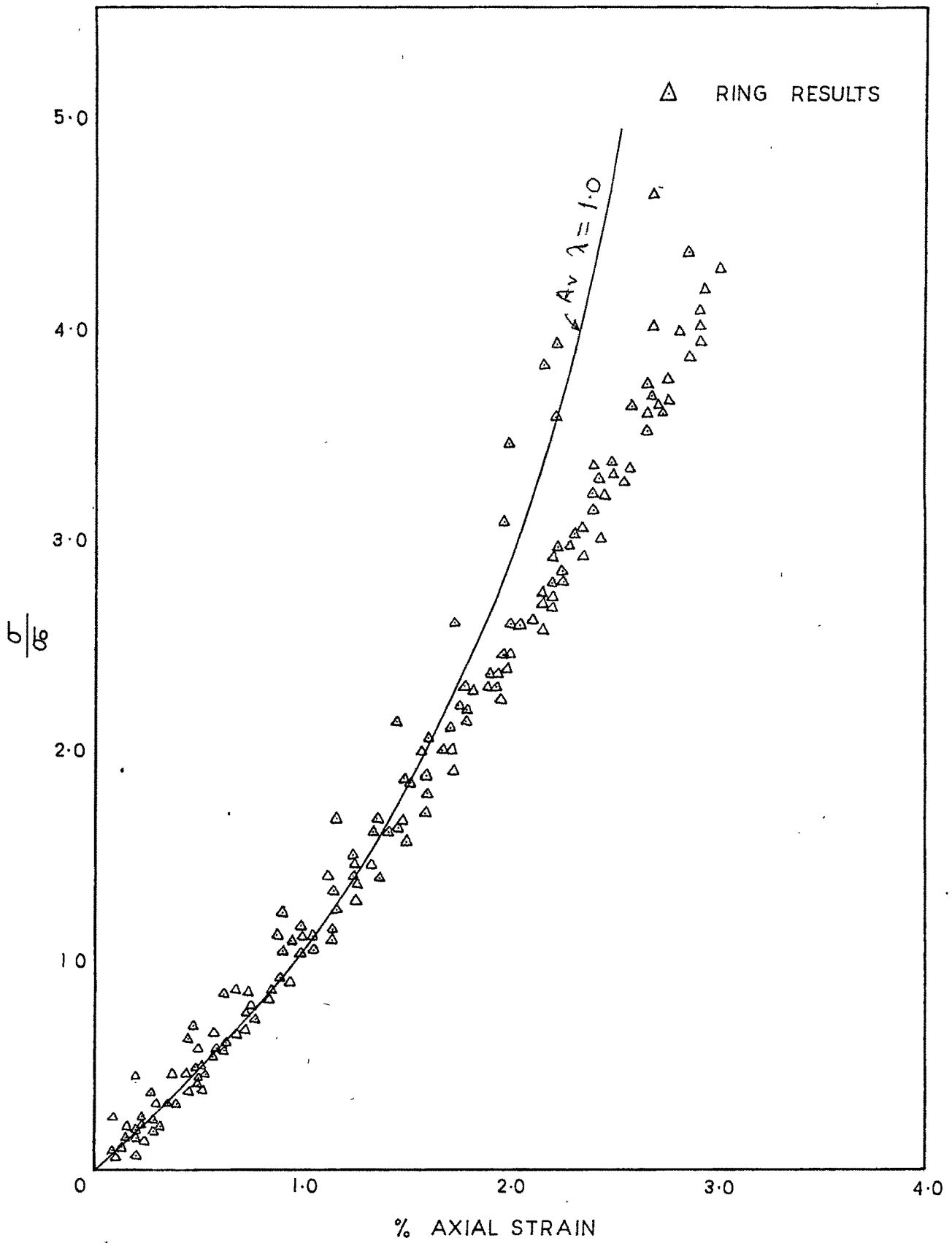

FIG. 6·50 $\frac{\sigma}{\sigma_0}$ Vs STRAIN

pre-existing flaws in proportion to a combinations of strains in the structure of the flaws. For simplicity the combinations of strains could be incorporated by a constant value of poisson's ratio. It is possible to visulaze that untile the stress ratio becomes unity the behaviour of the rock is non-linearly elastic and after reaching the limiting stress ratio of unity the crack is initiated in the material which propagates as per the failure critera for brittle materials. The average values of λ are approximately 1.2 and 1.0 for discs and rings respectively. The value of λ equal to unity signifies elastic law.

$$\sigma_{11} = E \frac{(1-\nu)}{(1+\nu)(1-2\nu)} \epsilon_{11}$$

if $\frac{(1-\nu)}{(1+\nu)(1-2\nu)} = \lambda = 1.0$

then $\sigma_{11} = E \epsilon_{11}$ if λ is equal,

to more than one the relation can be

$$\frac{\sigma_{11}}{\epsilon_{11}} = \frac{M}{E} = \lambda \quad \text{where}$$

$$M = E \frac{(1-\nu)}{(1+\nu)(1-2\nu)}$$

The departure of values from unity in case of disc could be due to not perfectly uniaxial test conditions in case of discs. The constitutive relationship for discs and rings are corresponding to $\nu = 0.25$ and $\nu = 0.15$ respectively. It may be mentioned that value of λ worked out independently from observing the axial and lateral strains from a test on disc using strain gauges is approximately

around 0.25. Fig 6.51 and Fig 6.52 show a plot between λ and rate of loading on log scale and λ against radii ratio respectively. From this it is clearly evident that the value of λ is equal to approximately 1.0 in case of rings and 1.2 in case of discs. The variations between the calculated curves and experimental curves may be due to the variation in the material parameters owing to structural defects in the individual test specimens. The departure in the later part of the curve can be attributed to the strain measurements specifically after the significant growth of cracks just at a point when the failure is imminent. The relationship is simple and general enough amneable to mathematical processes developed for elastic models. Subsequent to the unit stress ratio the crack is initiated and propagated and follows the classical behaviour for brittle materials.

6.6 Failure criterion:

In article 5.3.3 a failure criterion is proposed as an extension to the classical Griffith criterion which incorporates a parameter for pre-stress locked in the rock structures during the formation. It is expressed as

$$\tau^2 = \lambda \, To \, (\sigma + To)$$

where τ = Shear stress along the plane of failure

To = Maximum tensile stress

σ = Normal stress

n = $\frac{\text{Maximum compressive stress}}{\text{Maximum tensile stress}}$

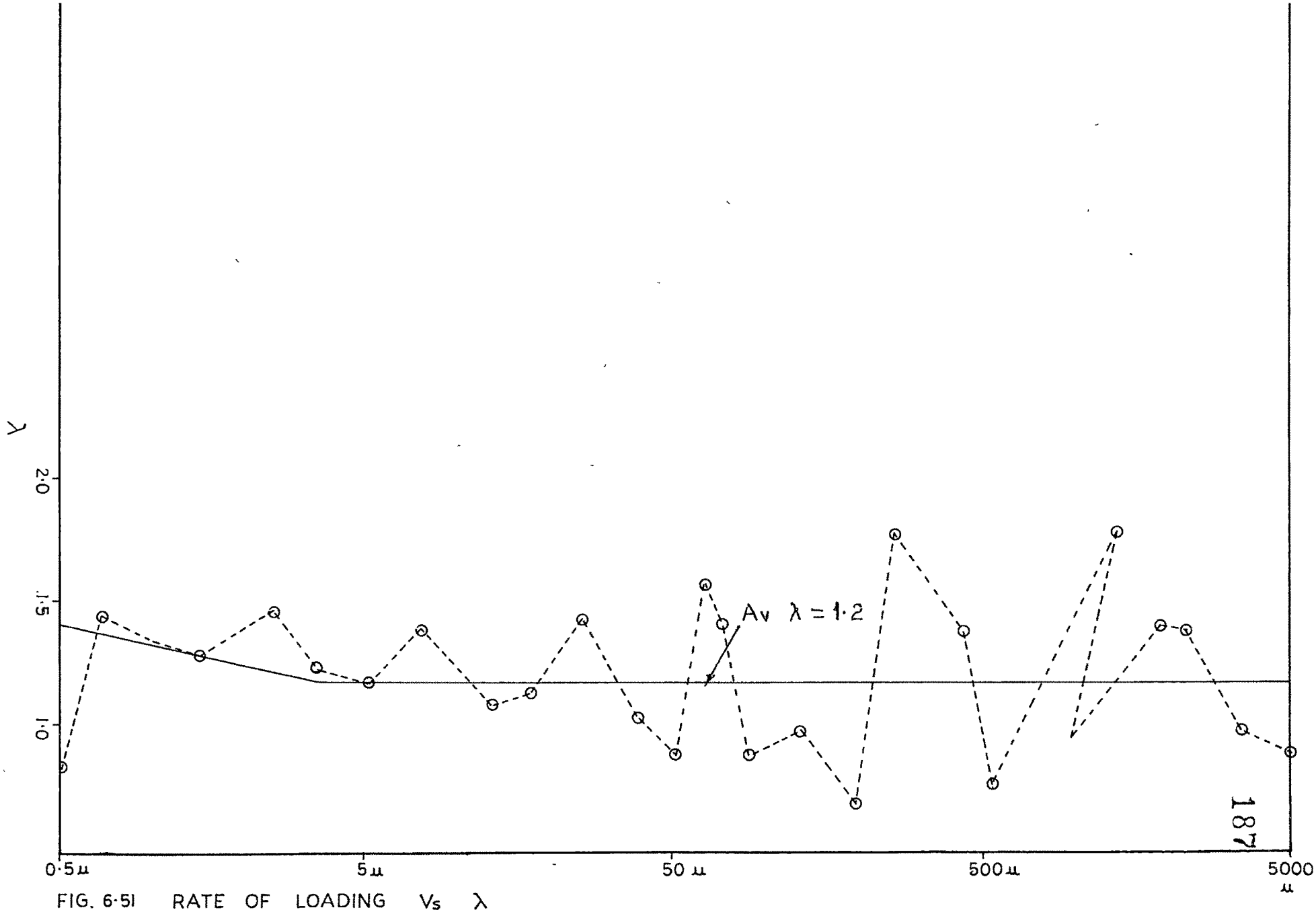

FIG. 6·51 RATE OF LOADING Vs λ

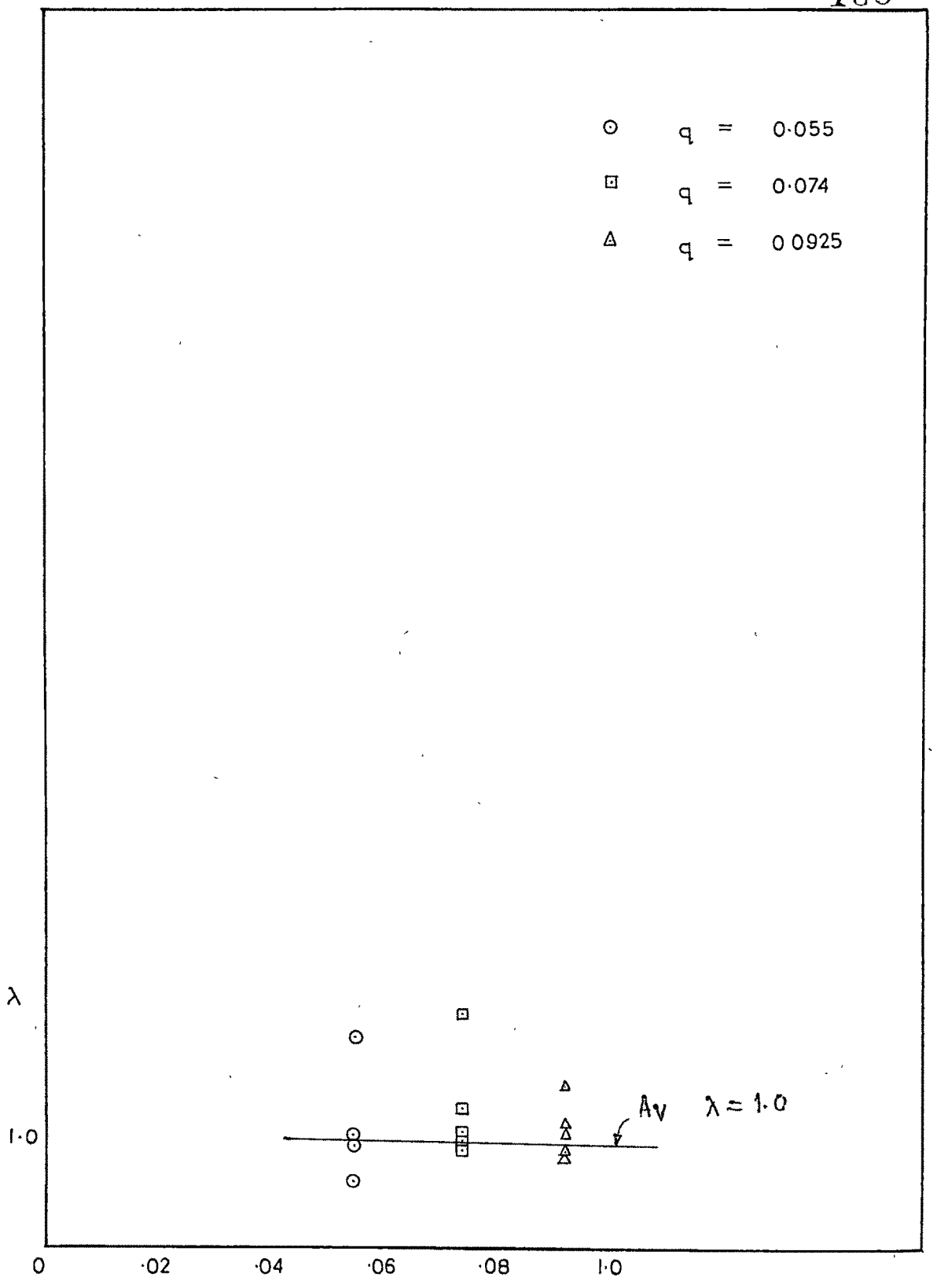

FIG. RADII RATIO (q)

and $\ast = (n\, T_o/2 - \sigma_o)/T_o$

Fig 6.53 and Fig 6.54 are the failure envelopes from the series of tests on discs and rings under diametral loading. The average value of $\ast$ is 4.15 for discs and 4.35 for rings. The Griffith value is 4 under the conditions of no pre-stress in the material. Thus the variation is due to the consequence of internal pre-stress locked during the formation of rock. (Table 6.4 A and 6.4 B)

6.7 Maximum tensile stress value:

The value of maximum tensile stress can be worked out from the failure criterion since it is the circle of stress touching the compressive stress circle in a Mohr's plot. Also it can be calculated from a formula obtained from theoretical analysis of disc and ring subjected to diametral loading. It is well known that the tensile stress values from ring formula over estimates to a very high degree approximately six times that of a disc. Table 6.3 A and 6.3 B presents the values of tensile stress from failure criteria, from disc and ring formula. From Fig 6.55 and Fig 6.56 it can be observed that values from the failure criteron and values from disc formula compares to a fair degree while there is no comparison with the values from ring formula. The Fig 6.57 and Fig 6.58 are the plots between To vs rate of speed and To vs radii ratio respectively. These plots show the similar pattern as in case of other stress parametets as discussed in article 6.4.

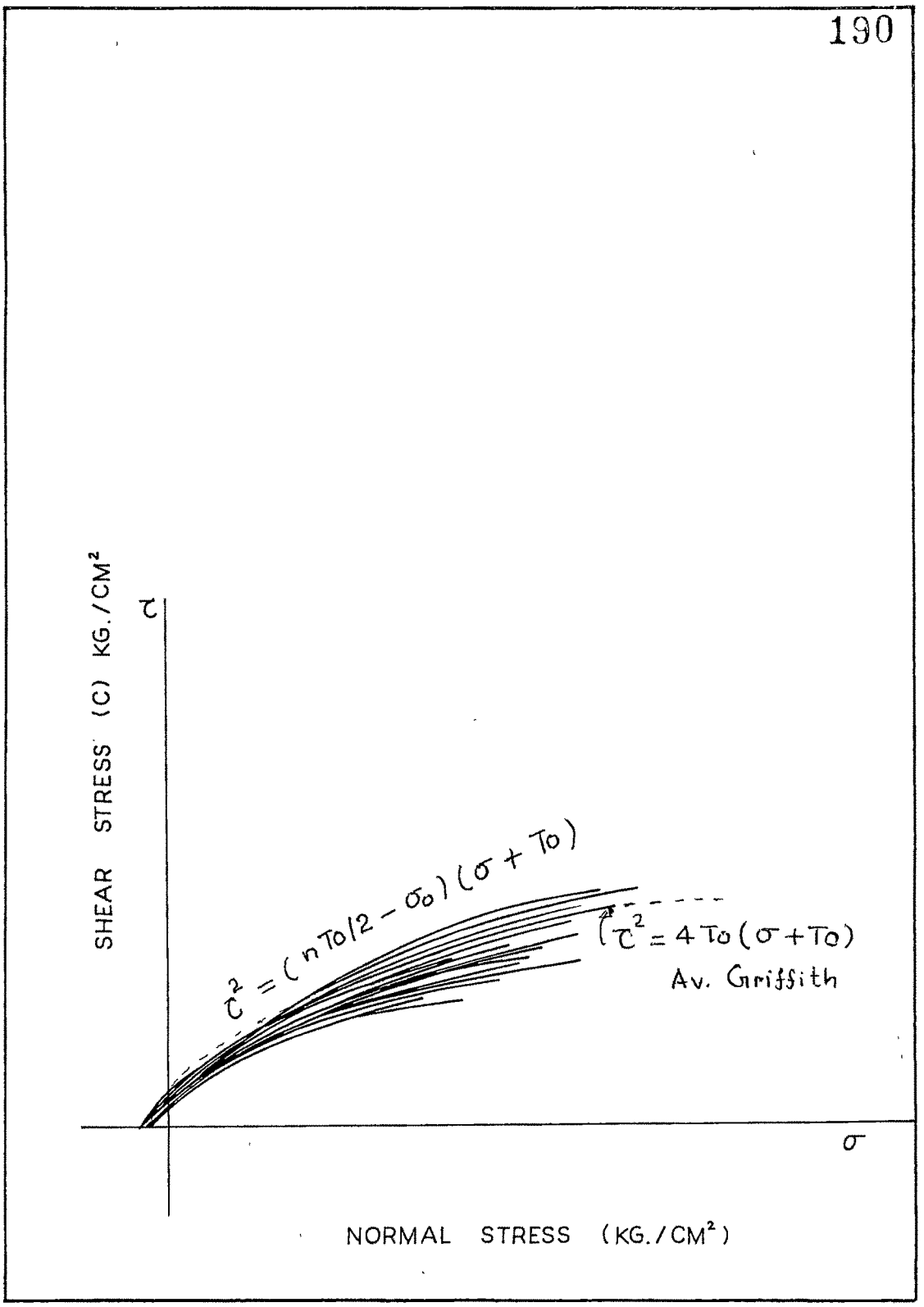

FIG. 6·53 FAILURE ENVELOPES FOR BASALTIC ROCK IN BRAZIL TEST ON DISCS

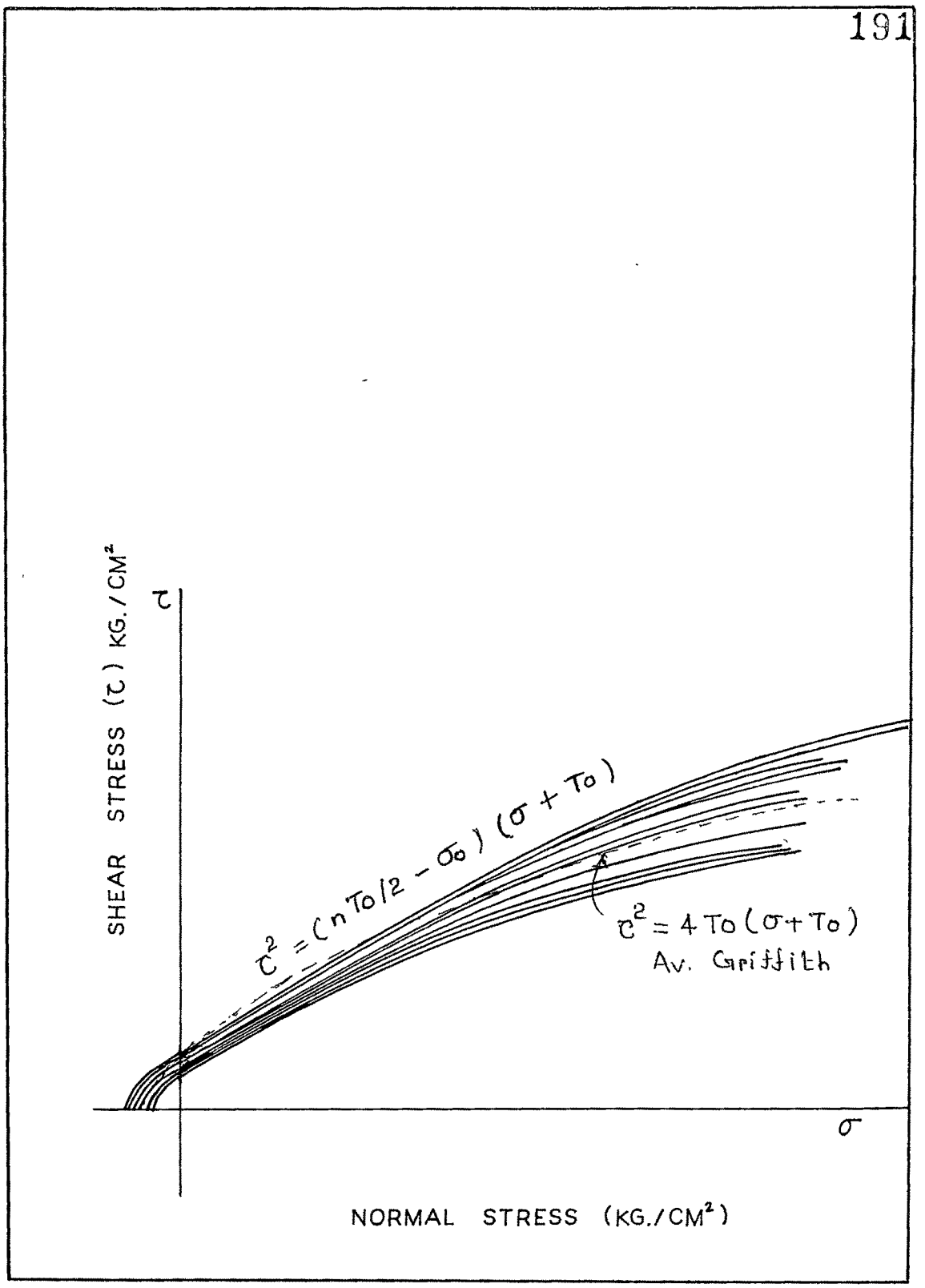

FIG. 6·54 FAILURE ENVELOPES FOR BASALTIC ROCK IN BRAZIL TEST ON RINGS

TABLE - 6.3 A MAXIMUM TENSILE STRESS VALUE

Sr. No.	Specimen Designation	To Theoretical $2P/\pi Dt$ Kg/cm^2	To Predicted Kg/cm^2
(1)	(2)	(3)	(4)
1.	Nx/D/0.48 μ/1	82.53	90.27
2.	Nx/D/0.66 μ/2	50.18	50.43
3.	Nx/D/0.96 μ/3	82.88	91.98
4.	Nx/D/1.44 μ/4	74.18	92.7
5.	Nx/D/1.95 μ/5	-	-
6.	Nx/D/2.4 μ/6	64.74	69.051
7.	Nx/D/3.3 μ/7	57.75	55.10
8.	Nx/D/4.8 μ/8	61.40	69.32
9.	Nx/D/7.2 μ/9	83.8	86.02
10.	Nx/D/9.6 μ/10	-	-
11.	Nx/D/12 μ/11	63.08	66.95
12.	Nx/D/16 μ/12	70.69	68.02
13.	Nx/D/24 μ/13	72.095	73.52
14.	Nx/D/36 μ/14	48.90	50.0
15.	Nx/D/48 μ/15	72.56	55.66
16.	Nx/D/60 μ/16	65.73	62.92
17.	Nx/D/82 μ/17	58.77	72.85
18.	Nx/D/120 μ/18	62.5	68.78
19.	Nx/D/180 μ/19	87.25	96.69
20.	Nx/D/240 μ/20	74.27	72.64

Table 6.3 A continued....

(1)	(2)	(3)	(4)
21.	Nx/D/300 μ/21	68.28	64.14
22.	Nx/D/410 μ/22	74.08	63.70
23.	Nx/D/610 μ/23	62.9	71.28
24.	Nx/D/900 μ/24	75.15	72.53
25.	Nx/D/1220 μ/25	82.39	86.54
26.	Nx/D/1520 μ/26	58.46	55.021
27.	Nx/D/2560 μ/27	64.84	61.52
28.	Nx/D/3050 μ/28	79.54	101.52
29.	Nx/D/4520 μ/29	75.54	81.35
30.	Nx/D/6100 μ/30	-	-

TABLE - 6.3 B MAXIMUM TENSILE STRESS VALUE

Sr. No.	Specimen Designation	To (The.) Ring Formula Kg/cm^2	To (The.) Disc Formula Kg/cm^2	To (Pred.) Kg/cm^2
1.	Nx/R/3Ø/1	807	131.95	146.1
2.	Nx/R/3Ø/2	792.64	129.50	152.34
3.	Nx/R/3Ø/3	829.66	135.56	160.13
4.	Nx/R/3Ø/4	496.83	81.18	88.08
5.	Nx/R/4Ø/5	738.07	118.83	136.93
6.	Nx/R/4Ø/6	673.22	108.39	114.74
7.	Nx/R/4Ø/7	775.61	124.87	149.94
8.	Nx/R/4Ø/8	721.85	116.22	124.8
9.	Nx/R/4Ø/9	725.72	116.84	131.74
10.	Nx/R/5Ø/10	875.95	138.41	150.86
11.	Nx/R/5Ø/11	809.73	127.95	135.8
12.	Nx/R/5Ø/12	706.26	111.60	113.56
13.	Nx/R/5Ø/13	621.22	98.16	91.0
14.	Nx/R/5Ø/14	646.62	102.18	99.96

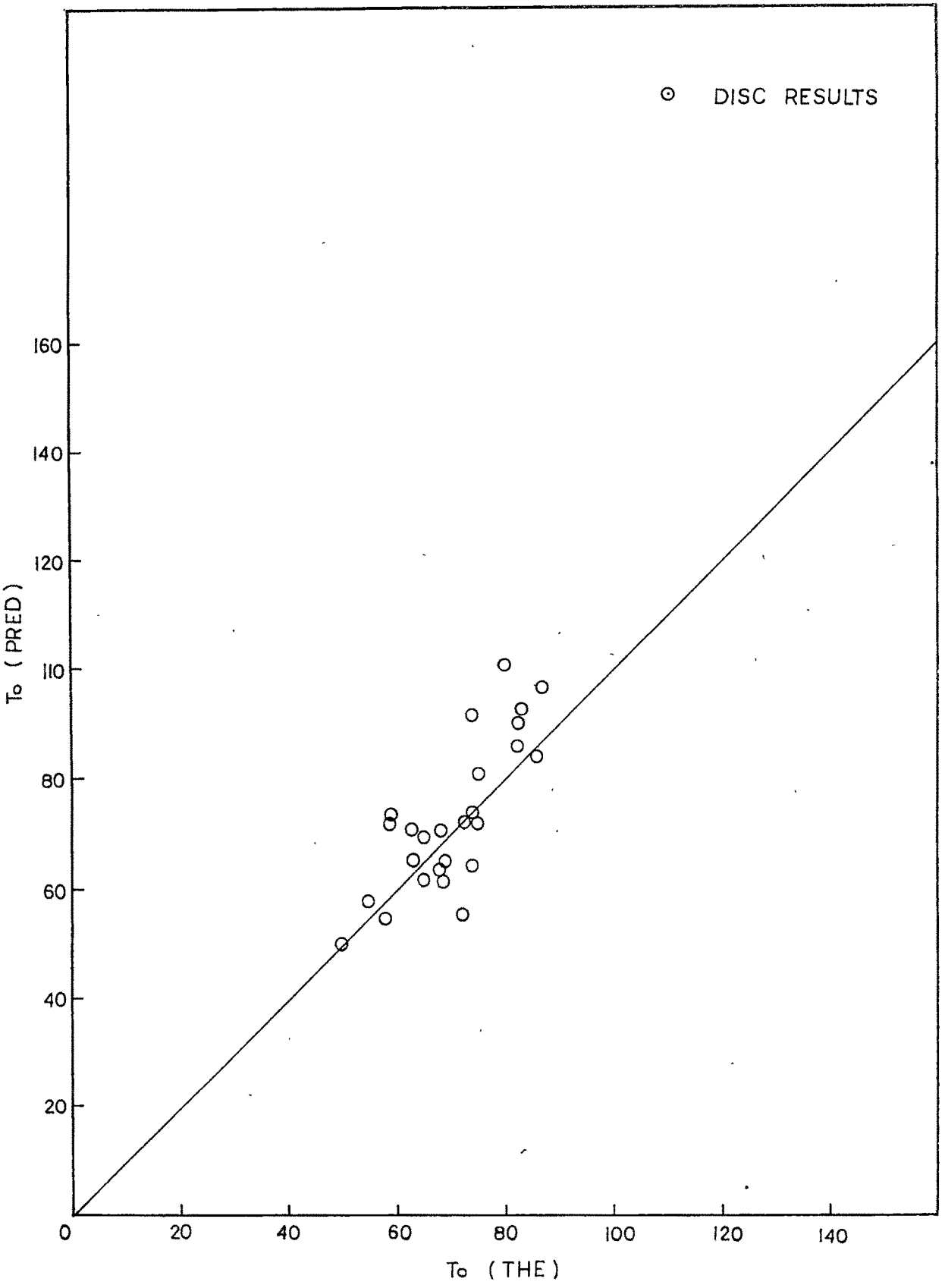

FIG. 6·55 To (THE) Vs To (PRED) IN BRAZIL TEST ON DISC SPECIMENS OF BASALT

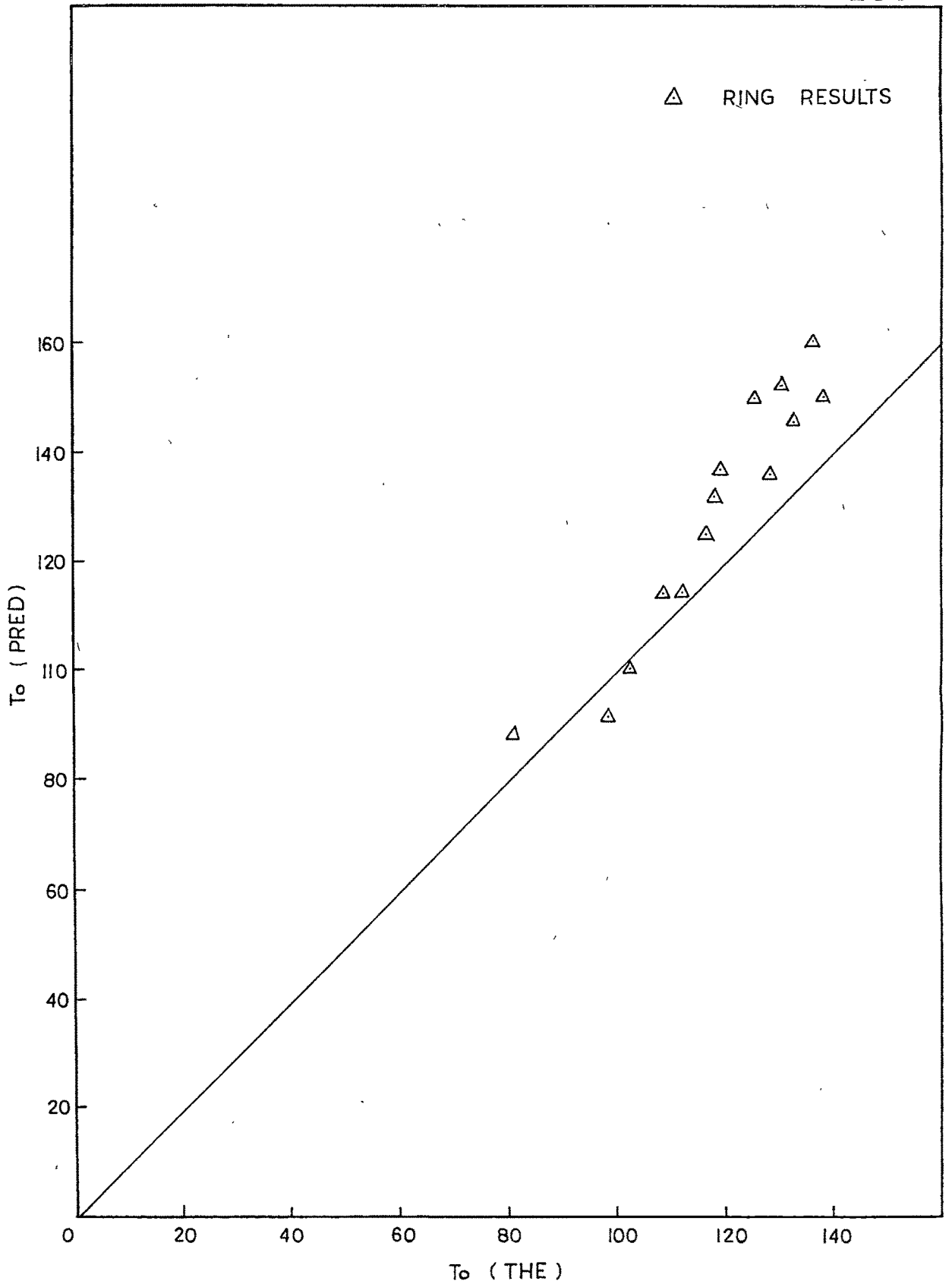

FIG. 6·56 To THE Vs To PRED IN BRAZIL TEST ON RING SPECIMENS OF BASALT

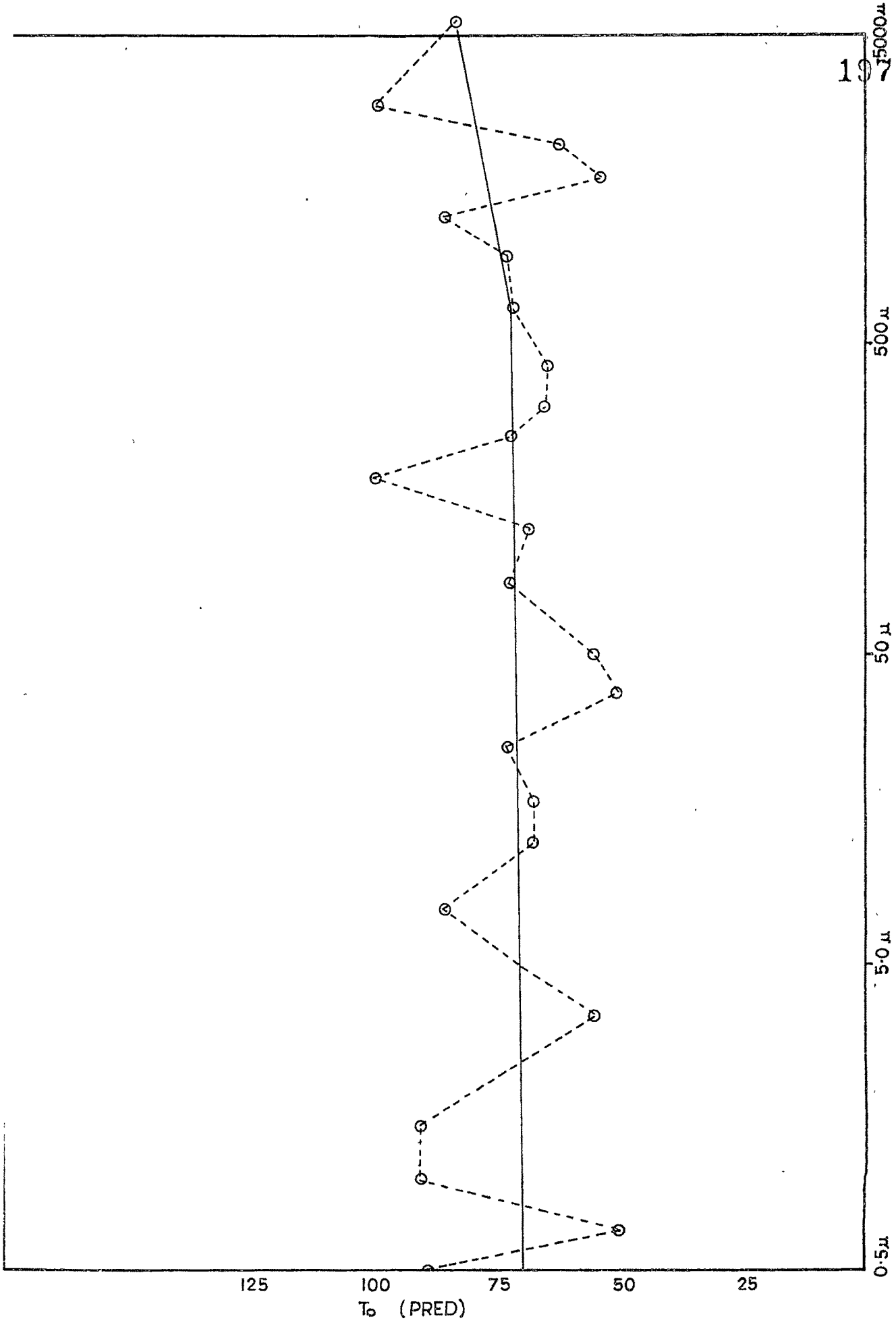

FIG. 6·57 RATE OF LOADING Vs To (PRED)

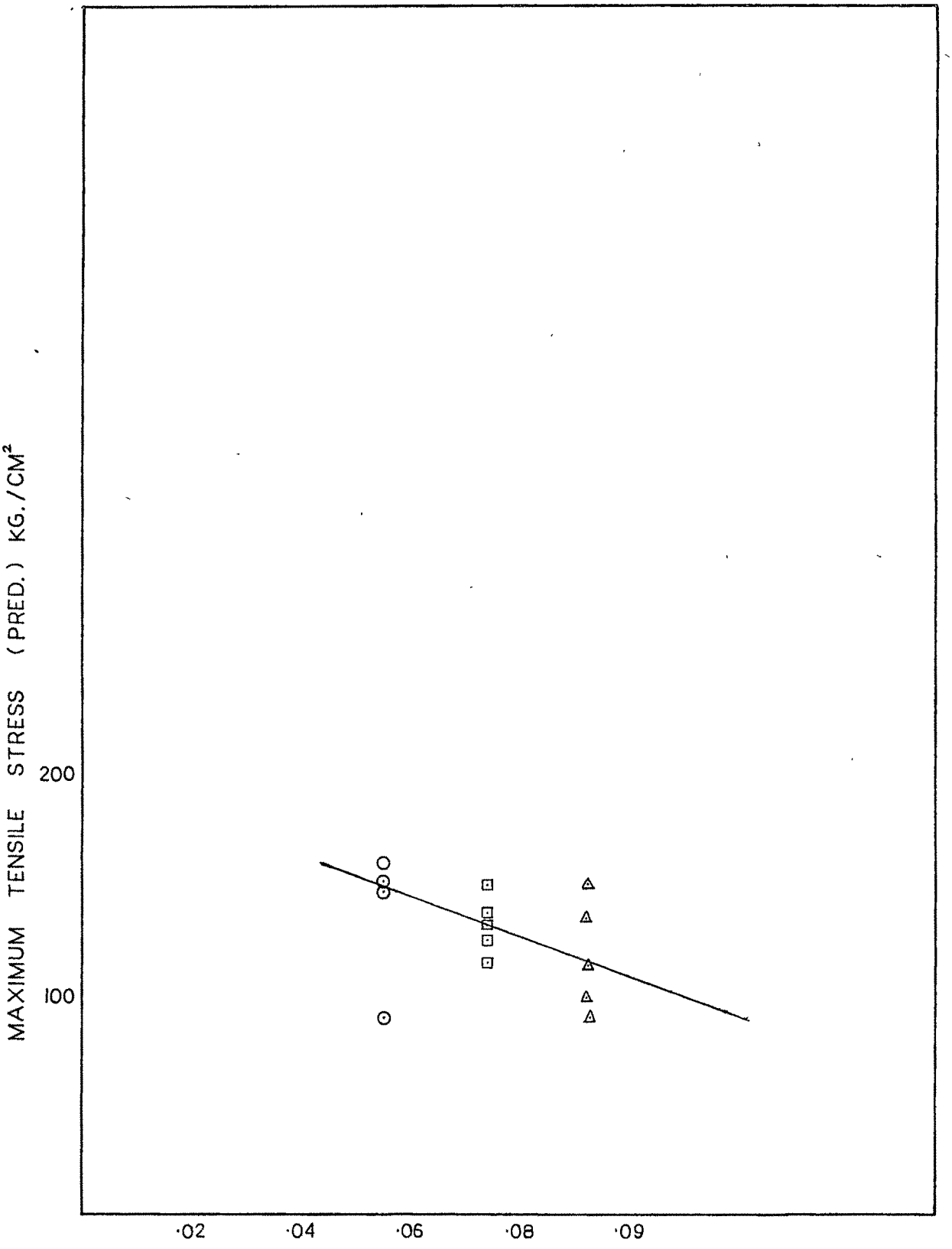
MAXIMUM TENSILE STRESS (PRED.) KG./CM²
200
100
·02
·04
·06
·08
·09
RADII RATIO (q)

FIG. 6·58

6.8 A critical stress ratio:

Griffith postulated that failure in a brittle material occurs when the ratio between uniaxial compressive strength and uniaxial tensile strength approaches the value 8. Further the Griffith condition is that the ratio corrosponds to the ratio of maximum compressive stress to maximum tensile stress. From the failure criterion derived during the present investigation the value of 'n' is equal to 8 when there is no pre-stress. From derived general failure criterion 'n_g' equals to

$$n_g = \frac{\sigma_m - \sigma_o}{To}$$

where $\sigma_m - \sigma_o$ is the stress difference on the flaw at the time of failure and To is the value of tensile stress at the time of failure. Table 6.4 A and 6.4 B gives the value of 'n' from series of tests on discs and rings. Thus the critical ratio in case of ricks in which the pre-stress is locked failure triggers when the stress ratio between the shear stress and the tensile stress at the flaw approximates the value equal to 8.

6.9 Crack initiation and propagation:

According to the Griffith's theory the test is only theoretically valid if fracture originates at centre which condition can only be achieved by distributed load for which purpose a special grip developed and designed as described in article 5.5 From the observations recorded and described in article 6.2.3 it can be seen that the primary fracture initiates near the centre of

TABLE - 6.4 A THE VALUES OF 'n_g' AND χ

Sr. No. (1)	Specimen Designation (2)	n_g (3)	χ (4)
1.	Nx/D/0.48 μ/1	8.75	4.375
2.	Nx/D/0.66 μ/2	8.04	4.02
3.	Nx/D/0.96 μ/3	8.87	4.435
4.	Nx/D/1.44 μ/4	9.99	4.99
5.	Nx/D/1.95 μ/5	-	-
6.	Nx/D/2.4 μ/6	8.63	4.31
7.	Nx/D/3.3 μ/7	7.63	3.81
8.	Nx/D/4.8 μ/8	8.27	4.13
9.	Nx/D/7.2 μ/9	8.21	4.105
10.	Nx/D/9.6 μ/10	-	-
11.	Nx/D/12 μ/11	8.49	4.245
12.	Nx/D/16 μ/12	7.7	3.85
13.	Nx/D/24 μ/13	9.03	4.51
14.	Nx/D/36 μ/14	8.18	4.09
15.	Nx/D/48 μ/15	6.13	3.06
16.	Nx/D/60 μ/16	7.66	3.83
17.	Nx/D/82 μ/17	9.91	4.95
18.	Nx/D/120 μ/18	8.8	4.4
19.	Nx/D/180 μ/19	8.86	4.43
20.	Nx/D/240 μ/20	7.82	3.91
21.	Nx/D/300 μ/21	7.51	3.75

Table 6.4 A contined....

(1)	(2)	(3)	(4)
22.	Nx/D/410 μ/22	6.67	3.33
23.	Nx/D/610 μ/23	9.06	4.53
24.	Nx/D/900 μ/24	7.72	3.86
25.	Nx/D/1220 μ/25	8.4	4.1
26.	Nx/D/1520 μ/26	7.52	3.76
27.	Nx/D/2560 μ/27	7.6	3.8
28.	Nx/D/3050 μ/28	10	5.0
29.	Nx/D/4520 μ/29	8.6	4.3
30.	Nx/D/6100 μ/30	-	-

TABLE - 6.4 B THE VALUES OF 'n_g' AND

Sr. No.	Specimen Designation	'n_g'	
1.	Nx/R/3Ø/1	8.86	4.43
2.	Nx/R/3Ø/2	9.4	4.7
3.	Nx/R/3Ø/3	9.45	4.72
4.	Nx/R/3Ø/4	8.68	4.34
5.	Nx/R/4Ø/5	9.21	4.60
6.	Nx/R/4Ø/6	8.47	4.235
7.	Nx/R/4Ø/7	9.6	4.8
8.	Nx/R/4Ø/8	8.6	4.3
9.	Nx/R/4Ø/9	9.03	4.51
10.	Nx/R/5Ø/10	8.72	4.36
11.	Nx/R/5Ø/11	8.49	4.245
12.	Nx/R/5Ø/12	8.14	4.07
13.	Nx/R/5Ø/13	7.75	3.87
14.	Nx/R/5Ø/14	7.80	3.9

the disc or near the hole of the ring and tend to coincide with the plane of the loaded diameter. The observed fracture patterns also corroborate with the typical fracture patterns observed by Colback (1966) and are in agreement with the findings by Mitchel (1961) and Rudnick et al (1963). While it validates the initiation of the fracture along the loaded diameter as expected in an ideal Brazilian test on discs and rings it further confirms the Griffith postulation that there initiates simultaneously a crack at very nearly the same load if there exists a critically oriented flaw. This phenomenous is clearly evident in the sample number Nx/R/4Ø/6, Nx/R/5Ø/10 and Nx/R/5Ø/12 in which the calcite veins are situated at some angles to the loaded diameter, along the loaded diameter and perpendicular to the loaded diameter. The fracture occured simultaneously along the flaw irrespective of the orientations of the flaw as seen in the sample number Nx/D/1.95 μ/5, Nx/D/12 μ/11, Nx/D/82 μ/17, Nx/D/610 μ/23 and Nx/D/2060 μ/27. Thus a concept of failure emerges out that in rock material which has inherent microcracks maximum falure stress is transferred instantaneously to the pre-existing flaws like microcracks, intrusions in the rock where the stress concentration might be maximum. This concept hitherto has been utilised in the development of a generalised Griffith criterion as developed during the present investigation.

6.10 Conclusions:

The analysis of the Brazil test on discs and rings of basalt rock subjected to diametral loading conducted under theoretical model of failure in rock material developed during the present investigation establishes the following conclusions:

6.10.1 Ceoncept of pre-stress in rock material:

The basic postulation on which the present investigation centered is that when hot lava solidifies as a consequence of cooling over a period of time a pre-stress is built in to the structure of the rock which resists the external stress on the rock material. As a censequence of series of thermal pressure cycles during the formation of the rock there develops flaws in to the rock structure in which these pre-stresses are locked. The pre-stress is therefore distributed throughout the structure of rock material whose values are not necessarily constant but from engineering considerations these values of pre-stress has been evaluated as a mean weighted material constant. From the experimental investigations conducted under Brazil test condition on discs and rings of two varieties of igneous basalt rocks confirm the postulation and established the material parameter for engineering use.

6.10.2 Mechanistic picture of the failure in rocks:

When an external stress is applied to a material whose structure essentially consist of

6.10 Conclusions:

The analysis of the Brazil test on discs and rings of basalt rock subjected to diametral loading conducted under theoretical model of failure in rock material developed during the present investigation establishes the following conclusions:

6.10.1 Ceoncept of pre-stress in rock material:

The basic postulation on which the present investigation centered is that when hot lava solidifies as a consequence of cooling over a period of time a pre-stress is built in to the structure of the rock which resists the external stress on the rock material. As a censequence of series of thermal pressure cycles during the formation of the rock there develops flaws in to the rock structure in which these pre-stresses are locked. The pre-stress is therefore distributed throughout the structure of rock material whose values are not necessarily constant but from engineering considerations these values of pre-stress has been evaluated as a mean weighted material constant. From the experimental investigations conducted under Brazil test condition on discs and rings of two varieties of igneous basalt rocks confirm the postulation and established the material parameter for engineering use.

6.10.2 Mechanistic picture of the failure in rocks:

When an external stress is applied to a material whose structure essentially consist of

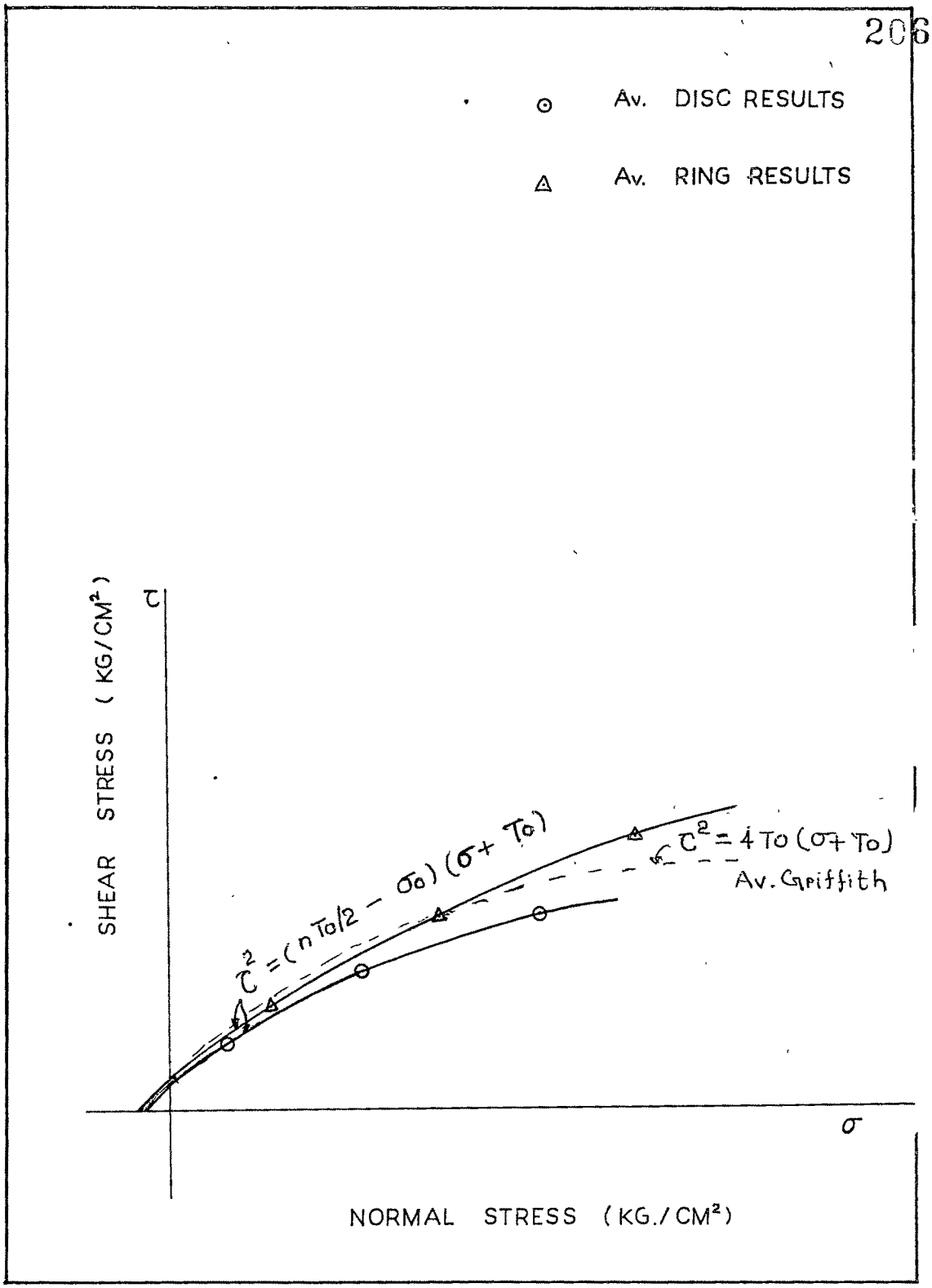

FIG. 6·59 FAILURE ENVELOPES FOR TWO VARIETIES OF BASALT IN BRAZIL TEST ON DISCS AND RINGS

$$\tau^2 = (n\,To/2 - \sigma_o) (\sigma + To)$$

6.10.4 Critical stress ratio for rock materials:

The critical stress combinations at the point of most favourably oriented flaw which triggers the failure is expressed as a ratio of stress difference between the excess compressive stress and the pre-stress to tensile stress. The average value of this critical ratio for the two varieties of basalt rock investigated is 8.73.

6.10.5 Constitutive relation for rock materials:

A hyperbolic constitutive stress-strain relation

$$\sigma/\sigma_o = \mathrm{Sin}\,(\lambda\epsilon)$$

for rock materials emerges out against experimental observations (Fig 6.60), whose parameters can be deduced from elastic considerations. Within elastic limit the relationship for uniaxial stress and strain is

$$\sigma_{11} = E (1 - \nu)/(1 + \nu) (1 - 2\nu)$$

With the dissipation of stored elastic energy at σ/σ_o greater than one the failure is triggered and follows the laws of crack dynamics.

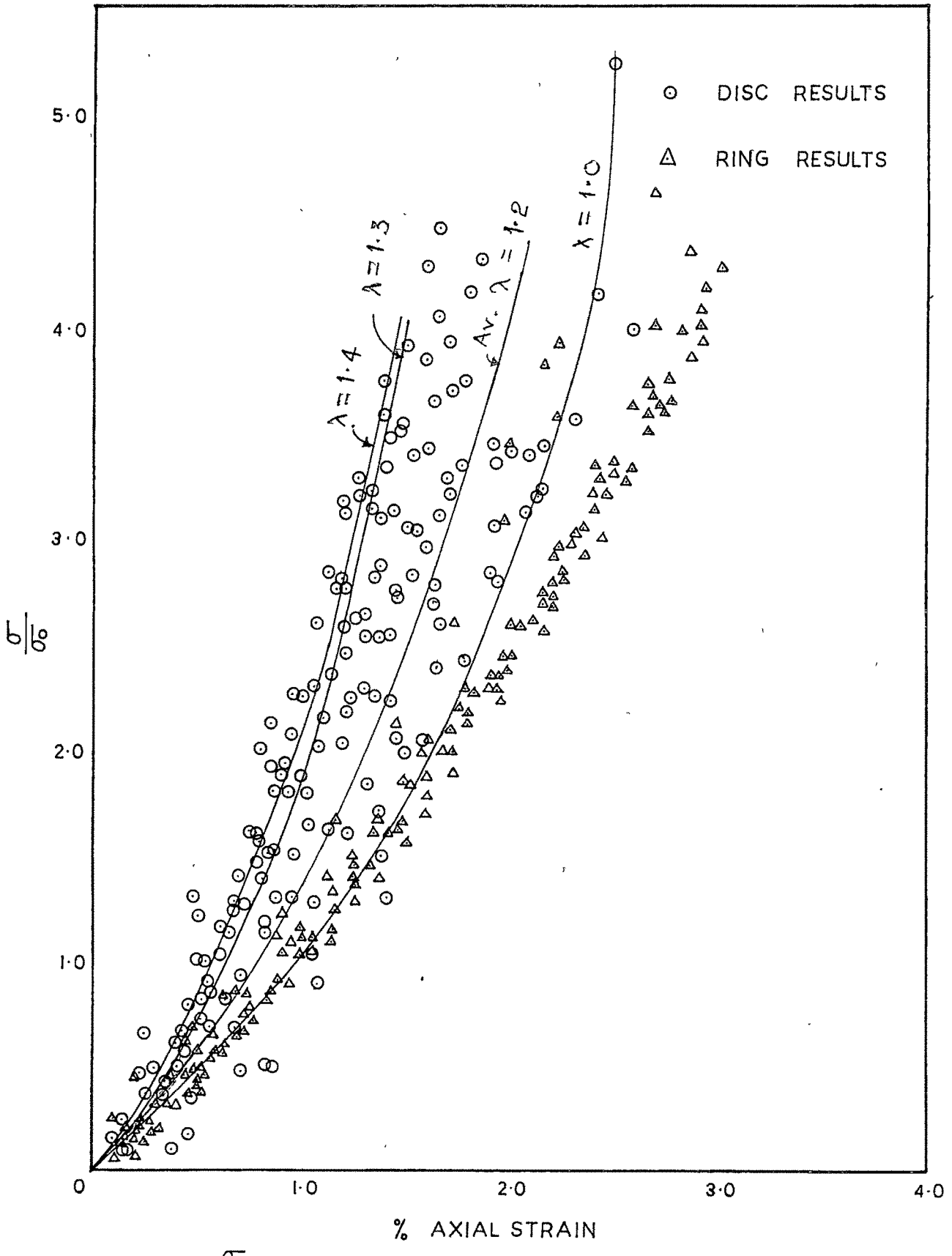

FIG. 6·60 $\frac{\sigma}{\sigma_0}$ Vs STRAIN